The Jamming of Dense Suspensions Under Imposed Stress

Colin Holmes

Thesis submitted for the degree of Doctor of Philosophy

School of Physics

University of Edinburgh

2004

"We're jammin'... I hope you like jammin' too."

Bob Marley

Abstract

Suspensions of solid particles within a solvent display a variety of interesting rheological behaviour. The viscosity can vary with applied stress, resulting in materials which become thinner or thicker as they are driven more strongly. Thickening can become so severe that the flow becomes erratic on a macroscopic level, suggesting that the material aquires a solid–like character, at least transiently. This idea is supported by recent experiments in which initially fluid suspensions are transformed into a persisting solid upon shearing.

Behaviour reminiscent of this can be observed in granular materials. For example, the flow of grain from a hopper under gravity is often halted as 'arches' of force bearing particles form. In such a situation, the solidity of the material arises only as a result of applied forces and transient flow.

There has been much speculation regarding the nature of these jamming phenomena, in particular whether or not there is a link between jamming and the glass transition. In this thesis, we present a model in which jamming is treated as a stress induced glass transition. This leads to predictions of the rheological behaviour and the structural dynamics in such a scenario. We also discuss the link between rheology and the glass transition more generally, arguing that common explanations for thickening in dense colloids are unlikely to be complete, as they essentially ignore the presence of the glass transition. Finally, we discuss the relevance of jamming phenomena to the industrial process of granulation.

Declaration

I declare that this thesis was written by myself and that the work presented has been carried out by myself, in collaboration with my supervisor Mike Cates. Additionally, the models described in Ch. 6 were studied in collaboration with Matthias Fuchs. The work presented here has not been submitted for any other qualification.

Acknowledgements

There are many people who have, in some way or other, helped ensure that my PhD studies have been both fruitful and enjoyable.

Firstly, I would like to thank my supervisor Mike Cates for his guidance throughout the course of my PhD. His enthusiasm, knowledge and guidance have been greatly appreciated. I would also like to thank Matthias Fuchs, for many patient discussions regarding mode–coupling theory, as well as Achod Aradian for discussions of rheology.

I am grateful to Wilson Poon, who latched onto my initial enthusiasm for condensed matter and encouraged me from an early stage. Similarly, Patrick Warren gave me an early opportunity to further my interest, and has also provided food for thought during my PhD studies.

My fellow students have helped in a number of ways, from providing computational help to post work pints. A particular mention must go to Otti and Dave who, along with myself, ensured that Room 4306 remained a tranquil working environment...

I thank all the members of E=mcc (the School of Physics' premier cricket team) and Torpedo Baird for nights in the pub, occasionally preceeded by some sport.

I am grateful to Unilever and the EPSRC for finanical support through a CASE award.

Finally I would like to thank my family and Joanna for all their support.

Contents

Chapter 1

Introduction

This thesis is concerned with the behaviour of complex fluids under flow, or their *rheology*. I begin by giving a brief introduction to complex fluids, explaining what they are and why they are interesting to study. I then introduce the subject of rheology, and conclude the chapter with a summary of the thesis.

1.1 What are complex fluids?

In *atomic* and *molecular* materials (*eg*, carbon and water respectively) the material is made up of a large number of particles (the individual atoms or molecules) interacting with one another. The structure of the material is homogeneous on lengthscales much larger than the typical atomic lengthscale of angstroms. In a *complex fluid*, this is not the case: rather, at least one component is significantly larger than the atomic lengthscale. For example, in *polymer solutions*, very long molecules are suspended in a liquid of much smaller molecules or atoms. Many properties of complex fluids (also known as soft matter) are governed by the behaviour of this large component, rather than by behaviour on the atomic scale, and this can give rise to rather interesting material properties. Some of the most common complex fluids are briefly introduced below. For a more in-depth discussion of complex fluids see, *eg* [1, 2].

1.1.1 Colloids

In colloidal systems, solid or liquid particles are dispersed within a liquid or gas. There is a range of particle sizes, from a few nm up to about $1\mu m$, for which particles are regarded as colloidal. Particles with sizes in this range are sufficiently large that the background fluid may be treated as continuous, whilst they are sufficiently small that Brownian motion is significant. This latter condition can be used to set a loose upper bound on the colloidal lengthscale by comparing the magnitude of the thermal energy to a typical gravitational potential energy. Everyday examples of colloidal systems include blood, milk and paint.

For a number of years now, physicists have studied model colloids, in which the interactions between the particles are well characterised. The simplest model system is the (nearly) hard sphere suspension. This is an approximate realisation of an idealised system of spherical particles which have no interactions, save for an arbitrarily large repulsion upon contact, which prevents overlap: an appealing analogy is 'microscopic ping-pong balls'. Computer simulation has demonstrated that the hard sphere system displays a thermodynamic phase transition between a disordered fluid and a crystalline solid at a certain particle concentration. Additionally, there is a nonequilibrium transition to an amorphous solid phase which occurs at high concentrations – this 'glass' state will be discussed in much more depth later. That colloids could mimic a hard sphere system has been demonstrated by comparing the phase behaviour of carefully prepared samples with the computer simulations, with great success. More generally, it is typical for colloidal systems to behave as a fluid (solid) at sufficiently low (high) concentrations.

1.1.2 Polymeric materials

As mentioned above, in a polymer solution, long chain-like molecules (polymers) are suspended within a molecular liquid. The polymers are made up of many ($\gtrsim 10^5$) *momomers* linked together in chains. As well as in solution, polymers can exist in a solid state (*eg*, rubber) and as a polymeric liquid. Solid polymers are very common in everyday life, for example in packaging. Such products are often processed either in a molten form or in solution.

1.1.3 Amphiphilic systems

Amphiphilic systems are composed of *surfactant* molecules, which have one end (the *head*) which likes to be surrounded by water, whilst the other end, called the *tail*, does not like to be in water – it prefers to be in oil. Because of this property, mixtures of surfactants with water/oil can lead to the spontaneous formation of complex structures which allow both ends of the molecules to reside within their favoured environment. Surfactants are used in many cleaning products to seperate oils from water.

1.2 Why are complex fluids interesting?

We are all familiar with the classical separation of matter into solids, liquids and gases. But there are, in reality, many materials which do not fit neatly into this classification. Consider the simple division between solids and liquids: a typical liquid such as water is easily made to flow, whilst solids (for example steel) are not. But what about a material such as toothpaste – is this a solid or a liquid? One one hand, toothpaste will flow if one squeezes the tube, but on the other hand it will happily sit on the brush, rather like a solid. It is evident then, that some materials are not easily categorised as solid or liquid. Complex fluids (of which toothpaste is an example) often fit into this category. (In fact, some authors choose this as their definition of a complex fluid *eg*, [1].) Another oft quoted example is that of 'silly putty'. If dropped, this material will bounce like a solid rubber ball, but will flow under gravity if left undisturbed on a surface for ten minutes or so. This sort of behaviour naturally provokes one's curiosity.

Another merit of studying complex fluids is that they allow easier study of many-body dynamics than atomic or molecular materials [3]. In atomic materials, these processes occur on short timescales ($\sim$ picoseconds) governed by atomic motion: this makes them very difficult to study. In complex fluids, the relevant dynamics is that of the large 'structural units' (colloidal particles, polymers...). As one might intuitively expect, these larger particles have slower dynamics, resulting in typical timescales being of the order of milliseconds or greater. These longer timescales are far more accesible to experimental techniques than those associated with atomic motion. For example, the process of crystallisation may be studied in colloidal systems

using microscopy [4], while such detailed studies of crystallisation in atomic or molecular systems would prove rather more difficult. Another attribute of complex fluids is that their slower dynamics makes it easier to perturb the system from equilibrium, for example by external forcing, and thus to study nonequilibrium situations. We will return to this point in the following section. These considerations point towards the fact that complex fluids provide an excellent 'laboratory' for the study of many-body dynamics. For further discussion of the physics which can be gleaned from the study of soft matter, see [3].

Finally, it is important to understand the physics of complex fluids because they are ubiquitous in industry. For instance shampoos, lubricants, foods and the aforementioned toothpaste are all examples of complex fluids. A greater understanding of the fundamental physics of these materials allows more efficient processing and the development of improved products.

1.3 Rheology

Rheology is the study of how a material deforms under an externally imposed stress, or conversely, the study of the stresses which result when a material is deformed in a prescribed manner. From the previous section, it is apparent that much of what makes soft matter interesting is its rheology. As a simple probe of rheology, consider the experiment schematically represented in Fig. 1.1. Exerting a given force upon each of the parallel plates imposes a certain *shear stress* upon the material, which results in its deformation. For a 'normal' solid, such as a lump of steel, this deformation is rather boring: a constant *shear strain* (γ), proportional to the applied stress, is maintained for as long as the stress is applied (*Hookean behaviour*). (The shear strain is the ratio of the distance moved by one of the plates to the perpendicular distance between them.) The ratio of the applied stress to this strain is the the material's *shear modulus*. What about a classic example of a liquid, such as water? Do the same experiment and one finds that the shear strain does not approach a constant value. Rather, the shear strain continually increases at a rate $\dot{\gamma}$ (the *shear rate*) proportional to the applied stress. In this case, the modulus is not a useful quantity: more relevant is the *viscosity*, defined as the ratio of the imposed stress to the shear rate.

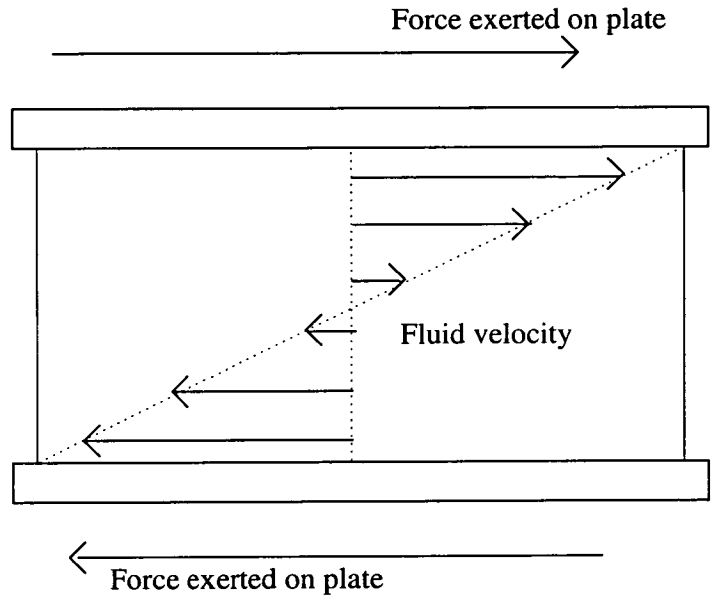

Figure 1.1: Application of shear stress to a material may be performed by enclosing the material between two parallel plates, and imposing a given force on the plates. This schematic figure shows a side on view of such a setup. In a liquid such as water, this results in 'simple shear flow': the flow velocity varies linearly from zero (at the midpoint between the plates) to a maximum velocity (equal to that of the plates themselves) adjacent to the boundary plates. The velocity gradient is known as the *shear rate* $\dot{\gamma}$.

But what about soft matter? In this case, the result often proves to be far from boring. Consider shearing a colloidal fluid: as before, application of a given shear stress leads to flow at some shear rate. However, unlike the case of water, the shear rate need not be simply proportional to the stress. Rather, in some cases one finds a highly nonlinear relationship between the two quantities (see, *eg*, [5]) – the viscosity can vary dramatically with the applied stress. A situation in which the viscosity increases with stress is known as *shear thickening*; a decreasing viscosity corresponds to *shear thinning*. Also, some materials can exhibit flows which change in time, perhaps chaotically, when subjected to a constant stress (*eg*, [6]).

What if our soft material is not a fluid, but rather is a solid, such as a colloidal crystal? If we impose a very small stress, then the behaviour will be similar to that of the steel mentioned above – a constant shear strain is maintained during the application of stress. However, on application of larger (but still rather modest) forces, we can cause the solid to yield and flow. Once this 'yield stress' has been exceeded, the material's mechanical response is similar to that of a liquid: the viscosity, rather than the elastic modulus, is a meaningful quantity. 'Honorary

liquids' created in this way can exhibit similar rheological phenomenology to materials which are liquids in their quiescent state.

So why do complex fluids display rheology which is so different to 'normal' materials? In particular, why do, *eg*, colloidal liquids not simply flow with a constant viscosity; and why are colloidal solids easy to 'shear melt'? To answer the first question, consider a fluid in thermal equilibrium. In such a system quantities such as the density field fluctuate, with fluctuations having a typical lifetime τ, which is fixed by the microscopic dynamics of the fluid. By shearing a fluid at shear rate $\dot{\gamma}$, we introduce a characteristic timescale of the flow: $\tau_{\dot{\gamma}} \sim 1/\dot{\gamma}$. If the shearing is sufficiently slow, this timescale will be very long compared to the material's intrinsic relaxation timescale τ. This means that, over the timescales on which shearing could perturb the fluid at a microscopic level, relaxation processes occur many times over. Thus the structure and dynamics of the material remain largely unchanged from from that of the quiescent state. In molecular fluids such as water, this condition is met at any feasible shear rate, due to the fast (picosecond) relaxation processes, and so sheared molecular liquids essentially remain in thermodynamic equilibrium: their viscosity, and other properties remain unchanged from the equilibrium values. In complex fluids however, typical relaxation times are much slower, of the order of milliseconds or longer. Therefore, whilst at low enough shear rates this equilibrium condition is met, the fluid may be driven out of equilibrium at easily attainable shear rates. In this case, the system has insufficient time to relax in the time taken for the shear to alter the material at a microscopic level. The structure and dynamics of the material can become altered from that in the unperturbed state, causing properties of the material – such as its viscosity – to change. So we see that, as claimed in the previous section, the long relaxation times of complex fluids make it much easier for us to drive them out of equilibrium, and thus to study nonequilibrium many–body processes.

We turn now to the second difference which we have identified – why can we easily shear melt a colloidal solid, but not a lump of steel? To answer this, we make a simple estimate of the shear modulus of these materials which, as mentioned above, is a measure of the stress which arises upon a shearing deformation. The modulus is an energy density, and so we consider the typical energy per unit volume in each material. In a typical 'hard' solid, the particles are joined by strong electronic bonds, with typical energies per atom of the order of electron volts,

and the relevant lengthscale is $\sim 10^{-10}m$. For a sheared colloid, entropy is the main source of elasticity, and so the energy scale is the thermal energy kT ($\sim \frac{1}{40}eV$ at room temperature), whilst the relevant lengthscale is $\sim 10^{-7}m$. Thus, a typical shear modulus of a metal is of the order 10^{10} times as large as that of a colloid! This suggests that it is easy to deform a colloidal solid to large strains, where at some point it will it yield and flow. In contrast, it is difficult to do this with steel. Once the material is flowing, the discussion above regarding the competition of timescales again comes into play, bringing with it all that this entails. Therefore, we see that both colloidal solids and fluids may easily be driven out of equilibrium and therefore display interesting rheology.

1.4 Thesis summary

In this thesis, we shall be interested in the rheology of dense colloids. In particular, we investigate the implications of a model in which shear thickening is due to the proximity to the glass transition. This model is discussed in the context of recent experiments in which shear thickening becomes so severe that a fluid is transformed into a solid upon shearing. We are interested in whether or not such a 'jammed solid' may be interpreted as a stress induced glass. Aspects of these experiments which lie outwith the scope of the simple model are also discussed.

The rest of this thesis is laid out as follows. In Chapters 2 and 3, background material on the subjects of rheology and the glass transition are presented. Following this, Ch. 4 provides a technical description of the mode-coupling theory of the glass transition (MCT), which is relevant to the work presented in this thesis.

In Ch. 5, we suggest an explanation of the experiments mentioned above. We also discuss their relationship to the industrial process of granulation, and identify the important physical quantities involved in this procedure. Following on from this, we argue that the glass transition is of relevance to shear thickening. This notion leads to the development, in Ch. 6, of a simple model, based upon MCT, of suspension rheology. The results of this model are presented in Chapters 7 and 8. In Ch. 9, we discuss these results in the context of experimental results and the rest of the thesis. Finally, in Ch. 10 we draw our conclusions and suggest ways in which work in this field might proceed.

Chapter 2

Rheology

In this chapter, we shall discuss the rheology of soft matter in more depth: we shall explain what it is in general that one would like to achieve, and discuss the relevant phenomenology of complex fluid rheology. We begin by introducing various tensors, which provide a framework for the quantitative description of stress and deformation. Much of the information in this chapter, and more, may be found in Refs. [1, 7, 8, 9].

2.1 A tensorial description

2.1.1 Deformation: the strain and velocity gradient tensors

In order to characterise deformation in a quantitative manner, we introduce the strain tensor $\underline{\underline{\mathbf{E}}}$, following Ref. [8]. The strain tensor is defined in the following way: consider a small element, at position $\mathbf{r}$, within a material. If the material is then deformed in some manner described by $\underline{\underline{\mathbf{E}}}$ then, under the deformation, $\mathbf{r} \rightarrow \mathbf{r}' \equiv \underline{\underline{\mathbf{E}}} \cdot \mathbf{r}$, as illustrated in Fig. 2.1.

Deformations for which $det\, \underline{\underline{\mathbf{E}}} = 1$ preserve a material's volume. These are the strains in which we shall be interested, as volumetric strains do not lead to the sorts of interesting behaviour which we have been discussing. The reason for this is that, like deformation in 'hard matter', these strains deform strong chemical bonds between molecules [8]. The modulus relevant to such strains (the *bulk modulus*) is therefore of the same order as the modulus of 'hard matter',

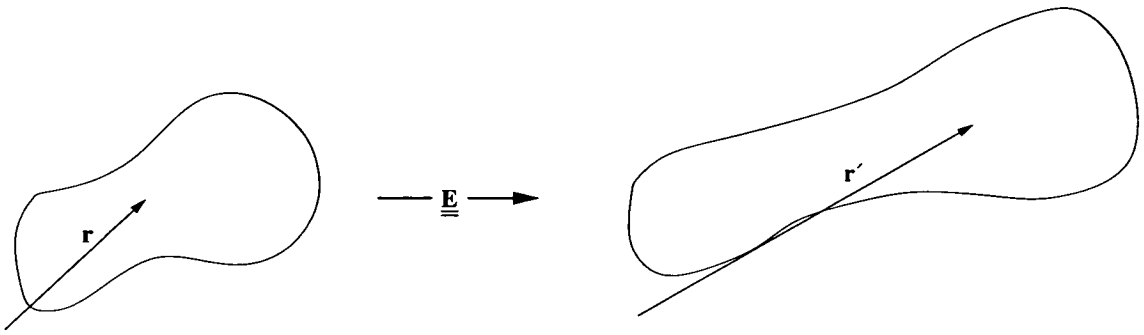

Figure 2.1: A deformation, such as the one illustrated above, may be represented by the strain tensor, which is defined in the main text.

and so these strains lead to the sort of 'boring' response discussed in the Introduction. We shall therefore ignore volumetric strains in future discussions.

For small strains, it is useful to split the strain tensor in the following way:

$$\underline{\underline{\mathbf{E}}} = \underline{\underline{\delta}} + \underline{\underline{\mathbf{e}}}, \tag{2.1}$$

where $\underline{\underline{\delta}}$ is the second rank identity tensor. Then, the *displacement* of a material element, $\mathbf{u} \equiv \mathbf{r}' - \mathbf{r} = \underline{\underline{\mathbf{e}}} \cdot \mathbf{r}$. If the strain is homogeneous, which we shall assume in the following, this is equivalent to $\underline{\underline{\mathbf{e}}} = (\nabla \mathbf{u})^T$.

In a flowing material, we have a time dependent deformation, which we consider to consist of a series of infinitesimal strains. In this case, the displacement field $\mathbf{u}(\mathbf{r})$ will vary in time: in a short time δt the material element at $\mathbf{r}$ is displaced by $\mathbf{u}(\mathbf{r}) = \mathbf{v}(\mathbf{r})\delta t$, where $\mathbf{v}(\mathbf{r})$ is the velocity field, and so $\dot{\mathbf{u}} = \mathbf{v}$.

By considering gradients of the velocity field, we can divide volume preserving deformations into *extensional* and *shearing* strains. In the former, velocity gradients are parallel to the velocity itself, whilst in the latter, gradients are perpendicular to the velocity. Mixed flows, containing both these components, may also occur. The gradient of the velocity field defines the aptly named *velocity gradient tensor* $\underline{\underline{\mathbf{K}}} \equiv (\nabla \mathbf{v})^T = \dot{\underline{\underline{\mathbf{e}}}}$. This object is related to the strain tensor, which we must generalise in the case of a flowing material: let the position of the material element, present at $\mathbf{r}(0)$ at $t = 0$, evolve in time according to $\mathbf{r}(t) = \underline{\underline{\mathbf{E}}}(t, 0) \cdot \mathbf{r}(0)$. Now consider the position of a material element at time $t + \delta t$. We can write this in several ways:

by definition of $\underline{\underline{\mathbf{E}}}$, we have

$$\mathbf{r}(t+\delta t) = \underline{\underline{\mathbf{E}}}(t+\delta t, 0) \cdot \mathbf{r}(0). \tag{2.2}$$

Alternatively, we may write

$$\begin{aligned} \mathbf{r}(t+\delta t) &= \mathbf{r}(t) + \mathbf{v}(\mathbf{r})\delta t & (2.3)\\ &= (\underline{\delta} + \underline{\underline{\mathbf{K}}}\delta t) \cdot \mathbf{r}(t) & (2.4)\\ &= (\underline{\delta} + \underline{\underline{\mathbf{K}}}\delta t) \cdot \underline{\underline{\mathbf{E}}}(t, 0) \cdot \mathbf{r}(0), & (2.5) \end{aligned}$$

where we have used $\mathbf{v} = \underline{\underline{\mathbf{K}}} \cdot \mathbf{r}$. Upon taking the limit $\delta t \to 0$, comparison of Eqs. 2.2 and 2.5 shows that

$$\underline{\underline{\mathbf{K}}} \cdot \underline{\underline{\mathbf{E}}} = \frac{\mathrm{d}\underline{\underline{\mathbf{E}}}}{\mathrm{d}t}. \tag{2.6}$$

This result links the strain and velocity gradient tensors. We now consider how to describe the state of stress in a material, using the *stress tensor*, before linking the state of stress in a material to its deformation.

2.1.2 The stress tensor

Consider a small cubic material element (Fig. 2.2). The faces of this volume element will experience forces from the material on the exterior of the cube: the stress tensor $\underline{\underline{\sigma}}$ is defined such that the force $d\mathbf{F}$, due to material outwith the cube, on a face with vector area $d\mathbf{A} = \mathbf{n}dA$ (with n the outward unit normal and dA the infinitesimal area of the face) is $d\mathbf{F} = \underline{\underline{\sigma}} \cdot \mathbf{dA}$. Except in unusual cases, the stress tensor is symmetric, as is shown by considering torques on an infinitesimal element [8].

As mentioned earlier in this chapter, the bulk moduli relevant to volumetric strains in soft materials are much larger than the moduli of volume preserving deformations. Very large stresses are required to produce even a small volume change. In this case, it is a good approximation to treat the bulk modulus as infinitly large, expressly forbidding volume changes. This condition is then enforced by the isotropic pressure $p = -(1/3)\,\mathrm{Tr}(\underline{\underline{\sigma}})$, which simply takes on the value necessary to prevent volume changes, and is therefore not an interesting quantity to study.

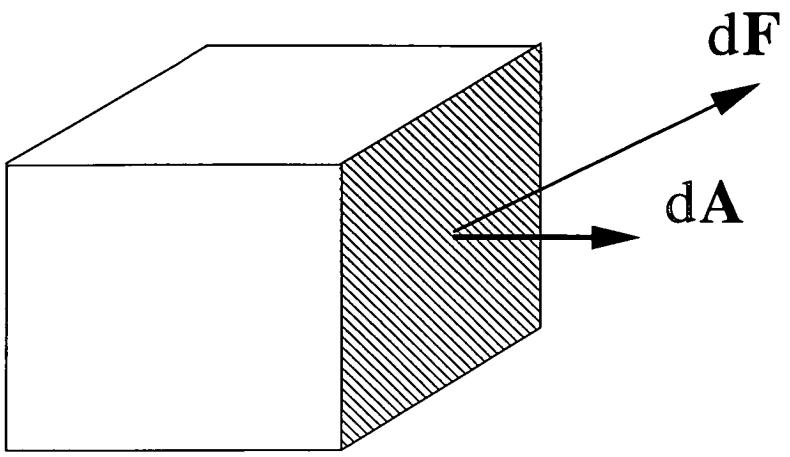

Figure 2.2: A cubic volume element. The face (shaded) with vector area $d\mathbf{A}$ experiences a force $d\mathbf{F} = \sigma d\mathbf{A}$.

Therefore, we concern ourselves only with determination of the stress tensor up to an additive isotropic term. From this, and the symmetry of the stress tensor, one can see that there are 5 independent numbers which specify the stress tensor: three shear stresses (σ_{12}, σ_{13} and σ_{23}) and two normal stress differences, usually chosen as $N_1 \equiv \sigma_{11} - \sigma_{22}$, and $N_2 \equiv \sigma_{22} - \sigma_{33}$.

2.1.3 The constitutive equation

In complete generality, a material's state of stress is linked to its deformation rate at all earlier times, and the present time. We may write this as a functional of the deformation rate:

$$\underline{\underline{\sigma}}(t) = \mathcal{F}[\underline{\underline{\mathbf{K}}}(t' \leq t)]. \tag{2.7}$$

It is this relationship, known as the *constitutive equation*, that rheologists wish to measure, and to understand from the microscopic physics. In some cases, a constitutive equation which is local in time may provide a suitable description of a material's rheological response, simplifying matters somewhat. An example of this situation is the constitutive equation for a Newtonian fluid, for which $\underline{\underline{\sigma}} = \eta(\underline{\underline{\mathbf{K}}} + \underline{\underline{\mathbf{K}}}^T)$, with η the shear viscosity – a constant property of the material. Another simple constitutive equation is that of the ideal Hookean solid: $\underline{\underline{\sigma}} = G\underline{\underline{\mathbf{E}}} \cdot \underline{\underline{\mathbf{E}}}^T$, where G is the material's *shear modulus* [10], again a property of the material. (This is couched in terms of the deformation tensor, rather than velocity gradients, but as we have seen, these are

related.) These two simple models are the archetypes of a viscous liquid and an elastic solid. Upon application of a shear stress, the Newtonian fluid flows at some shear rate determined by its viscosity, whilst the Hookean solid develops a fixed shear strain. Many real materials are well modelled by these idealised cases, at least in some regime, but outside these cases the behaviour is often much richer. Example constitutive equations in more complex models (along with examples of the tensors describing stress and deformation) may be found in Refs. [7, 8, 9, 10].

2.1.4 An example: simple shear flow

In the following discussion of the rheology of complex fluids, we shall be concerned in particular with simple shear flow. Therefore, we now define this in terms of the tensors introduced above.

In simple shear, the fluid flows in in a given direction (which we choose to be the x–direction) with a constant velocity gradient in an orthogonal direction (the y–direction). The flow field does not vary in the z–direction. Therefore the velocity field is $\mathbf{v}(t) = \dot{\gamma}(t)y\hat{\mathbf{x}}$, with $\hat{\mathbf{x}}$ a unit vector in the x direction. $\dot{\gamma}(t)$ is the *shear rate*. The velocity gradient tensor is

$$\underline{\underline{\mathbf{K}}} = \begin{pmatrix} 0 & \dot{\gamma}(t) & 0 \\ 0 & 0 & 0 \\ 0 & 0 & 0 \end{pmatrix}. \tag{2.8}$$

We can use Eq. 2.6 to give the strain tensor as

$$\underline{\underline{\mathbf{E}}}(t,0) = \begin{pmatrix} 1 & \gamma & 0 \\ 0 & 1 & 0 \\ 0 & 0 & 1 \end{pmatrix}, \tag{2.9}$$

where $\gamma = \int_0^t \dot{\gamma}(t')\mathrm{d}t'$, the accumulated shear strain. In *steady shear*, $\dot{\gamma}(t)$ is a constant and $\gamma = \dot{\gamma}t$.

The constitutive equation given above allows us to calculate the stress in a Newtonian fluid

undergoing shear flow. This gives

$$\underline{\underline{\sigma}} = \begin{pmatrix} 0 & \eta\dot{\gamma} & 0 \\ \eta\dot{\gamma} & 0 & 0 \\ 0 & 0 & 0 \end{pmatrix}. \tag{2.10}$$

For the Newtonian fluid in simple shear, the only stress that develops is a shear stress. In complex fluids significant normal stresses can also develop. However, experiments and theory often focus upon the relationship between the material's shear stress (simply denoted σ) and the shear rate – unlike the case in Newtonian fluids, the relationship $\sigma(\dot{\gamma})$ may be significantly more complicated than a simple linear function.

The viscosity is not a useful quantity in the description of the Hookean solid. Using the constitutive equation given above, one can calculate the stress in a Hookean solid undergoing shear flow. Doing so, one finds that in order to make this material flow, we would need an ever increasing stress, since the shear stress scales with the shear strain: the viscosity is divergent. A more natural way to study the Hookean solid's response to shear is to ask what stress results due to a given constant strain, the answer being provided by the material's shear modulus.

Having introduced the quantities used to describe a material's rheology, we go on now to discuss the experimental techniques used to measure these quantities, before providing a summary of the experimental phenomenology.

2.2 Experimental techniques

2.2.1 Basic principles

In order to investigate the rheology of a complex fluid, one uses a device known as a *rheometer*. This imposes a fixed deformation upon a material, and measures the resulting stresses (or vice–versa), allowing experimental determination of a material's rheological behaviour.

We can categorise rheometers depending upon whether they impose shear or extensional flow (for fundamental studies, it is generally desirable to impose one or the other, rather than a mixed flow, which can be very difficult to analyse). Shear rheometers can be further categorised into

those which impose flow through *drag*, and those which impose flow by setting up a pressure gradient. Colloidal rheology, in which we shall be primarily interested, is very often performed using drag imposed shear flow, and so we shall concentrate upon this technique. However, it is worth bearing in mind that extensional flows can provide information which cannot be deduced from results of shear experiments (see [8] for an example). See [10] for details of other techniques.

Drag flows

In drag flows, the sample is held between two solid surfaces (the *plates*), which are driven with a prescribed force (or with a prescribed relative velocity), creating a flow in the material. If the driving force is controlled, then the mean shear stress at the boundary of the material is fixed, and the resulting shear rate is measured. If, instead, the velocity is controlled, then this fixes the mean shear rate across the sample, and the resulting shear stress is measured. Additionally, normal stresses can be measured in some experiments.

2.2.2 Time dependent shear and viscoelasticity

The simplest rheometer geometry is that of two parallel sliding plates (illustrated in Ch. 1). This set-up has the advantage that (assuming the flow remains homogeneous) it imposes uniform simple shear flow, which allows for (relatively) simple analysis. This geometry is commonly used to perform experiments with a time–dependent strain. In contrast, steady shear is rather problematic, as the plates quickly become displaced far from one another. This problem is solved by using rotational devices, described in Sec. 2.2.3.

Time dependent strain experiments reveal that many complex fluids are *viscoelastic* – they display characteristics of both an elastic solid and a viscous fluid. As an example, consider the following experiment: impose a shear deformation

$$\gamma = \gamma_o \theta(t - t_o), \tag{2.11}$$

where θ is the Heaviside step function. This is known as a *step–strain*. Under such a defor-

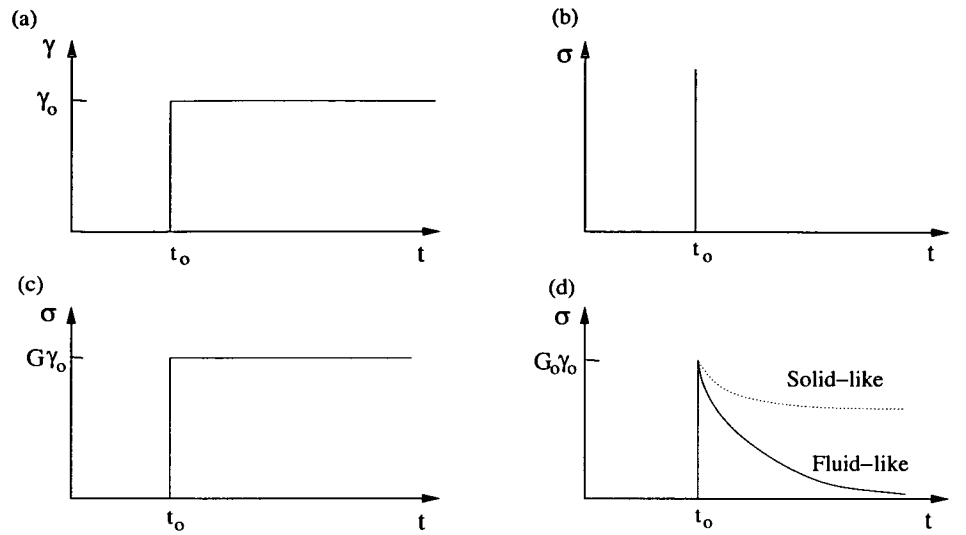

Figure 2.3: A step–strain experiment (a), and the resulting stress response in (b) a viscous fluid; (c) an elastic solid of modulus G; and (d) solid and fluid like viscoelastic materials, with instantaneous modulus G_o (defined in main text).

mation, an ideal Hookean solid with shear modulus G will develop a shear stress $\sigma = G\gamma$ as soon as the strain is imposed. This stress then remains constant for the duration of the strain. In an ideal Newtonian fluid, the shear stress will again rise sharply as the strain is imposed, but will instantaneously relax back to zero (formally, the stress is a Dirac–delta function). In a viscoelastic material, the stresses which arise are not simply proportional to either the strain or strain rate, and so do not show such simple behaviour. Rather, the stress which is created upon the step–strain relaxes from its initial value over time. If the stress relaxes back to zero, then the material is said to be 'fluidlike', whilst if it does not, the material is 'solidlike'. The stress response of fluidlike and solidlike viscoelastic materials, as well as that of the idealised solid and liquid, are shown in Fig. 2.3. It should be noted that all real materials are viscoelastic to some extent, but this property is only obvious if the time for the stress to decay to its final value is comparable to the timescales probed by the experiment. Accordingly, the classification of a material as solidlike or fluidlike may depend upon the experiment. For example, a material will appear solidlike if an experiment is performed on a timescales shorter than the relaxation of the stress, whilst a longer experiment may categorise it as fluidlike (*cf* the earlier example of silly putty).

If a step–strain experiment is performed with a sufficiently small strain amplitude, one can characterise the results in terms of a linear time–dependent modulus, $G(t)$, defined via $\sigma(t) = G(t - t_o)\gamma_o$. (Note that we have also assumed time–translational invarience (TTI), which will not hold in all situations – see [11] for a formulation without this assumption. Situations in which TTI does not hold will be discussed in Sec. 3.4.) $G(t)$ is often written as the product of an 'instantaneous modulus' G_o and a 'memory function' for the stress, $\mu(t)$. Using $G(t)$ one can, at least theoretically, make a distinction between solidlike and fluidlike behaviour which is independent of experiment: *viz*, materials for which $\lim_{t\to\infty} G(t) = 0$ are liquid, whilst those for which $\lim_{t\to\infty} G(t) \neq 0$ are solid. The question of whether such a distinction is useful – *ie*, whether relaxation times truly diverge – will crop up in a later chapter.

We can link the response to an arbitary strain to $G(t)$ (provided we remain in the linear response regime). Consider decomposing an arbitary strain $\gamma(t)$ into a series of strains $\delta\gamma(t')$: if we remain in the linear regime, we can superpose the effects of strains at all earlier times to give

$$\sigma(t) = \sum_{\delta\gamma} G(t - t')\delta\gamma(t') \tag{2.12}$$

which becomes, in the limit $\delta\gamma(t') \to 0$,

$$\sigma(t) = \int_{-\infty}^{t} G(t - t')\dot{\gamma}(t')\mathrm{d}t'. \tag{2.13}$$

Thus we see that the shear stress due to any linear shear deformation is characterised by the function $G(t)$. (In fact, the response to *any* volume–preserving linear deformation is encompassed by $G(t)$ [10].)

In addition to the step–strain experiment discussed above, there are several other time–dependent techniques which probe a material's linear rheological properties. Particularly common is the technique of oscillatory shear, whereby a sample is subjected to an oscillatory shear strain $\gamma = \gamma_o \mathrm{e}^{i\omega t}$. This provides data in the frequency domain in the form of the *storage and loss moduli* $G'(\omega)$ and $G''(\omega)$. There quantities are the real (elastic modulus) and imaginary (loss modulus) parts of the *complex modulus* $G^*(\omega) \equiv i\omega \int_0^\infty G(t)\mathrm{e}^{i\omega t}\mathrm{d}t$, which represents the stress response to an oscillatory strain via $\sigma = \gamma_o \mathrm{e}^{i\omega t} G^*(\omega)$. The elastic modulus represents the stress which is in phase with the strain (corresponding to storage of energy), whilst the loss modulus represents the out–of–phase response, which corresponds to dissipation of energy.

Typically, the balance between elastic and viscous behaviour shifts towards a more elastic response as frequency is increased, again reflecting the dependence of mechanical response upon the timescale probed.

Having discussed time dependent measurements, we shall turn now to discuss *steady shear rheology*, which is a common probe of a material's *nonlinear* behaviour. For more on linear response, see Refs. [1, 8, 9, 10].

2.2.3 Steady shear flow

In order to make measurements in steady shear flow, a rotational device such as a *cone-and-plate* or a *Coutte* rheometer is often used. These are illustrated schematically in Fig. 2.4. In these geometries the flow can be made to approach uniform simple shear flow, and so they are a practical alternative to the parallel plates in steady shear experiments. Additionally, the cone–and–plate device is useful for measuring normal stresses as well as the shear stress.

To investigate a material's steady shear rheology, one applies a constant shear stress (shear rate), to the sample and measures the steady state value of the resulting shear rate (shear stress), and normal stresses if possible. By performing steady shear measurements at a range of stresses/shear rates, one builds up the material's *flow curve* $\sigma(\dot{\gamma})$. Alternatively, the same information may be presented in terms of the shear viscosity $\eta \equiv \sigma/\dot{\gamma}$, either as a function of the applied shear stress, $\eta(\sigma)$, or as a function of applied shear rate $\eta(\dot{\gamma})$. (The distinction between the two controlled variables may be important, since there need not be a one–to–one relationship between the shear stress and the shear rate.) The viscosity in the limit of vanishing shear rate is the *zero–shear viscosity*.

Results in steady shear can often be linked to those made in time dependent shear experiments. In particular, the zero–shear viscosity may be expressed as an integral of the stress relaxation function $G(t)$: for a constant (infinitesimal) shear rate, Eq. 2.13 becomes

$$\sigma(t) = \dot{\gamma} \int_0^\infty G(t)\mathrm{d}t. \tag{2.14}$$

Comparison with the definition of the zero–shear viscosity gives

$$\eta = \int_0^\infty G(t)\mathrm{d}t. \tag{2.15}$$

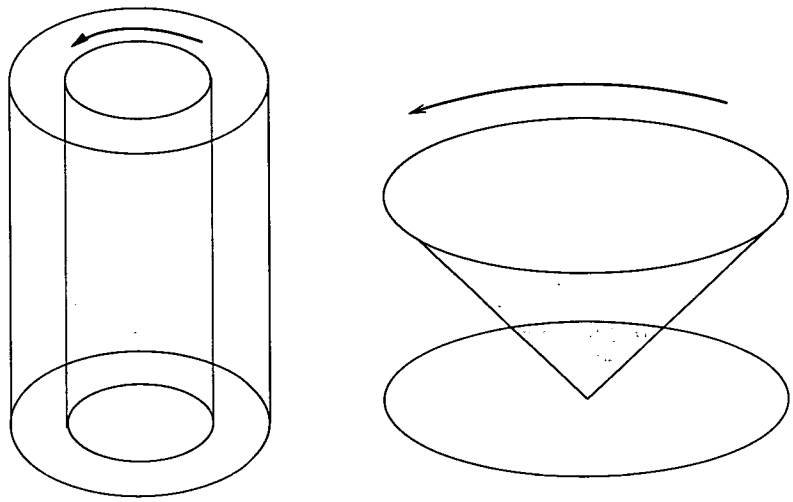

Figure 2.4: Schematic pictures of a Coutte (left) and a cone and plate rheometer. In the Coutte cell, the sample sits between the rotating inner cylinder and the stationary outer cylinder. In the cone and plate, the sample sits between the cone and the plate. In reality, the angle between the cone and plate is much smaller than that depicted – about 5 to 10°.

Thus, materials which have the quality of being solid, as defined in terms of stress relaxation, are also seen to have a divergent zero–shear viscosity. This fits with our intuitive idea of a solid mechanical response.

2.2.4 Experimental difficulties

Lest we give the impression that experimental rheology is a straightforward task, we briefly outline some difficulties which may occur. One of the most common difficulties faced by rheologists is 'wall–slip' – the slippage of the sample against the rheometer plates. If wall–slip occurs, the shear rate in the sample will be (perhaps significantly) less than that which is apparent. This is often a problem in concentrated suspensions, in which the flow may be erratic. Another problem which is common in concentrated colloids is that of accurately determining the volume fraction of experimental samples. This is a problem, not just in rheology, but with any experiment using these systems. However, as we shall see, the rheological properties of suspensions can be extremely sensitive to volume fraction, and so this difficulty is especially pertinent to rheology.

A final complication is that samples may not remain homogeneous when sheared: rather, the

system can undergo a separation into two nonequilibrium 'phases' [12]. Whilst this should not be regarded as a 'problem', but rather as an interesting phenomenon in its own right, it nontheless makes the analysis of experimental data rather more difficult than it might at first appear. We shall not concern ourselves further with the difficulties faced by experimentalists, but it is worth bearing in mind that such difficulties do exist. For further details regarding experimental rheology, see *eg*, [10].

2.3 Phenomenology of complex fluid rheology

In this section, we describe several phenomena which are of interest: much of what we discuss regards hard sphere colloids, as these systems are of primary importance in this thesis. A review of hard sphere colloids from 1996 [13] provides a useful survey of the literature available at the time, and is a good starting point for the newcomer to this subject.

2.3.1 Linear rheology of hard sphere colloids

In hard sphere colloids, the zero–shear viscosity is observed to strongly increase with the concentration (this is usually expressed in terms of the volume fraction $\phi = 4\pi a^3\rho/3$, where ρ is the number density and a is the particle radius). Dilute suspensions have a viscosity close to that of the solvent, as calculated by Einstein [14, 15] and Batchelor [16]. In contrast, concentrated suspensions exhibit large viscosities – *eg*, close to the onset of crystallisation, the viscosity of a hard sphere suspension is ~ 50 times that of the solvent. Experiments suggest that the viscosity may diverge at some volume fraction in the region of 60% [17, 18, 19, 20, 21, 22]. However, other experiments suggest differing values for this volume fraction, possibly indicative of difficulties in accurately measuring volume fractions and verifying whether particles truly behave as hard spheres [18]. Note that, for $\phi > 0.494$, the equillibrium state is (either partly or wholly) a crystalline solid, whose zero–shear viscosity would be divergent: viscosity measurements in this regime are performed not upon the equilibrium state, but upon metastable fluid samples.

The strong increase in viscosity is associated with the slow–down of structural relaxation as the *glass transition* is approached: this is the subject of the following chapter, and so we shall

not go into the underlying causes of this behaviour. However, there is a range of complex fluids (known as 'soft glassy materials' [23]) which exhibit similar rheological behaviour, attributed to the presence in all these materials of slow structural relaxations. We now give a brief survey of these generic features.

2.3.2 Soft glassy materials

Many soft materials appear to have an infinite zero–shear viscosity (they are solid by our earlier definition), but yield and flow upon the imposition of a shear stress exceeding their *yield stress* σ_y [9]. The low shear behaviour of such materials is typically described by the expression

$$\sigma = \sigma_y + \dot{\gamma}^p; \quad 1 > p > 0. \tag{2.16}$$

This describes either a *Herschel–Bulkley fluid*, or a *power–law fluid* if $\sigma_y = 0$. This suggests that the presence of a flow has the effect of speeding up the material's relaxation processes from the rate in the unsheared, quiescent state, lowering the viscosity.

The definition of a solid as a material with an infinite zero–shear viscosity is not wholly satisfactory, since this does not imply the existence of a finite elastic modulus (which is another way in which one might define the onset of solid behaviour) [11]. A material subjected to a stress below its yield stress may 'creep' forever with an ever–decreasing shear rate whose time integral diverges: thus the steady state shear rate is zero (and the material has infinite viscosity), whilst the steady state strain is infinite (resulting in zero elastic modulus).

In addition to this yielding behaviour, the linear viscoelastic spectrum of soft materials is intriguing. The loss modulus $G''(\omega)$ often appears to be constant or increasing as the frequency is lowered [24, 25, 26, 27], in contrast to the requirement, from linear response theory, that $G''(\omega)$ is an odd function [9]. This behaviour has been interpreted as an effect of *aging* – the system's relaxation processes become ever slower as the age of the system increases. Thus measurements at decreasing frequencies, which require the system to be increasingly old, reveal relaxation processes on longer and longer timescales. A model (the *soft glassy rheology* (SGR) model) which reproduces much of the phenomenology of such materials has been developed [11, 23, 28]. We will discuss aging, which is associated with the glass transition, in the following chapter.

2.3.3 Thinning, thickening and jamming

If the viscosity of a fluid increases with increasing shear stress, the material is said to be *shear thickening*, whilst a decreasing viscosity is referred to as *shear thinning* (thus the power law and Herschel–Bulkley fluids are shear thinning at low shear rates). Thinning and thickening occur in a range of complex fluids [1], but for brevity we will concentrate upon colloidal suspensions.

Before we go on to discuss this subject, it will be useful to introduce the *Peclet number*, a dimensionless group obtained by taking the ratio of a material's diffusive relaxation time to the timescale of the shearing. Taking the diffusive relaxation time as that in a dilute system gives the Peclet number as [1]

$$\mathrm{Pe} = \frac{6\pi\eta a^3\dot{\gamma}}{kT}, \tag{2.17}$$

where η is the solvent viscosity, a is the particle radius and kT sets the thermal energy. Thus, in a dilute system, for Peclet numbers much less than unity, the Brownian diffusive dynamics dominate and shear is a perturbation, whilst for Peclet numbers much larger than unity, the suspension properties are largely governed by the shearing motion. In a concentrated suspension, the dynamics do not correspond to a simple diffusion process: in this case, one can define the Peclet number in a variety of ways [1, 13, 29].

A number of experiments have been performed in order to elucidate the behaviour of suspensions of well–characterised particles in steady shear flow, *eg* [5, 30, 31, 32, 33]. 'Stokesian dynamics' simulations have also played an important role [34, 35, 36, 37, 38]. At low volume fractions, suspensions generally behave as a Newtonian fluid. At higher volume fractions, hard sphere suspensions can show shear thinning in a range of shear rates, with thickening occuring at higher shear rates [31, 32]. This scenario is generally in agreement with the simulations, which (for $\phi = 0.45$ for example) predict shear thinning at Peclet numbers of order unity, with thickening at Pe of order 100 [35].

The nature of the thickening depends upon the concentration. Moderately concentrated colloids show gradual thickening whilst in very concentrated samples the thickening can become very pronounced: indeed, the shear rate can show a region where it *decreases* as the shear stress is increased [30, 33]! This is illustrated by the experimental data shown in Fig. 2.5. In controlled

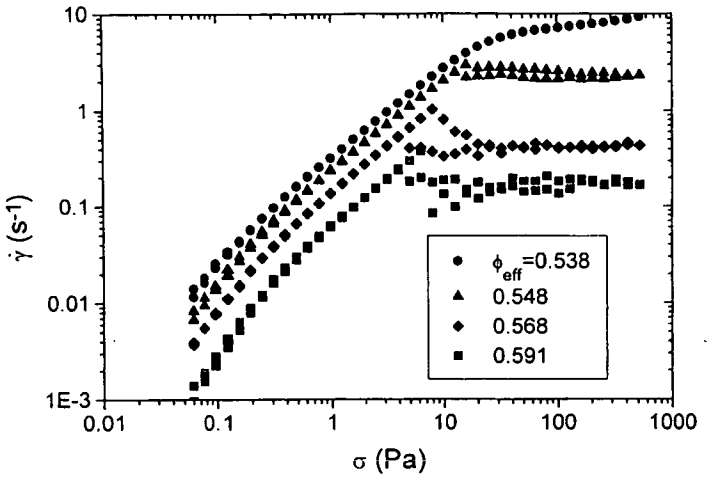

Figure 2.5: Experimental data from Ref. [30], showing strong shear thickening in controlled stress rheometry of concentrated hard sphere colloids. In the most concentrated samples, beyond a certain stress, the shear rate appears rather erratic. Where more than a single value of shear rate is indicated for a single stress, the upper shear rate is that measured upon initially increasing the stress, and the lower is the value measured upon subsequently decreasing the stress. Note that, in this diagram, the axes are interchanged with respect to later figures of this type.

shear rate experiments, this can lead to a discontinuous jump in the measured viscosity. In the strongly shear–thickened state, researchers observe that the flow becomes very erratic [30, 32, 33], and that samples can fracture. This seems to suggest the continual formation and breakup of some load–bearing structure within the thickening suspension, strongly resisting the flow. Also, the origin of the thickening may change with concentration: in the most concentrated systems, the large stresses generated by shearing appears to arise from elasticity, rather than from a dissipative process [32]. This situation is reversed at lower concentrations.

Common explanations for thickening

There are two commonly cited explanations for thickening: these are 'hydrodynamic clustering' [35] and an 'order–disorder transition' [39, 40]. In the latter scenario, the increase in viscosity is due to a loss of order in the flow. It is known that there is a regime of shear rate for which the particles become arranged into flowing layers [35, 41] which are disrupted at higher shear rates. The loss of order in the flow is then supposed to result in the observed thickening,

as particles are no longer able to easily flow past one another, as they can in the layered flow. However, in recent years, evidence has been presented which suggest that shear thickening need not be accompanied by an order–disorder transition. Radiation scattering experiments have found thickening which does not consistently coincide with a loss of order [31, 41]. Optical measurements suggest that the thickening is due to an increase in that portion of the stress mediated by hydrodynamic interactions between the particles. This, it is claimed, is not consistent with the order–disorder transition scenario [31]. Simulations paint a similar picture [35]. However, at least in some cases, there appears to be a correlation between a transition to disorder and shear thickening [42], and some authors remain unconvinced by the evidence against the order–disorder scenario: it has been argued that scattering may not resolve weak order present in layered states, and that the optical measurements in fact do not preclude the relevance of an order–disorder transition [43].

The hydrodynamic clustering scenario is more widely accepted, but a detailed picture of this scenario is still emerging [44]. The idea is that clusters, roughly at 45° to the flow direction, form when the system is strongly sheared [36, 37, 45]. The particles in these clusters are driven close together, leading to strong hydrodynamic lubrication forces which resist the relative motion of particles in close proximity. The formation of these clusters is supposed to lead to the observed rise in viscosity. In recent work it has been suggested that, in hard spheres, the onset of thickening is related to the formation of a contact network between particle surfaces [44]. The network arises when the flow is sufficiently fast that the relaxation of an interparticle contact is slower than the characteristic shearing timescale. This signals the important role of particle surfaces in colloid rheology. This point is backed up by simulations of hard spheres without polymer coatings or Brownian motion [36, 37], in which there appears to be no steady–state flow. Gaps between particles collapse, giving rise to enormous lubrication forces and causing the simulations to fail. This suggests the possibility that the system becomes 'jammed' into a solidlike state. This singularity may be resolved by modelling the polymer coatings, or by including Brownian motion in the simulations.

2.3.4 Shear banding and rheochaos

In extreme cases of shear thinning and thickening, it is possible that the flow curve becomes nonmonotonic [30, 33, 46, 47]: a schematic flowcurve of a shear thinning material with this property is sketched in Fig. 2.6. The portion of this flow curve with negative slope is mechanically unstable – small inhomogeneities in the shear rate tend to grow. This may be illustrated by considering a simple application of the Navier–Stokes equations [48]. This means that materials with such a flow curve, subjected to a shear rate in the range $\dot{\gamma}_1 < \dot{\gamma} < \dot{\gamma}_2$ cannot indefinitely sustain homogeneous flow. In practice, the material will typically separate into two (or more) 'bands' [49, 50], which correspond to stable states. Different types of banding are possible [51]: the coexisting bands will have equal shear rate, or equal shear stress depending upon their orientation.

For brevity, we consider only the case represented in Fig. 2.6, in which the bands have differing values of the shear rate and equal shear stresses. The average of the shear rate across these bands must, of course, correspond to that applied to the system (assuming that the shear rate is the controlled variable). As the applied shear rate is increased beyond $\dot{\gamma}_1$, one then finds a plateau in the shear stress [50], as the system balances the proportion of the two states to satisfy the imposed shear rate. (Actually, the system may separate at shear rates lower than $\dot{\gamma}_1$. The 'selected stress' at which banding occurs is a subject of theoretical interest [52].) Whichever form of banding takes place, one does not expect to *observe* a flow curve such as that of Fig. 2.6: such a curve represents underlying constitutive behaviour, rather than the measured macroscopic behaviour. Note that banding is also reported in shear thickening systems [53], suggesting an underlying 'S'–shaped flow curve. There is a large body of theoretical work on inhomogeneous flows (see *eg* [51, 52, 54, 55, 56]), some of which takes advantage of the analogies with thermodynamic phase transitions.

In recent years, there have been reports of oscillatory, and possibly chaotic, variations in the viscosity of systems under steady applied stress or shear rate in the vicinity of the banding–instability [57, 58, 59, 60]. The presence of macroscopic choas in a viscoelastic material at low Reynolds numbers has been termed *rheochaos* [61]. One explanation for such behaviour might be that the system has banded, and that the position of the interface between bands does

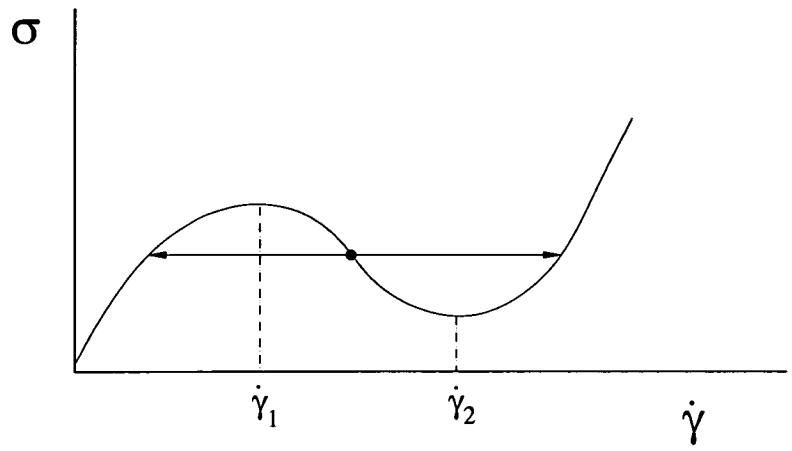

Figure 2.6: The flow curve of an extremely shear thinning material. The portion of the curve with negative slope is unstable, and so this is not the flow curve which is measured. Rather, an applied shear rate $\dot{\gamma}_1 < \dot{\gamma} < \dot{\gamma}_2$ causes the system to 'shear–band': one way in which this can occur (illustrated by the arrows) is for the system to split into states on the stable part of the flowcurve which have equal shear stresses, but differing shear rates.

not reach a steady state. An alternative is that the temporal oscillations could occur without spatial inhomogeneities: this possibility has been investigated in some simple shear thickening models [61, 62, 63]. Fluidity models [54, 64], in which the relaxation time (of a Maxwell model) evolves in time according to some specified dynamics, might offer another avenue of study. These approaches are in keeping with the idea that systems displaying such oscillations must have some relevant timescale which is much longer than the others in the system (an example of such a long relaxation timescale might be the time to equilibrate the distribution of chain lengths in wormlike micelles). The study of this subject is in its infancy, but promises to be of much interest [65, 66].

Chapter 3

The Glass Transition

We begin this chapter with a rather rough definition of the glass transition. This will be followed by an introduction to the way in which we describe the microscopic dynamics of the liquid state, since this is central to descriptions of the glass transition. We shall then discuss the glass transition in more depth. The chapter concludes with a discussion of some recent ideas regarding links between the glass transition and some other (seemingly quite different) physical situations.

Before we begin however, the reader should be aware that this chapter is in no way a complete description of the subject. For a more complete introduction to the physics of glasses, the reader is directed to other sources: Refs. [1, 67, 68, 69] provide useful starting points. In particular, we shall say nothing of thermodynamic aspects of the glass transition. The thermodynamic viewpoint is that there is, lurking beneath experimental obserations, a thermodynamic singularity of some kind, perhaps a second-order phase transition to a thermodynamic glass state. Although interesting, this viewpoint is not particularly relevant to the current work, and so we do not go into any detail.

3.1 A working definition

As a liquid is cooled, typically one expects that, at some temperature, the material undergoes a first order phase transition into a crystalline solid state. However, crystallisation takes time, and

so it is often possible to *supercool* a liquid without undergoing such a phase transition[1]. In this situation, we may continue cooling without the equilibrium transition intervening. Upon doing so, a wide range of liquids are observed to become more and more viscous as they become colder. This effect becomes considerably more pronounced as the temperature is decreased: the (zero-shear) viscosity may increase through several orders of magnitude upon a relatively modest alteration of temperature. At some point, the material barely flows under a modest stress (*eg*, that provided by gravity), if indeed it flows at all. The material now appears more like a solid than it does a liquid. However, its microscopic *structure* is disordered, like that of the higher temperature (unambiguously liquid) state [70] (we provide a quantitative measure of structure in Sec. 3.2 below). We call this low–temperature state the *glass*.

This is obviously rather imprecise: how viscous does the material need to be for it to be classed as a glass rather than a liquid? This can be quantified by choosing an arbitary value of the zero–shear viscosity at which one declares the material to be a glass: a typical value is of the order $10^{12} Pas$. Making such a declaration may be of practical use, but is not of much help in pinning down the nature of the transition.

Colloids

The above describes, crudely, the glass transition in a wide range of liquids. However in colloidal systems, which are of prime importance in this thesis, the rôle of temperature is, to a variable extent, reduced. Consider a system of hard spheres, for which there are no direct interactions between particles, except for an infinite repulsion upon contact. In this case, there is no potential energy scale with which to compare the thermal energy, and so the temperature is irrelevant (beyond setting a timescale, via the typical velocity of a particle with kinetic energy $\sim kT$). In this case, the glass transition (as well as equilibrium phase behaviour) is governed solely by the density of the system: beyond a volume fraction $\phi \approx 0.58$, the system appears to be in a glassy state [71].

Interactions in colloidal systems are often represented by hard-core repulsion, either with or without some additional finite potential at larger separations. If the additional potential is

[1] But note that the phenomena described here need not occur at temperatures below the melting point [68]. Despite this, the terminology of 'supercooled liquids' is invariably used.

negligible, then the physics is controlled solely by the volume fraction, whilst if it is non-negligible, the temperature plays a part. The above discussion regarding the viscosity of the system upon altering the temperature also holds, appropriately altered, in the concentration dependent case.

3.2 Liquid state dynamics

In order to improve upon the rough definition given above, we need to provide an introduction to the microscopic dynamics of the liquid state, as this subject is intimately related to the glass transition. For a more complete introduction to this subject, see a suitable monograph such as that by Hansen and McDonald [72]. Alternatively, for a specific account of the dynamics of colloidal suspensions, see [73].

3.2.1 Microscopic density fields

We begin by defining the microscopic number density at position $\mathbf{r}$ and time t as

$$\rho(\mathbf{r},t) = \sum_i \delta(\mathbf{r} - \mathbf{r}_i), \tag{3.1}$$

where the sum is over all particles in the system, and $\mathbf{r}_i$ is the position of particle i (with a suppressed time argument). We can also introduce microscopic density fields for quantities such as the current density

$$\mathbf{j}(\mathbf{r},t) = \sum_i \mathbf{v}_i \delta(\mathbf{r} - \mathbf{r}_i), \tag{3.2}$$

where $\mathbf{v}_i$ is the velocity of particle i. We can decompose such densities into Fourier components. The Fourier transformed number density is

$$\rho(\mathbf{q},t) = \sum_i \mathrm{e}^{-i\mathbf{q}\cdot\mathbf{r}_i(t)}, \tag{3.3}$$

and the transformed current is

$$\mathbf{j}(\mathbf{q},t) = \sum_i \mathbf{v}_i \mathrm{e}^{-i\mathbf{q}\cdot\mathbf{r}_i(t)}. \tag{3.4}$$

These quantities are referred to as the density and current fluctuations at wavevector $\mathbf{q}$ and time t. Such fluctuations will appear frequently within various *correlation functions*, which are now introduced.

3.2.2 Correlation functions

Consider two (often complex) variables A and B which are useful in the description of a many–body system. Possible examples include the number and current densities at given point in a fluid, and the magnetisation at some point in a spin system. From these quantities we form a correlation function (or *correlator*)

$$\phi_{AB}(t,t') = \langle A(t+t')B^*(t)\rangle, \tag{3.5}$$

where the angled brackets represent an equilibrium statistical average. This quantity tells us how strongly the value of the variable A at time $t+t'$ is correlated with the value of B at time t. If A and B are the same variable then ϕ is an *autocorrelator*. If the two quantities are measured at the same time (*ie*, $t' = 0$), ϕ is an *equal–time correlator*. Correlation functions between quantities measured at different times are often referred to as *time correlations functions*. In the main, correlations decrease with t': this is intuitively sensible. For example, consider the velocity autocorrelator of a chosen colloidal particle. If it has a certain velocity at a given time, then a sufficiently short time later it will have a similar velocity. In contrast, a few days later, the velocity will be completely uncorrelated from the initial value. The time on which correlation becomes lost provides a measure of typical relaxation times.

In many situations, a many–body system will have time translational invarience (TTI) and the origin of the time t is immaterial. In such cases, time correlation functions have a single time argument and equal–time correlators are time–independent. In some situations, discussed in Sec. 3.4, this is not the case.

3.2.3 Density correlators

Taking the equal–time autocorrelator of density fluctuations (divided by the total number of particles in the system) gives the *static structure factor*

$$S(\mathbf{q}) = \frac{1}{N}\langle\rho(\mathbf{q},t)\rho(-\mathbf{q},t)\rangle. \tag{3.6}$$

Here, by ascribing $S(q)$ no time–dependence, we have assumed TTI: if this is not applicable, the thermal average may vary in time. This quantity provides a description of the time-averaged structure in a liquid and is essentially the Fourier transform of the well-known pair distribution function $g(\mathbf{r})$ [72].

We can also calculate time correlations of density fluctuations: these are expressed by

$$\phi_{\mathbf{q}}(t) = \frac{1}{NS(\mathbf{q})}\langle\rho(\mathbf{q},t)\rho(-\mathbf{q},0)\rangle \tag{3.7}$$

which is normalised such that $\phi_{\mathbf{q}}(0) = 1$. We have again assumed TTI. This quantity is the *normalised intermediate scattering function*, but is known loosely as a *density correlator*. It can be measured in radiation scattering experiments, as can $S(\mathbf{q})$ [73].

This quantity describes the correlation between the density fluctuation at wavevector $\mathbf{q}$ with itself at a later time. In order to get a feel for what this means, consider a small region of volume $v \sim l^3$ within a bulk fluid. At any instant in time, the density in this region will be the mean number density in the system, plus some temporal fluctuation about this mean due to thermal motion. The Fourier decomposition of this fluctuation will be dominated by modes with $|\mathbf{q}| \sim |\mathbf{q}^*| \equiv 2\pi/l$, and therefore its decay is largely encompassed by the decay of fluctuations at these wavevectors. This is essentially the information contained within the density correlator $\phi_{\mathbf{q}^*}(t)$. So, in short, $\phi_{\mathbf{q}}(t)$ describes the relaxation of fluctuations on lengthscales $l \sim 2\pi/q$.

An example calculation: density correlators in dilute systems

In order to make things more concrete, we perform a simple calculation of the density correlator in a dilute colloidal system. For the sake of simplicity, we consider the *coarse grained local number density*, denoted $n(\mathbf{r},t)$. This quantity is not the microscopic density used earlier, as

it does not resolve individual particles: rather it is the number density familiar from classical Navier-Stokes fluid mechanics. However, at sufficiently small wavevectors, the two coincide.

In a dilute colloidal system, interactions are negligible, and the density obeys a simple diffusion equation [2]:

$$\frac{\partial n(\mathbf{r},t)}{\partial t} = D\nabla^2 n(\mathbf{r},t), \tag{3.8}$$

where the constant is the Stokes-Einstein diffusion coefficient, $D = \frac{kT}{6\pi\eta a}$ with η the solvent shear viscosity and a the particle radius. Fourier transforming and solving leads to $n(\mathbf{q},t) = n(\mathbf{q},0)\mathrm{e}^{-q^2Dt}$. Forming the density correlator, we have that $\phi_{\mathbf{q}}(t) = \mathrm{e}^{-q^2Dt}$. The system 'loses memory' of density fluctuations at wavevector $\mathbf{q}$ on a timescale $\tau \sim 1/Dq^2$. With the general meaning of the density correlators given a little earlier, this tells us that fluctuations of size l take a time $\tau \sim l^2/D$ to decay. The fact that longer wavelength fluctuations take longer to decay is a consequence of particle conservation: in order to relax a fluctuation, particles must be diffusively transported over distances of order the fluctuation size.

Density correlators in concentrated systems

This exponential form has been verified in dilute colloids [74]. In more concentrated colloids however, interactions between the particles cause this simple argument to fail: the dynamics are not simply diffusive [73], and the density correlators obtain a complicated dependence upon both $\mathbf{q}$ and t. A typical density correlator in a dense liquid is shown in Fig. 3.1. It consists of an early time relaxation from unity (known as the β-relaxation), followed by a later relaxation (the α-relaxation) towards zero. In a dense system, the time taken for the structural relaxation – that is, the time for the system to relax a fluctuation – can become much longer than the 'bare' relaxation time found in dilute systems. Physically, the two relaxation processes can be heuristically understood within the *cage picture* of a dense liquid, schematically illustrated in Fig. 3.2. The β relaxation corresponds to a particle moving within a cage formed by its neighbours, whilst the α relaxation corresponds to escape from the cage. In contrast to the situation in dilute colloids, the calculation of a density correlator in a dense suspension is a difficult task: this is the subject of Chapter 4.

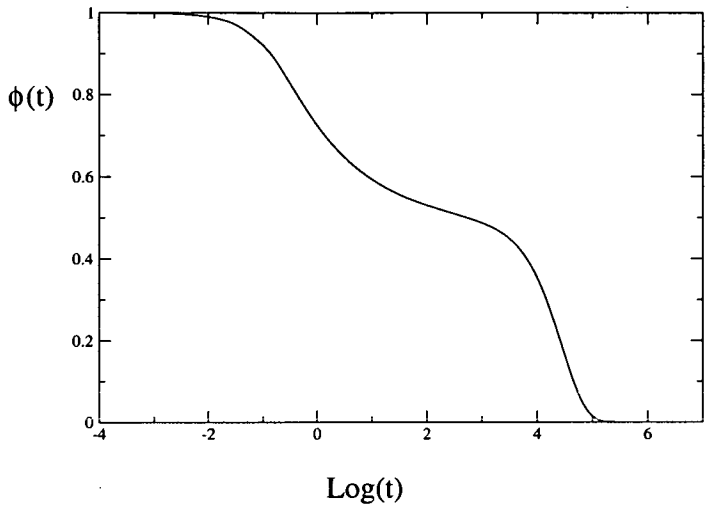

Figure 3.1: A typical density correlator in a dense liquid: the two–stage relaxation process is evident. The time has been scaled by a characteristic microscopic timescale.

3.3 The nature of the glass transition

Having described it in rough terms, we now begin to explore more precise descriptions of the glass transition.

3.3.1 The idealised glass transition

As mentioned above, close to the glass transition the zero–shear viscosity can increase through several orders of magnitude due to a modest alteration in temperature or volume fraction. This is illustrated in Fig. 3.3, which shows the zero–shear viscosity vs. volume fraction for a hard sphere colloid system. This suggests there might in fact be a divergence of the viscosity at some point, thus identifying the transition in a concrete manner: *viz.* at the transition, the viscosity diverges.

Note that it is important that we specify the zero–shear viscosity if we are to define the glass transition in this manner. This is because a material whose zero– shear viscosity is divergent may have a finite viscosity at nonzero shear rates (Sec. 2.3.2). Therefore, an experiment

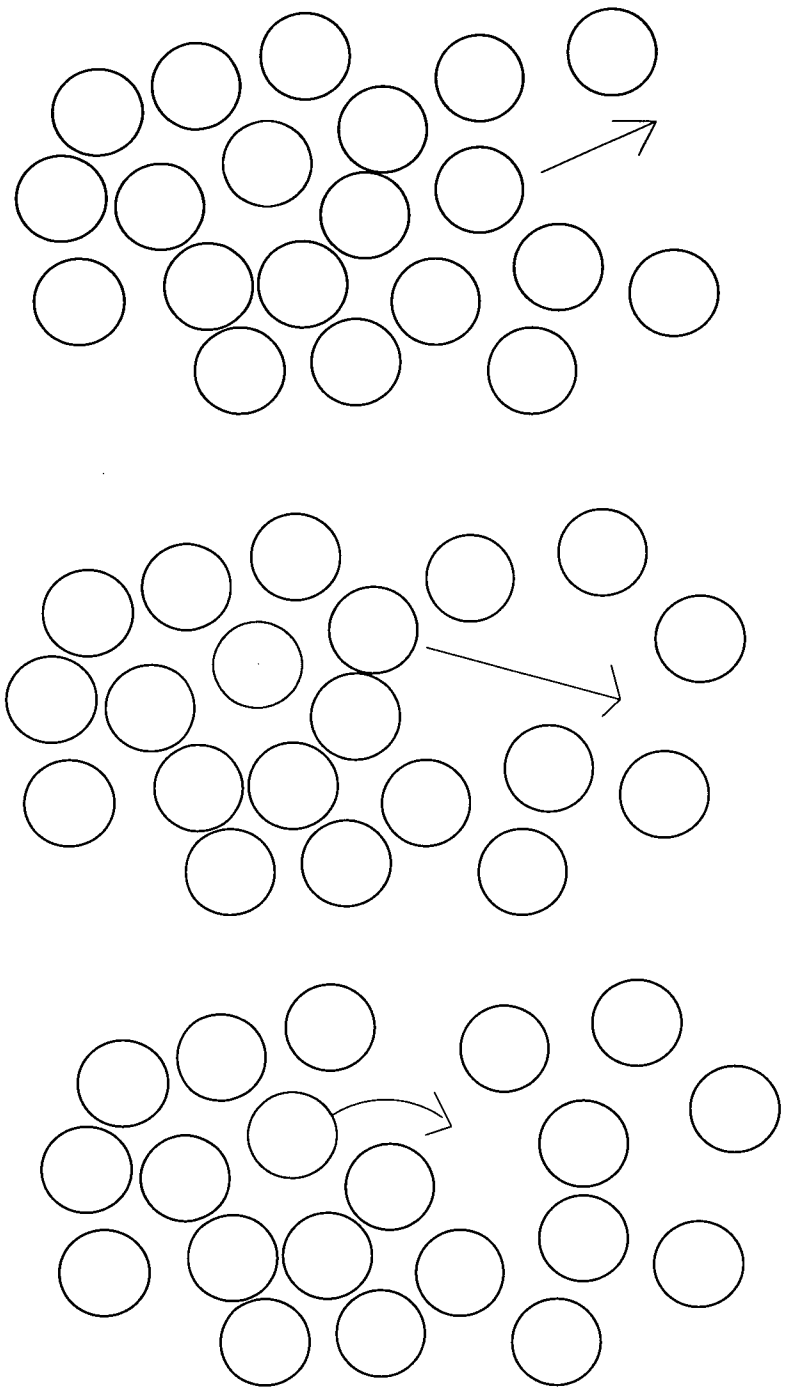

Figure 3.2: The 'cage picture' of a dense liquid. Consider any particle in a dense liquid, such as the dark shaded one shown here. The chosen particle is surrounded by a 'cage' of its neighbours, which tend to hinder its motion. The chosen particle itself plays a part in the caging of neighbouring particles. The β relaxation corresponds to a particle moving within its cage, whilst the α relaxation is related to a particle escaping from its cage, due to the cooperative motion of many particles. For example, here our shaded particle can only escape from the cage if, *eg*, the adjacent shaded particle moves out of its way. In turn, this particle can only move if one of *its* adjacent particles can move...

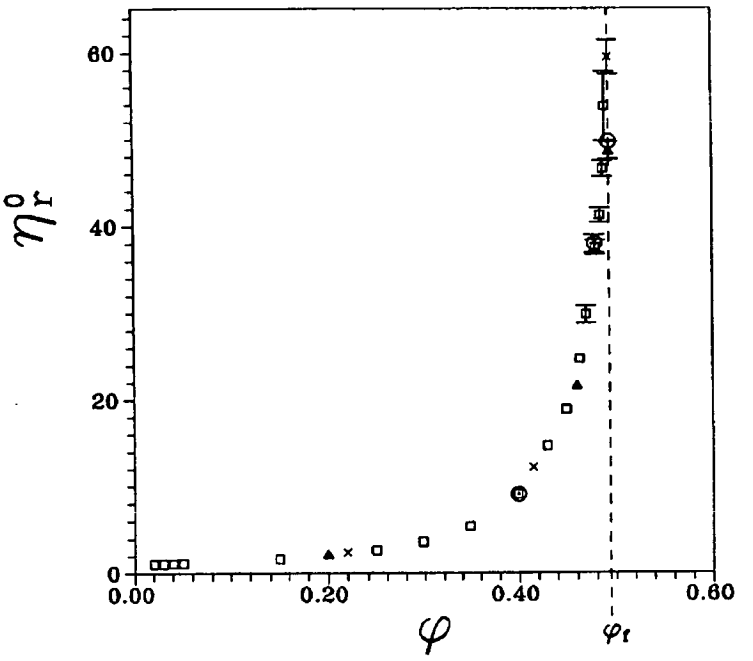

Figure 3.3: The relative viscosity ($\eta_r \equiv \eta/\eta_s$, with η_s the solvent viscosity) as a function of volume fraction for a colloidal hard sphere system. The freezing concentration of hard spheres is shown as the dashed vertical line. Data is shown for particles of three different radii: $301nm$[□]and[○]; $500nm$[×]; and $240nm$[▲]. The vertical dashed line represents the concentration $\varphi_f = 0.494$ at which, in equilibrium, crystals first appear. Recall from Ch. 2 that viscosity measurements at concentrations above this point are carried out on a metastable fluid, rather than on the equilibrium state. From [18].

which aims to ascertain whether or not a sample is a glass or a liquid, by measuring the viscosity, must be performed at very small (in principle, infinitesimal) shear rate, and is thus a formidable task. This difficulty suggests that we search for a description of the glass transition which does not involve external forcing. This can be done by consideration of a liquid's internal dynamics: measurements of the dynamics and viscometry of systems approaching a glass transition shows that as the viscosity of a liquid increases, so does the structural relaxation timescale [17]. As with the variation in viscosity, the increase in relaxation time with the relevant control parameter can become very pronounced, perhaps suggesting a divergence. Thus another possible definition of the glass transition may be proposed in these terms: *viz.*, in a glass, density correlators do not decay to zero in any finite time. Such a transition implies that the microscopic structure of the material is fixed when it is quenched into the glassy state: particles are unable to escape from their cage of nearest neighbours. The loss of diffusion over long distances within the material means that it is unable to sample phase space adequately, and is thus unable to reach the equilibrium state: it is said to be *nonergodic*.

The divergence of the structural relaxation timescale and the zero–shear viscosity may coincide [17, 73, 75]. The transition defined via the divergence of either of these quantities is referred to as an *idealised glass transition*. This is in keeping with our common experience that a glass has the character of a solid (although recall from Ch. 2 that a divergent viscosity does not necessarily imply a finite elastic modulus), and is therefore an appealingly simple idea.

So, does the idea of a divergence at the glass transition stand up to scrutiny? At least in molecular glasses, the answer appears to be that it does not [1]. However, for colloidal systems, in which we are interested, an ideal glass transition may well occur: light scattering experiments on hard-sphere systems show an apparent arrest of the structural relaxation at a volume fraction $\phi \approx 0.58$ [71, 76, 77, 78]. Measurements of the zero–shear viscosity in these systems suggest the existence of a divergence at a similar concentration (see Fig. 3.3) [18, 79], although other experiments suggest a divergence closer to the *random close packing* limit [19, 21, 22]. (Random close packing is the supposed maximum volume fraction possible for an non–crystalline packing of spheres: $\phi_{RCP} \approx 0.64$.) These two groups of experiments were performed using different experimental systems, that are nontheless both supposed to represent a hard–sphere suspension. As mentioned in Ch. 2, there are various possible reasons for the discrepancy [18].

3.3.2 Relaxation and experimental timescales

There is an obvious difficulty in verifying the existence of an idealised glass transition. Consider measuring $\phi_{\mathbf{q}}(t)$ in a dense colloidal sample, and noting that the correlation functions do not decay on some timescale (defined by the patience of the experimentalist!) long compared with the bare dynamics of the system: one concludes that the system is in a glassy state. But a more patient experimentalist might wait for a little longer, and detect a relaxation at some point after his colleague has departed. So one experimentalist claims the system is a glass, the other claims it is liquid. This example points towards the fact that it is not possible to find, experimentally, that a timescale has actually diverged. (Of course, one can infer a divergence by fitting a plot of relaxation time *vs.* concentration to a suitable functional form.) Rather, one can say only that the relaxation timescale exceeds that of the experiment. This then, allows us to define the glass transition in another manner; we can say that a system is, or is not, a glass on the longest timescale probed by the experiment. From this point of view, there is no sharp transition, rather there is a continuum of behaviour dependent on the experimental timescales. This is related to our discussion of the time–dependent modulus $G(t)$ in Ch. 2: a viscoelastic material appears solidlike if one probes it on sufficiently short timescales, whilst it is liquidlike on longer timescales. In an ideal glass state, $G(t)$ will not relax to zero in any finite time.

There are further consequences if the experimental timescale is defined by the rate at which a control parameter is altered. For example, consider measuring the properties of a liquid as it is cooled. Doing so, one notices that (for example) the specific heat has a notable change in functional form at some temperature [69]. However, repeat the experiment at a lower cooling rate (thus probing longer timescales) and it is found that the liquidlike behaviour persists for lower temperatures. This is because the point at which the system 'falls out of equilibrium' and behaves in a glassy manner depends upon the timescale that we probe. Again, the point at which glassy behaviour begins depends upon the timescale probed, but it also introduces *history dependent behaviour*: the material's behaviour now depends not only upon its temperature, but also upon the manner in which that temperature was reached. The phenomenon of *aging* is a particularly interesting example of history dependent behaviour, and will be discussed in the following section.

3.4 Aging

Under 'normal' conditions (including, but not restricted to, thermal equilibrium), materials are time translationally invarient (TTI): measured quantities do not depend upon the time at which the experiment is performed. However, in other situations, this is no longer true: in both conventional glasses and the soft glassy materials discussed in Sec. 2.3.2, the dynamics and mechanical properties change in time. This is known as *aging*.

In order to study aging, one must be able to obtain a reproducible starting state, from which the evolution of the system can be monitored: the production of such a state is referred to as *sample preparation*. We denote the time at which the sample is prepared as t_0. The experiment begins at a time $t_0 + t_w$, where t_w is the *waiting time*, defining the *age* of the sample. In many materials, as we have discussed, temperature plays an important rôle: in these systems, sample preparation consists of a quench from some high temperature to a low temperature glassy state. In hard sphere colloids, the obvious analogue of this would be a concentration quench, but this is not practical. Rather, one makes use of the fact that strong shearing reverses aging - a sample, prepared at some point in the past, may be 'rejuvenated' by shearing at a high shear rate: it behaves as if it was created at the time the shearing is ceased, rather than at the true (earlier) preparation time [80]. Thus, t_0 may be chosen as the time at which an initial strong shearing is stopped.

With the ability to create a reproducible starting point, one can perform the relevant experiments upon the system, after the desired waiting time. The internal dynamics may be studied by radiation scattering [80, 81], in which case one finds that the relaxation of correlations becomes slower as the waiting time is increased. Rheological measurements [81] show that the systems also tends to become 'stiffer' with increasing waiting time – hardly surprising, given the association between slow dynamics and rheological response discussed in Sec. 3.3.1. Relaxation times typically go as a positive power of the waiting time: $\tau \sim t_w^{\mu}$. The exponent μ is system dependent, typically less than unity. Note that such aging scenarios suggest that, in the limit of long waiting times, relaxation times grow without bound, in keeping with the idea of the ideal glass transition.

Both the SGR [11, 23, 28], and the fluidity [64] approaches mentioned in Ch. 2 have been

used to study aging theoretically. Of particular interest to us is the rejuventing effect of *flow* upon soft matter: the relaxation dynamics tends to speed up in a flowing system [82], a point to which we shall return in Chapter 6. This effect is present in both the fluidity model and the SGR model. The resulting competition between glassy dynamics and flow is key to much of the interesting rheology of soft glassy materials. Refs. [9, 83] provide good starting points for the reader interested in the competition between glassy dynamics and flow–induced rejuvenation in soft matter.

Looking slightly further afield, similar physics appears outwith soft matter: in driven spin–glass models [84], there is an interplay between the intrinsic dynamics and external driving which is reminiscent of that between shearing and glassiness in sheared glasses (although its precise nature may differ between different systems: compare the 'shear thinning exponents' in the spin–glass model [84] with those of [29] which models sheared colloids).

We shall say no more here on the subject of aging – the work presented in this thesis is unsuitable for the description of aging effects, and so it is not directly relevant.

3.5 Jamming and the glass transition

In 1998, Cates and co-workers [85] discussed the notion of *jamming* under external stress in dense suspensions and granular materials. We have seen in Ch. 2 that colloidal suspensions can show discontinuous shear thickening, whereby the material shows an abrupt change in mechanical response at some applied stress/shear rate. Simulations investigating this phenomenon, performed in the absence of Brownian motion [36, 37], suggested a catastrophic jamming up of the system, possibly leading to a static, jammed state. Motivated by these simulations, Cates *et al* considered the mechanical properties of a jammed system of particles. They argued that idealised jammed materials – that is, materials whose solidity arises as the result of some applied stress – have unique mechanical properties. In particular, such materials can statically support a macroscopic stress in one direction (the direction of the load which resulted in the solidity in the first place), whilst small loads in a different direction result in the catastrophic failure of the material. The reason for this highly nonlinear response is that the structure of

the material adapts to support an initially imposed stress. If a different stress is then applied, the material's structure is completely incapable of supporting this structure, leading to failure. (Note however that, in time, the material may be able to adapt to support this new load, causing it to re-jam.) This property was described as *fragility*. For an example of such a response, consider a simple bucket of sand. Upon filling a bucket with sand, the material adopts a structure which allows it to support the weight of the higher grains. If the bucket is then tilted, altering the direction of gravity in the reference frame of the bucket, the sand then flows like a liquid, since its structure is not 'designed' to deal with the new stress field. However, stand on a bucket of sand and it will support your weight – not a property of a bucket of water.

Liu and Nagel [86] then suggested that the notion of jammed states could be generalised. They conjectured that the jamming transition discussed above, and the glass transition, are two specific limits of a generic nonequilibrium fluid–solid transition. Other examples might be gelation in colloid-polymer mixtures [87] [2], or the solidification as the shear stress on a flowing material is decreased below its yield stress [88].

Whilst Liu and Nagel referred quite generally to this postulated class of transitions as 'jamming transitions', we will reserve this name for transitions which occur under external forcing, à la Cates *et al.* Of course, in a sense the conventional glass transition occurs under external forcing, since there is an externally controlled isotropic pressure. Therefore, one should be slightly more specific: we will regard transitions as *jamming* transitions if they occur due to an applied deviatoric stress, in keeping with the spirit of Ref. [85]. The question then, is whether jamming transitions, gelation and the glass transition (and others) can be shown to have a common description. An obvious analogy may be made with equilibrium phase transitions, for which seemingly very different phenomena can be shown to display universal behaviour.

Liu and Nagel's conjecture has been the subject of much interest. Trappe and co–workers [88] studied fluid–solid transitions in an attractive colloidal system. By increasing the density or attraction strength, or by lowering an applied stress, they induced transitions from a fluid to a solid. They found that signatures of a solid state, such as the appearance of an elastic

[2] Gelation is an attraction mediated transition from an ergodic fluid to a nonergodic low-density gel structure. Similiarly to the glass transition, this is a many-body phenomenon: the bonds which form between particles are not so large that bonds are irreversible, but the fact that there are many bonds causes structural arrest.

modulus, appeared with similar functional forms regardless of the way in which the transition was induced. Other work [87] examines the link between the glass transition and gelation using the mode–coupling theory described in Ch. 4.

3.5.1 Colloidal jamming

In this thesis, we are primarily interested in the link between jamming (as defined above) and the glass transition. In order to elucidate the link between jamming, which is most easily observed in granulars, and the glass transition which appears in microscopic thermal systems, the most profitable system to study would seem to be colloids. These combine the particulate nature of powders and grains with the thermal properties of atomic and molecular systems. By varying the size of the particles in a suspension, from radii $a \sim 1nm \rightarrow 100\mu m$, one can span the gap between conventional thermodynamic systems and granular materials. By doing so, one might hope to answer questions such as whether materials may jam in the presence of significant Brownian motion: from the viewpoint of Liu and Nagel, such a jammed state would resemble a glass, albeit one which is anisotropic. An alternative would be that sufficient Brownian motion precludes the formation of a static jammed state, possibly resulting in the discontinuous thickening observed in dense colloids.

Bertrand and coworkers have observed jamming in suspensions of irregular particles (mean radius $a \approx 3\mu m$) [42]. They found that, whilst moderately concentrated samples shear thickened, denser samples were transformed from a liquid "into a persisting paste by moderate shearing". We shall discuss some interpretations of these experiments in Ch. 5. For now we note that such behaviour seems unlikely to be explained by hydrodynamic explanations for shear thickening (see Sec. 2.3.3), since in the resulting solid state there is no large scale flow. (One could conceive of a situation in which interparticle gaps close with an ever–decreasing rate, maintaining a constant hydrodynamic stress, but this seems somewhat far–fetched.)

Experiments have also been performed upon suspensions of smaller particles ($a = 300 - -1000nm$) [89] in narrowing channel flow. These particles will be affected by Brownian motion to a greater extent, and so one might imagine that the tendency to jam will be decreased. Indeed, no transition from a flowing to a statically jammed state is found in these experiments.

However transient jamming is observed – the flow noticeably slows, then speeds up in a stick–slip like motion. This work seems related to the deformation of geological structures [90].

These intriguing studies suggest links between the flows of colloids, and those in granular materials. The question of whether jamming, such as that found by Bertrand *et al*, can be treated as a generalisation of the glass transition is a major theme of the work presented in this thesis. We return to interpretations of these experiments in Ch. 5. In the following chapter, we provide a technical introduction to a succesful theory of the glass transition, the mode–coupling theory. Firstly though, we briefly discuss an industrial situation in which jamming appears particularly relevant.

Granulation

Jamming may have some bearing upon the industrial process of *high shear granulation*. This refers to the formation of macroscopic granules from the mixture of fine powder with a fluid, known as the *binder*. By mixing the two together (in apparatus not unlike an oversized food blender) one creates a pasty mixture, out of which individual granules form.

It seems that the physics of jamming is relevant to this process: suspensions used in some granulation processes can show jamming behaviour – suspensions of zeolite (used as a water softener in washing powder) particles (radius $a \approx 1\mu m$) within a binder exhibit similar bistability to that observed by Bertrand [91]. Squashing the material between two plates may transform fluid samples into a dry, brittle solid. Upon vibration, the material is returned to its original state.

Since these materials are capable of such jamming, it is tempting to associate the formation of granules from a strongly sheared paste with the fracture observed in strongly sheared dense colloids: *viz*, fracture, as a result of jamming, results in solid lumps of material, *ie*, granules. Once the stress is removed, the granules might either remain in the solid, jammed state or they could relax back into a fluid state (in Ch. 5 we discuss some criteria for the jammed state to persist). This suggests a scenario in which the granules can be either in a wet, fluid state or in a dry jammed state. As granules may grow via collision and coalesence [92], the difference may be crucial. If colliding granules are in a jammed state, they will not coalesce. In contrast if

one of them is in a fluid state, it can melt its jammed neighbour, and then coalesce with it [91]. Therefore, the ability to understand, and therefore control jamming might have an important part to play in improving granulation processes. We discuss ideas relevant to this process in Ch. 5.

Chapter 4

The Mode Coupling Theory of the Glass Transition

This chapter introduces the reader to the mode-coupling theory of the glass transition (MCT). We begin by defining the relevant quantities and introducing the equations which govern these quantities. We then study these (initially rather intractable) equations, allowing physical insight to suggest ways in which to simplify them.

4.1 Dynamical variables and correlations

We define the state of a classical dynamical system of N particles in terms of a phase space vector

$$\mathbf{\Gamma} = (q_1, q_2, \ldots q_{3N}, p_1, p_2, \ldots p_{3N}). \tag{4.1}$$

Here the $\{q_i\}$ and the $\{p_i\}$ are the usual $3N$ coordinates and $3N$ momenta required in a Hamiltonian description [93]. Thus any dynamical variable A_i is specified by $\mathbf{\Gamma}$: $A_i = A_i(\mathbf{\Gamma})$.

The evolution of the system is governed by

$$\dot{\mathbf{\Gamma}} = \{\mathbf{\Gamma}, H\}, \tag{4.2}$$

where the braces $\{,\}$ indicate a Poisson bracket, $\dot{\mathbf{\Gamma}} = \frac{d\mathbf{\Gamma}}{dt}$, and H is the Hamiltonian of the system. (More generally, a quantity u with explicit time dependence evolves according to $\dot{u} = \{u, H\} + \frac{\partial u}{\partial t}$.)

We now define the *Liouville operator* $i\mathcal{L} = \{\ , H\}$, which results in

$$\dot{\mathbf{\Gamma}} = i\mathcal{L}\mathbf{\Gamma}, \tag{4.3}$$

which is formally solved by

$$\mathbf{\Gamma}(t) = \mathrm{e}^{i\mathcal{L}t}\mathbf{\Gamma}(0). \tag{4.4}$$

Now, the dynamical properties $\{A\}$ are a function (solely) of $\mathbf{\Gamma}$ and so evolve in time in a similar way: the value of a dynamical variable A_i at time t is

$$A_i(t) = \mathrm{e}^{i\mathcal{L}t}A_i. \tag{4.5}$$

The absence of a time argument signals a quantity evaluated at $t = 0$.

It will help us to regard the dynamical variables A_i as vectors in a Hilbert space: their complex conjugates A_i^* play the role of the dual vectors. The scalar product $(A_i(t), A_j^*(t'))$ between two 'vectors' is defined by means of a correlation function: $(A_i(t), A_j^*(t')) \equiv \langle A_i(t)A_j^*(t')\rangle$ where the angled brackets denote an average over the phase space probability distribution. Thus two uncorrelated variables are 'orthogonal'. Recall from Sec. 3.2.2 that the correlation function between two variables A_i and A_j is defined as $\phi_{ij}(t) \equiv \langle A_i(t)A_j^*\rangle$, where we have assumed TTI. In terms of the Hilbert space notation, the correlation is the scalar product $\phi_{ij} \equiv (A_i(t), A_j^*)$.

We now define a *projection operator* $\mathcal{P}$, which projects an arbitary Hilbert space vector B onto the subspace spanned by a chosen set of variables $\{A_i\}$. We define

$$\mathcal{P}B \equiv (B, \mathbf{A}^\dagger) \cdot \underline{\underline{\chi}}^{-1} \cdot \mathbf{A} \tag{4.6}$$

where $\mathbf{A}$ is a column vector containing the elements of $\{A_i\}$, $\mathbf{A}^\dagger$ is its Hermitian conjugate, and the matrix $\underline{\underline{\chi}} = (\mathbf{A}, \mathbf{A}^\dagger)$. We also define $\mathcal{Q} \equiv 1 - \mathcal{P}$ which projects onto the subspace orthogonal to that spanned by the $\{A_i\}$. In matrix notation, the correlation functions $\phi_{ij}(t)$ are

the elements of the *correlation matrix* $\underline{\underline{\Phi}}(t) = (\mathbf{A}(t), \mathbf{A}^\dagger)$. Via formalism based on these projection operators, one can derive formal equations of motion for the evolution of the $\{A_i\}$, and for the correlations between them: these equations are derived in Appendix A. The evolution of the dynamical variables is governed by a *generalised Langevin equation*

$$\dot{\mathbf{A}} = i\underline{\underline{\Omega}} \cdot \mathbf{A}(t) + \mathbf{F}(t) - \int_0^t \mathrm{d}t' \underline{\underline{\mathbf{M}}}(t') \cdot \mathbf{A}(t-t'). \tag{4.7}$$

The *frequency matrix* $\underline{\underline{\Omega}}$ is defined by $i\underline{\underline{\Omega}} \equiv (i\mathcal{L}\mathbf{A}, \mathbf{A}^\dagger) \cdot \underline{\underline{\chi}}^{-1}$; $\mathbf{F}(t) \equiv \mathrm{e}^{i\mathcal{Q}\mathcal{L}t} \mathcal{Q} i\mathcal{L}\mathbf{A}$ is the *random force*; and $\underline{\underline{\mathbf{M}}}(t) \equiv (\mathbf{F}, \mathrm{e}^{-i\mathcal{Q}\mathcal{L}t}\mathbf{F}^\dagger) \cdot \underline{\underline{\chi}}^{-1}$ is the *matrix of memory functions*. The memory functions are so called since they parameterise the way in which the system's state at a given time is affected by past states – *ie*, they describe memory effects in the system. A similar equation to Eq. 4.7 governs the correlation functions (see Appendix A for a derivation)

$$\dot{\underline{\underline{\Phi}}}(t) = i\underline{\underline{\Omega}} \cdot \underline{\underline{\Phi}} - \int_0^t \mathrm{d}t' \underline{\underline{\mathbf{M}}}(t') \cdot \underline{\underline{\Phi}}(t-t'). \tag{4.8}$$

In this equation, the random force term does not appear because it is uncorrelated with the slow variables $\{A_i\}$. In frequency space, this becomes

$$(z\underline{\underline{\mathbf{I}}} + \underline{\underline{\Omega}} + \tilde{\underline{\underline{\mathbf{M}}}}(z)) \cdot \tilde{\underline{\underline{\Phi}}}(z) + \underline{\underline{\chi}} = 0, \tag{4.9}$$

where the Laplace transform of an arbitary function $f(t)$ is

$$L[f(t)] \equiv \tilde{f}(z) \equiv i \int_0^\infty \mathrm{d}t\, \mathrm{e}^{izt} f(t), \tag{4.10}$$

and $\underline{\underline{\mathbf{I}}}$ is the identity matrix.

These equations are simply formal restatements of Eq. 4.5. In order to profit from the formalism, for a given physical problem we must make a suitable choice of the set $\{A_i\}$: if we choose these variables such that they evolve on a slower timescale than all other variables in the problem, then the equations simplify considerably. A simple example of such a separation of timescales is the diffusion of a colloidal particle in a molecular solvent: in this problem, the position and momentum of the colloidal particle are, to a good approximation, constant on the timescale of the molecular motion. Therefore, they constitute a set of 'slow variables'.

If we can choose a set of variables in this way, all the variables orthogonal to the subspace spanned by $\{A_i\}$ are regarded as 'fast'. The fluctuating force $\mathbf{F}(t)$ resides in this fast subspace

and so arises from the quickly fluctuating variables. This is the sense in which it is a *random force* acting upon $\mathbf{A}$: it fluctuates quickly, even on timescales such that $\mathbf{A}$ is approximately constant – this is reminiscent of the random force acting upon a colloidal particle in a solvent. Therefore, correlations of $\mathbf{F}$ (that is, the elements of $\underline{\underline{\mathbf{M}}}$) should be short–lived on timescales relevant to the slow variables. If we assume a perfect separation of timescales (a Markovian approximation), we can take $\mathbf{F}$ to be δ–correlated in time. This reduces the integral over $\underline{\underline{\mathbf{M}}}$ in Eq. 4.7 to an instantaneous friction term, resulting in a form rather similar to the Langevin equation of Brownian motion [94].

For the Markovian assumption to be useful, we should ideally include within the set $\{A_i\}$ *all* slowly fluctuating variables – if we do not, the memory functions will have slowly varying components, and the Markovian assumption will fail. However, if we assume that the components of $\mathbf{A}$ are slow, products of slow modes $A_i A_j$ also seem likely to contain a slow component. This may not be catastrophic if the variables of interest do not couple strongly to these nonlinear variables. But, close to the glass transition (as well as close to phase transitions, the situation for which mode–coupling was originally developed) such nonlinear fluctuations *do* matter, and hence we must go beyond the Markovian approximation. The mode–coupling theory is a way in which one can include coupling to these nonlinear fluctuations.

4.2 Applying the formalism to supercooled liquids

We now apply the Zwanzig–Mori formalism to the study of supercooled liquids. We shall be interested in calculating density correlators since (Ch. 3) they are experimentally accessible, and show a characteristic change in the vicinity of the glass transition. They may also be regarded as slow, since they obey a local conservation law (this was illustrated in Sec. 3.2.3). Thus, one of our slow variables shall be the density fluctuations $\rho_{\mathbf{q}} = \sum_i \mathrm{e}^{-i\mathbf{q}\cdot\mathbf{r}_i}$.

These are coupled, through the equation of continuity, to the longitudinal current (density). The equation of continuity is $\frac{\partial \rho(\mathbf{r},t)}{\partial t} + \nabla \cdot \mathbf{j}(\mathbf{r},t) = 0$ which becomes, in Fourier space, $\dot{\rho}_{\mathbf{q}} = q j_{\mathbf{q}}$, where the longitudinal current is $j_{\mathbf{q}} = \hat{\mathbf{q}} \cdot \mathbf{j}_{\mathbf{q}}$. Because of this coupling, we include the longitudinal currents in our set of slow variables. In contrast, transverse currents are not coupled to density fluctuations and so we do not include them in the set.

With this choice of slow variables, we have

$$\mathbf{A} = \begin{pmatrix} \rho_{\mathbf{q}} \\ j_{\mathbf{q}} \end{pmatrix}. \tag{4.11}$$

We now evaluate the various matrices arising in Eq. 4.9 when it is applied to this situation. Many of the matrix elements will turn out to be zero (from symmetry considerations, variables of opposite parity under time–reversal are orthogonal, due to the fact that averages are invariant under time–reversal). The only nonzero elements of the static correlation matrix $\underline{\underline{\chi}}$ are the diagonal elements. These are given by the static correlation between density fluctuations $\langle \rho_{\mathbf{q}} \rho_{\mathbf{q}}^* \rangle = NS(\mathbf{q})$; and longitudinal currents $\langle j_{\mathbf{q}} j_{\mathbf{q}}^* \rangle = N\langle v_{\mathbf{q}}^2 \rangle = NkT/m$, where m is the particle mass. In the final equality, classical equipartition of energy has been used to write the mean square velocity in terms of the thermal energy. The *frequency matrix* $\underline{\underline{\Omega}}$ is also determined by static correlations. It contains only off–diagonal elements. The nonzero elements are $\Omega_{12} = q$ and $\Omega_{21} = qkT/mS(q)$.

The only nonzero memory function is the element M_{22}. This is, in the time domain, the random force correlator

$$M_{22}(t) \equiv M_{\mathbf{q}}(t) = \left(Qi\mathcal{L}j_{\mathbf{q}}, \mathrm{e}^{-Qi\mathcal{L}Qt}(Qi\mathcal{L}j_{\mathbf{q}})^* \right) \left(\frac{m}{NkT} \right). \tag{4.12}$$

The matrix equation for the correlations now becomes

$$\begin{pmatrix} z & q \\ \frac{kTq}{mS(q)} & z + \tilde{M}_{\mathbf{q}}(z) \end{pmatrix} \begin{pmatrix} \tilde{\phi}_{\rho\rho}(z) & \tilde{\phi}_{\rho j}(z) \\ \tilde{\phi}_{j\rho}(z) & \tilde{\phi}_{jj}(z) \end{pmatrix} = -N \begin{pmatrix} S(q) & 0 \\ 0 & kT/m \end{pmatrix} \tag{4.13}$$

where an obvious notation has been used to denote the elements of $\underline{\underline{\tilde{\Phi}}}$. Solving this simple matrix equation, we find that the density–density correlations obey

$$\tilde{\phi}_{\mathbf{q}}(z) \equiv \tilde{\phi}_{\rho\rho}(z)/NS(q) = \frac{-1}{z - \frac{\Omega_q^2}{z + \tilde{M}(z)}} \tag{4.14}$$

where $\Omega_{\mathbf{q}}^2 \equiv \frac{kTq^2}{mS(q)}$ and we have defined the correlator such that it is unity at $t = 0$. Expressed in the time domain, this equation becomes

$$\ddot{\phi}_{\mathbf{q}}(t) + \Omega_q^2 \phi_{\mathbf{q}}(t) + \int_0^t M_{\mathbf{q}}(t - t')\dot{\phi}_{\mathbf{q}}(t') = 0. \tag{4.15}$$

This equation is the basis for the mode–coupling description of the glass transition. It is solved, by approximating the random force correlator (or memory function) $M_{\mathbf{q}}(t)$ in a way which has became known as the mode–coupling approximation. We now discuss this approximation in the context of the glass transition.

4.3 The mode coupling approximation

The mode–coupling approximation reduces the memory function to a somewhat more tractable form, whilst attempting to account for the nonlinear coupling between variables ignored by the Markovian approximation. As we shall not require it in this thesis, we do not go through the mathematical derivation in detail, instead referring the interested reader to Refs. [95, 96]. However, the theoretical models which we shall discuss are extensions to 'schematic MCT models', which are themselves simplifications of the full theory. Therefore, we shall explain the basic procedure, employing physical insight where possible.

As discussed in the previous section, the fluctuating forces can aquire a slow component, even although they are orthogonal to the 'slow subspace', through nonlinear coupling between slow variables. This can result in their correlations (the memory function) decaying on timescales comparable to those of the slow variables, rather than the much faster decay assumed in the Markovian approach. In order to capture this slow decay, one approximates the fluctuating forces by their projections onto the simplest nonlinear variables – that between density pairs $\rho_{\mathbf{q}}\rho_{\mathbf{p}}$. These are the simplest variables which have a component orthogonal to the $\{A_i\}$, and which we expect to possess a slow component. Also, density fluctuations are coupled to the (longitudinal) currents, the fluctuations of which occur due to forces in the system. If we take these forces to arise from pair interactions, one might expect that fluctuations of density pairs are key to an understanding of fluctuations in currents, and therefore in the densities. By assuming that these couplings provide the main contribution to slow parts of the memory function, we allow the memory function to aquire a slow component, rather than (as in the Markovian approach) simply treating it as quickly decaying.

To make the approximation one defines a new projection operator $\mathcal{P}_2$, which projects onto all density pairs $\rho_{\mathbf{q}}\rho_{\mathbf{p}}$, and replaces the fluctuating forces F in the memory function by their

projections $\mathcal{P}_2 F$. This gives the memory function as $(\mathcal{P}_2 F, \mathrm{e}^{-i\mathcal{Q}\mathcal{L}\mathcal{Q}t}(\mathcal{P}_2 F)^*)$. In making this approximation, we lose the quickly decaying part of the memory function – referred to as the 'regular part'. We shall put this part back in later, although we shall not concern ourselves too much, as it is not particularly relevant to studies of the glass transition [95].

The next approximation consists of replacing the 'projected evolution operator' $\mathrm{e}^{-i\mathcal{Q}\mathcal{L}\mathcal{Q}t}$ with the standard evolution operator $\mathrm{e}^{-i\mathcal{L}t}$ within the memory function. This approximation allows F to aquire components parallel to $\{A_i\}$ as it evolves in time according to the classical equations of motion. Without this approximation, the evolution of F would be constrained such that it remained orthogonal to the $\{A_i\}$ – *ie*, $F(t)$ could never become correlated with these variables. One might make a rather hand–waving argument that the fluctuating force should be allowed to become correlated with the slow variables: we are interested in the approach to an arrested state, in which density fluctuations and currents are arrested. As these will determine the forces upon the particles, it seems reasonable to assume that these forces will become arrested too, and so are likely to be correlated with the other slow variables.

The procedure described above results in the memory function containing fourth–order density correlations. These are split into a product of pair correlations so that the equations may be closed. This approximation has no obvious physical justification other than a hope that second order correlations are sufficient to capture the important physics. These approximations are uncontrolled, in the sense that there is no expansion in a small quantity. The only true justification (or otherwise) can come from the comparison of results with experiment.

As well as the main approximations outlined here, a (less drastic) 'convolution approximation' is used in determining the mode–coupling expression for the memory function – see Ref. [95]. This series of simplifications results in an expression of the form

$$M_{\mathbf{q}}(t) \approx \frac{1}{2(2\pi)^3} \int \mathrm{d}\mathbf{k}\, V(q, k, |\mathbf{q}-\mathbf{k}|)\phi_{\mathbf{k}}(t)\phi_{\mathbf{q}-\mathbf{k}}(t), \tag{4.16}$$

where the 'vertex' V is given by

$$V(q, k, |\mathbf{q}-\mathbf{k}|) = \frac{N}{Vq^2} S(q)S(k)S(|\mathbf{q}-\mathbf{k}|)\Big(\hat{\mathbf{q}} \cdot [\mathbf{k}c(k) + (\mathbf{q}-\mathbf{k})c(|\mathbf{q}-\mathbf{k}|)]\Big)^2. \tag{4.17}$$

The most important thing to note is that the vertex depends solely upon the static structure of the system via $S(q)$ (in a system of number density ρ its close relation, the *direct correlation*

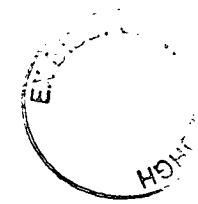

function $c(q)$, is fixed by $S(q) = 1/(1 - \rho c(q))$ [72]). This is where variables such as mean density, interparticle potentials and temperature enter the theory. These fix the static structure, which in turn fixes the coupling to nonlinear fluctuations which the memory function describes. The density correlators must then be calculated self–consistently.

4.3.1 MCT for colloids

So far in this chapter, we have outlined the mode–coupling theory as it applies to a classical deterministic system, via a Hamiltonian description. This is the original manner in which MCT was developed, and is suitable for the description of a classical atomic liquid, whose phase space vector evolves according to the deterministic laws of classical mechanics. However, in this thesis, we are interested in colloidal systems, for which the microscopic dynamics are stochastic rather than deterministic (unless one explicitly includes solvent degrees of freedom). Does the MCT formalism developed above, which describes the slow dynamics of a deterministic system, carry over to the case of Brownian dynamics? Since MCT describes dynamics, this is not obvious *a priori*. However, one can develop formalism [97], based upon the Smoluchowski description which, upon making mode–coupling approximations, leads to the same late–time dynamics as that of the deterministic approach presented above. More generally, the memory function descriptions of deterministic and Markovian processes (obeying detailed balance) are closely related [98].

This means that we can use the formalism developed above to describe the glassy dynamics, due to particle caging, of a colloidal system. Of course, the cases of deterministic and stochastic dynamics lead to differing results for the short–time dynamics. In our formalism, we have thrown away any information about this regime by discarding the regular part of the memory function. To complete the description of either a deterministic or stochastic system, we can now put this regular part back in, 'by–hand', choosing it to recover the correct dynamics in the absence of particle caging (*ie*, far from the glass transition). Provided it is quickly decaying, the choice of this contribution does not affect the position of glass transitions within parameter space, nor the characteristic late–time decays one finds in the vicinity of the transition.

In dilute colloids, in which the cage effect is not present, correlations decay exponentially (Ch.

3). Thus, in the absence of the mode–coupling contribution to the memory function, $\phi(t)$ should be of exponential form. This may be achieved if we choose the regular contribution such that it results in an instantaneous friction term: *ie*, $\int_0^\infty M_{\mathbf{q}}^{Reg}(t-t')\dot{\phi}(t') = \nu_{\mathbf{q}}\dot{\phi}(t)$. Additionally, we neglect the inertial term in Eq. 4.15, to give

$$\phi_{\mathbf{q}}(t) + \tau_o\dot{\phi}_{\mathbf{q}}(t) + \int_0^t m_{\mathbf{q}}(t-t')\dot{\phi}_{\mathbf{q}}(t')\mathrm{d}t' = 0, \tag{4.18}$$

where $\tau_o = \nu_{\mathbf{q}}/\Omega_{\mathbf{q}}^2$ and $m_{\mathbf{q}}(t) = M_{\mathbf{q}}(t)/\Omega_{\mathbf{q}}^2$ [99].

4.4 Solutions of MCT

We now discuss some features of the solutions to MCT, as simplified versions of it (discussed in the following section) shall later become the basis for a model of colloid rheology. We do not go into the details of obtaining these solutions: Ref. [95] provides somewhat more mathematical detail.

The parameter space of mode–coupling theory is defined by the values of $S(q)$ at each wavevector. This (infinite dimensional) parameter space splits into regions of 'weak' and 'strong' coupling. In the weak coupling (corresponding to 'high temperature' or, in the language of colloids, 'low density') region, the density correlators decay to zero on a timescale set by the coupling. This corresponds to a liquid: particles are free to diffuse over long distances in the fluid, and an initial spontaneous fluctuation relaxes totally over a sufficiently long timescale – in the language of Ch. 3, this is the α–relaxation time. As the coupling is increased towards a transition point, this timescale becomes increasingly long according to a power law, diverging at the transition. At this point the correlations no longer decay to zero in any finite time – the α relaxation timescale has diverged. The system is now within the strong coupling regime: the long–time limit of the correlation functions is nonzero. We write $\lim_{t\to\infty}\phi_{\mathbf{q}} = f_{\mathbf{q}}$. This long–time limit is known as the nonergodicity parameter and jumps discontinuously from zero to a finite value at the transition: upon further increasing the coupling, there is a characteristic square–root increase in $f_{\mathbf{q}}$ from the transition value [95]. These strong–coupling solutions corresponds to the glass, in which particles are not free to roam: rather they are trapped within their

cages, thus preventing an initial density fluctuation from fully relaxing. Thus MCT (at least in its simplest incarnation) predicts an idealised glass transition in strongly coupled systems.

MCT makes several predictions as to the nature of the relaxation processes in the vicinity of the transition. Density correlation functions (and indeed *all* correlation functions of variables with a slow component [100]) are predicted to show a characteristic two–stage relaxation (cf Fig. 3.1). There is a β–decay towards a plateau, which, on the low–coupling side of the transition, is followed by an α–relaxation towards zero (on a timescale which diverges with the power–law discussed above). The timescale for the β–relaxation onto the plateau also diverges as the transition is approached, but (obviously) always remains less than that of the α process. MCT also makes predictions regarding correlation functions close to the transition: in particular, the functional form of the decays onto, and from, the plateau region are universal (up to their amplitude) – the correlations at all wavevectors show the same temporal variation. In the vicinity of an MCT transition, the final relaxation towards zero is well fitted by a *stretched exponential* ($\mathrm{e}^{-t^a}, a < 1$), in accordance with many experimental systems close to a glass transition [100].

Finally, we note that, as well as diverging timescales, the transition exhibits a divergence of the zero–shear viscosity, in accordance with the notion that a glass has the character of a solid (Ch. 3). The shear viscosity is controlled by transverse current correlations, which may be expressed in terms of density fluctuations within the MCT [101, 102]. The viscosity is expressed as the integral of density correlations, and so diverges with the α–relaxation timescale.

Comparison with experiment: colloids

This section would be incomplete without some comparison of MCT to experiments. We restrict attention to colloids, in which we are primarily interested.

MCT predicts that there is a glass transition in a system of Brownian hard spheres at a volume fraction $\phi = 0.516$ [102]. This contrasts with the experimental value, $\phi \approx 0.58$. However, many of the predictions of the MCT regarding the glass transition appear to hold: there is reasonable agreement between the variation of the nonergodicity parameters with wavenumber

[103]; and predictions of the dynamics in systems approaching the transition appear consistent with experiments [77] – in particular, scaling laws predicted by MCT [95] are found to hold.

Further evidence for the usefulness of MCT comes from comparison with experiments on attractive colloids. MCT predicts the melting of colloidal glasses upon adding short ranged attrations, followed by a subsequent loss of ergodicity as the attraction strength is increased. Experiments appear to confirm this scenario [104].

So, although it is certainly not 'correct', many believe MCT to be the most succesful theory of the colloidal glass transition. Despite its successes, others dislike the theory, due to the rather arbitary nature of some of the approximations used. The author's viewpoint is that MCT is too successful to discard, even if the approximations are not understood. Rather than simply criticise these approximations then, it would seem sensible to further our understanding of them, and if possible, make improvements.

For the purposes of this thesis, we regard MCT as providing a suitable description of the glass transition in colloids. For more details on the comparison of MCT with real colloidal systems, see [105] and references therein.

4.5 Schematic models of the glass transition

Solution of the full mode–coupling theory is an involved task due to the coupling between fluctuations at all wavevectors. However, it has been found that many features of the solutions to these equations survive a rather drastic simplification which results in *schematic models*. One presumes there to be a single dominant wavenumber in the system (the typical inverse interparticle separation), and throws away all coupling of the fluctuations at this wavenumber to other density modes – this means that we consider fluctuations at wavevectors which lie on a shell in q–space.

Mathematically, this corresponds to approximating the static structure factor by a single peak $S(q) \sim \delta(q - q_o)$. In this case, there is only one equation (rather than an infinity corresponding to the spectrum of wavevectors), and the memory function is no longer an integral over

wavevectors, but reduces to a quadratic product of density fluctuations, with a coupling constant representative of the height of the main peak in $S(q)$ [100, 102]. The parameter space is one dimensional as the only parameter is the single coupling constant of the theory. This model is known as the F2–model. It is defined by the equations

$$\ddot{\phi}(t) + \Omega^2\phi(t) + \nu\dot{\phi}(t) + \int_0^t \mathrm{d}t' m(t-t')\dot{\phi}(t') = 0, \tag{4.19}$$

with

$$m(t) = v_2\phi^2(t). \tag{4.20}$$

The F2–model has an idealised glass transition at $v_2 = 4$. The model shows much of the phenomenology of the full theory, with the exception that, close to the transition, the final decay of correlation functions has an exponential form, as opposed to the (apparent) stretched–exponential found in the full theory.

Including fluctuations at the subsequent peaks of $S(q)$ leads to progressively more complicated models. Including N δ–function contributions leads to a system of N coupled equations for N correlation functions. The inclusion of an infinity of wavevectors recovers the full theory. On a less sure footing, one can also generalise the F2–model to cases in which, although there is still a single correlator, the memory function is some other polynomial in the correlation function: for example, the F12–model has $m(t) = v_1\phi(t) + v_2\phi^2(t)$. In this model, the simple exponential decay at late times goes over to a stretched relaxation more in keeping with that found in the full theory.

Thus we see that schematic models can capture the essence of the MCT. The features of a variety of schematic models are discussed in [95]. Refs. [102] and [106] study the F2–model in particular. Obviously restricting attention to these models, one throws away some predictive power. However, these simplified descriptions were useful in the early development of MCT, and so one might hope that such an approach might once again be fruitful as one seeks to extend MCT, for example to deal with deal with sheared systems.

Chapter 5

Jamming In Suspensions

5.1 Introduction

In the previous chapters, we have introduced the background physics relevant to this thesis. This has been rather extensive, since the work presented here combines the physics of the glass transition with that of colloidal rheology and the notion of jamming under imposed stress.

In the remainder of the thesis, shall consider the physics of jamming in suspensions and, in particular, whether there is a link to the glass transition. We begin by discussing the nature of stress transmission within jammed suspensions, making comparisons with both granular and molecular systems. In this chapter we shall also discuss the link between shear thickening and jamming, discussing the rôle of hydrodynamic interactions in these phenomena.

5.1.1 Mechanical or thermodynamic jamming?

As discussed briefly in Ch. 3, Liu and Nagel suggested a correspondance between solidity in a range of out of equilibrium situations. These included jammed granular materials as well as glasses. In granular materials the nature of jamming is, in one sense, trivial – that is, there is no ambiguity in the manner in which stress is propogated through the material. Forces are transmitted by direct interparticle contacts. The common picture is of a stress bearing network of particles in contact, with the temperature irrelevant compared to other energy scales (*eg*, a

typical gravitational energy in the system). Thus thermal fluctuations are negligible: there is no thermal motion tending to return particle distributions towards a free energy minimum.

At the other end of the spectrum, we have molecular materials. In this case, thermodynamics plays the leading rôle in governing the response to stress: in a glass, applied forces are supported not due to chains of rigid particles in contact, but because deformation perturbs the microstructure from its equilibrium state, resulting in thermodynamic forces (both energetic and entropic).

Many materials lie in between these two extremes (fine powders, suspension of both non–Brownian ($a \gtrsim 1\mu m$) and colloidal ($a \lesssim 1\mu m$) particles). Somewhere in the middle of this range, the nature of jamming becomes rather blurred: at what point does solidity cease to arise from a contact network and instead come about as the result of thermodynamic forces? In colloidal glasses, solidity is ascribed to thermodynamics: deformations result in a free energy penalty, appearing macroscopically as elasticity. To what extent can shear–induced solidity be attributed to this mechanism, and to what extent is it due to a network of contacts? The former case might be thought of as a stress induced glass transition, whilst the second has more in common with a granular material. Of course, the answer to this question is likely to depend crucially upon the particle size.

5.1.2 Outline

In Ch. 6 we shall proceed upon the assumption that jammed colloids may be treated as a stress–induced glass. Working on this assumption, we formulate a simple model of stress–induced glassiness, building upon schematic MCT models of the glass transition. The remainder of this chapter is split into two parts. Firstly, we shall consider some issues, relevant to both the thermal and mechanical jamming scenarios, which are ignored in our simple model. These relate to the interplay between bulk and surface properties which, we believe, are key to interpreting experiments such as that of Bertrand *et al* [42], and to understanding the process of high shear granulation. Secondly, we shall consider the rôle played by solvent–mediated hydrodynamic interactions in jamming suspensions. This feature, obviously not present in granulars, is often held responsible for shear thickening in dense colloids and, in part, for the divergence in the

zero–shear viscosity of colloids [107]. We shall argue that hydrodynamics are not primarily responsible for these phenomena.

5.2 Simple ideas on jamming

In this section, we discuss a simple picture of jamming in dense suspensions, as observed in the experiments of [42, 91]. In order to do so, we consider the phenomenon of *dilatancy* – the expansion of deforming particulate materials.

5.2.1 Dilatancy

Dilatancy, first documented by Reynolds [108], occurs because, in order to flow, particles need more room than they have in dense packings, as schematically illustrated in Fig. 5.1. It is easily observed: go for a walk on a wet beach, and you will notice that the sand around your feet appears to dry. This occurs as the dense packing expands to allow the particles to pass one another as the material deforms. This draws the water in to fill the additional pore space, drying the surface of the sand. There is a lower bound on the concentration of sand (or any granular material) ϕ_d at which this occurs : for $\phi \leq \phi_d$ there is no expansion upon deformation – the particles have sufficient room to flow past one another. In contrast, for $\phi > \phi_d$, the particles have insufficient room, and the volume fraction of a flowing material is lowered to ϕ_d. For non–Brownian hard spheres in the absence of gravity $\phi_d \approx 0.555$ [109]. This is connected to soil mechanics [110], in which deformed soils tend to a *critical state* density.

The precise rôle of dilatancy within shear thickening remains something of a mystery, despite the fact that the two phenomena have long been thought to be related. (In the past, the word dilatancy was used to refer to thickening.) In suspensions, the sample cannot simply expand, as the concentration is fixed by the constituents. In slow flows, we might expect that large scale dilation is not neccessary, as relaxation processes allow particles to find their way past their neighbours. But, within faster flows, thermal motion cannot prevent dilation of the packing. In a simplistic explanation for thickening, one then argues that particles must protrude from the fluid–surface, giving rise to large surface forces, ultimately resulting in the large stresses

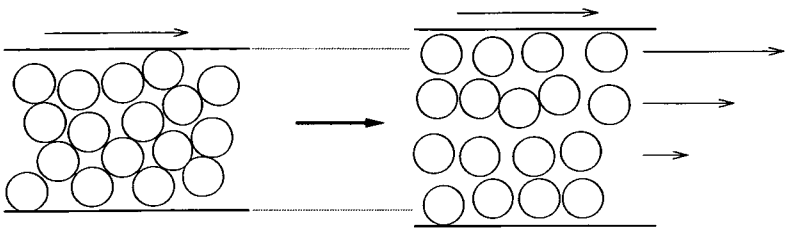

Figure 5.1: An illustration of the dilation of dense packings upon shearing. In the left hand picture, the particles are unable to flow easily, since particles pack tightly into the interstices between their neighbours. In order to flow freely, the packing must expand orthogonal to the flow direction, allowing the particles to easily flow past their neighbours. This phenomenon is responsible for the drying of wet sand when it is stood upon: the dilation of the particles' packing creates causes fluid to rush in to fill the additional pore space, resulting in a drying at the surface of the material.

measured at the rheometer plates. Such a scenario is given credence by the loss of gloss often observed at the surface of suspensions [30], but it does not feature greatly in current explanations of thickening [13].

5.2.2 Jamming and granulation

In the experiments of Ref. [42], initially fluid samples of some suspensions were transformed into a solid state by shearing. Upon vibration, these samples melted back into the initial fluid state. These observations point towards the existence, in the jammed state, of some metastable structure. Presumably, whilst thermal fluctuations are not sufficient to overcome the energy barrier to relaxation back into the initial fluid state, the energy input by vibration is. This suggests two main questions: firstly, what is the difference (on the microscopic level) between the statically jammed state and the initial fluid? And secondly, what provides the energy barrier to rearrangement from the jammed solid into the fluid state – *ie*, why does the solidity persist after cessation of shear?

The first of these questions seems related to shear thickening: a strongly thickened state has a solidlike quality. In the experiments, it seems that the thickened state persists after the shearing is removed. With this in mind, a simple scenario which accounts for the observations is as follows: consider a finite, dense sample of a hard sphere colloid. As the sample is deformed, the bulk concentration is lowered to ϕ_d and the material shear thickens. The solvent fills the increased pore space between the particles, sucking it from the sample boundaries, drying the

surface. As well as lowering the concentration, the deformation alters the microstructure, so that particles are less efficiently packed than in the equilibrium structure, lowering the entropy. The free energy will also be raised by the surface energy cost of particles protruding from the interface. However, the system cannot relax to its free energy minimum, as the capillary forces squeeze the sample tightly, holding it in an expanded, stressed structure. To relax, work must be done against the capillary forces.

We now consider the quantities of interest in such a scenario, comparing the relevant energy/stress scales, with the aim of elucidating the relevance of jamming to granulation. We also argue that there are restrictions on the size of samples which can dilate without fracturing.

Stress scales

Firstly, we estimate the magnitude of the forces acting upon a particle, of radius a, protruding from a solvent of surface tension γ. If a particle, initially contained within the fluid, is wholly removed from it, an interfacial area $A = 4\pi a^2$ is created between the (solid) particle and the air, whilst the same interfacial area between the solid and the fluid is lost. If the solvent wets the particle surface [70], the interfacial energy cost of removing the particle is then given by $\Delta E = 4\pi\gamma a^2$, setting the typical scale of the interfacial energy cost of a particle protruding from the interface as $E \sim \gamma a^2$.

If the surface of the solvent–air interface is curved, there is a difference between the pressure of the solvent (P_s) and that of the surrounding atmosphere (P_a), given by $\Delta P \equiv P_s - P_a = \gamma(1/R_1 + 1/R_2)$, where R_1, R_2 are the principal radii of curvature of the surface on the fluid side [70]. The mean curvature $\kappa \equiv (1/R_1 + 1/R_2)$ can vary over the surface, its variation being determined by hydrostatic pressure differences in the solvent (and, technically, in the atmosphere). However, even leaving aside this complication, it does not seem easy to estimate this curvature. Consider a spherical droplet of suspension, of radius R: if no particles protrude from the surface, then the mean curvature is $\kappa = 2/R$. The pressure within the fluid droplet is greater than that of the surrounding atmosphere with $\Delta P = 2\gamma/R$. This suggests that a particle protruding from the interface will be pushed out by the pressure difference (in conflict with minimisation of the interfacial energy). We can estimate the magnitude of this force as

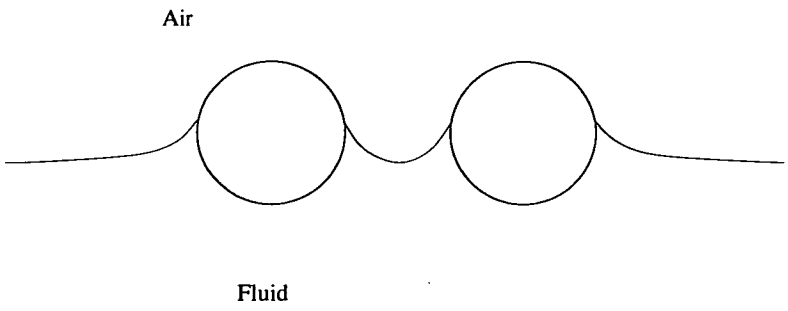

Figure 5.2: A schematic illustration of the dimpled fluid–air interface which could arise if particles protrude from the interface. Such a situation could result in decreased positive curvature (with respect to the case of a spherical droplet), or in negative curvature. One should note that this diagram is in 2–D: the curvature in the orthogonal plane may be of opposite sign, so the mean curvature at a point may be of either sign.

$F_{\Delta P} \sim (\Delta P)a^2 \sim 2\gamma a^2/R$: if the droplet is significantly larger than the individual particles ($R \gg a$), then this force is much less than that arising from the interfacial energy cost, which is of the order $F_{int} \sim \gamma a$.

However, if many particles protrude from the fluid surface, it is not clear that its curvature remains close to $\kappa \sim 2/R$: if the contact angle between the solvent and the particle surface is small, it seems that the surface must take on a dimpled appearance as illustrated schematically in Fig. 5.2. This dimpling could reduce the magnitude of ΔP, or even change its sign. If the curvature changes sign, we expect that $|\kappa| \lesssim 1/a$, since a is the smallest lengthscale in the problem. Thus, the dimpling might result in a force $F_{\Delta P} \sim \gamma a$ tending to keep particles within the droplet. This is of the same order, and of the same sense, as the force resulting from the interfacial energy cost.

Therefore, regardless of the dimpling effect, in a (roughly spherical) droplet of radius $R \gg a$, we expect an inwards capillary force of order $F \sim \gamma a$ acting upon particles protruding from the fluid–air interface. The maximum number of particles $\mathcal{N}$ which may be at the surface scales as $\mathcal{N} \sim (R/a)^2$, and so the typical energy cost of protruding particles is $E \sim \mathcal{N}\gamma a^2 = \gamma R^2$, corresponding to a typical (normal, compressive) stress $\sigma_\gamma \sim \gamma/R$ from capillarity.

In a thermal system, this should be compared to the typical thermal energy density. If the latter is far greater than the capillary stress, we expect that an energy barrier due to capillary forces is easily overcome. The typical thermal energy density is just given by $E_{thermal} \sim kT/a^3$. Then

a jammed droplet of typical dimension R may be maintained by capillary forces provided $R \lesssim \gamma a^3/kT$. Note that this criterion does not ask whether we can create a jammed state, but rather whether such a state, assumed *a priori* to exist, can survive. Depending upon the particle size, this gives a maximum droplet size which ranges from a few millimetres for $50nm$ radius particles, to several metres for particles of radius $1\mu m$. Thus, it seems that macroscopic jammed droplets of colloidal particles may be sustained by capillary forces.

In a granulation process, as well as in a rheological experiment, the externally imposed stress provides another scale of stress. In order to *create* a jammed state, sustained by capillary forces, external forcing must be sufficient to surmount the capillary energy barrier in the first place – thus, we expect that, to do so, an external stress $\sigma_{ext} \sim \gamma/R$ is required. Except for very small droplets, this stress ($\sigma_{ext} \sim 1Pa$ for $R \sim 3cm$) is easily applied. (However, as mentioned during our discussion of dilatancy above, one might also require a sufficiently fast flow in order to cause dilation.) On the other hand, we expect that droplets which are already in a jammed state may be melted by application of a stress $\sigma_{shear} \gg \sigma_\gamma$. This suggests then, that (for example in a granulation process) large lumps of material might become jammed, but could also be 'melted' by the external forces. In contrast, sufficiently small lumps are more difficult to jam, or to melt.

By considering the extent of dilatancy, we now argue that, if a suspension can only flow through dilation, it will tend to break up. This suggests how granules might form out of a strongly mixed paste.

Fracture and granulation

In a dilating sample, particles are pushed through the fluid surface. We can estimate the extent of this as follows. Consider the deformation of a sample at volume fraction ϕ. Initially, the total volume is V, and so the volume occupied by the particles and solvent are, respectively, $V_p = V\phi$ and $V_{sol} = V(1-\phi)$. Upon deformation the sample dilates so that the volume fraction is reduced to ϕ_d. The volume of the particulate packing (as opposed to the actual volume of the particles) increases to a value V_p^{final}, whilst the solvent resides within a volume V_s^{final}. Of course, neither the volume of particles nor solvent has changed, so $V_p^{final}\phi_d = V\phi$

and $V_s^{final}(1-\phi_d) = V(1-\phi)$.

$V_p^{final} > V_s^{final}$ and so, after dilation, part of the material is dry – *ie*, it lies outwith the solvent. If we consider the (overly) simple case in which both the initial and dilated samples are a spherical droplet, this dry region is a layer of thickness

$$r_{dry} = R\left(\left(\frac{\phi}{\phi_d}\right)^{1/3} - \left(\frac{1-\phi}{1-\phi_d}\right)^{1/3}\right) \tag{5.1}$$

at the surface, with R the radius of the initial droplet.

The experiments of [109] suggest that, in order to flow, a dense packing of spheres dilates to a bulk concentration $\phi = 0.555$. Taking this as the bulk concentration of our dilated droplet (*ie*, $\phi_d = 0.555$) the thickness of the dry layer varies from zero (at $\phi = 0.555$) to around ten percent of the sample size R (at $\phi \approx 0.64$). If the thickness of this layer is much greater than the particle size, this picture suggests that, during the deformation, layers of particles are shed by the dilating suspension. However, this is not observed experimentally, suggesting that a picture of homogeneous dilation is too simplistic: rather, in strongly sheared dense suspensions, one can observe fracture of the sample [32, 33]. This suggests that the material chooses to create additional surfaces, resulting in fracture, rather than shed particles. The idea that flowing colloids do not dilate homogeneously is consistent with experiments [89].

If fracture occurs in preference to shedding particles, Eq. 5.1 suggests a limit on the size of samples which can flow without fracturing. This criterion for flow without fracture is quite stringent. For example, taking $\phi = 0.58$, it suggests that samples will fracture if $R \gg 25a$. Thus, dense macroscopic samples can fracture if sheared sufficiently strongly.

If this occurs, it provides a mechanism for smaller lumps of material to form, as occurs in a granulation process. From the order of magnitude calculations above, these smaller granules are more robust: sufficiently small lumps can dilate and flow without fracture if external forcing demands it. Alternatively, if forcing is sufficiently weak and if thermal motion is not too great, they could remain as rigid, jammed solids. The final result will depend upon which criteria are satisfied and which are not. This, in turn depends upon the system parameters.

At present, we have not worked out the details of this picture. However, even in the rough form described here, it suggests how the result of shearing dense pastes, as in high shear granulation,

might be understood by considering the effect of dilatancy, and the typical stresses which arise.

Summary

We believe that the ideas described above are key to understanding the persisting shear induced solids found experimentally, and that these ideas are relevant to the process of high shear granulation. However, it is evident that we do not have a detailed picture of the microstructure in a jammed sample. Nor do we have a picture of the pathways betwen the two macroscopic states. In order to produce a detailed theory, it seems that a better description of the microscopic structure of the jammed state is required. This would enable one to construct detailed pathways between the two macroscopic states of the system, allowing more precise calculation of the energy barrier to relaxation, as well as the stress required for to create the jammed state. Computer simulation might provide a suitable avenue of attack for this problem.

We now leave these questions, and turn instead to discuss the mechanisms behind shear thickening, which we have largely ignored in the above discussion.

5.3 The rôle of hydrodynamics

Shear thickening is often discussed in terms of hydrodynamic interactions without reference to the cage effect which, in the MCT, is responsible for the large (zero–shear) viscosity observed in dense colloids. Hydrodynamic theories [107] thus ignore the presence of the glass transition. If one attributes the rise in viscosity to the presence of the dynamical glass transition, then the viscosity diverges at $\phi \approx 0.58$ (consistent with some experimental observations, whilst inconsistent with others: see [18] and the discussion in Ch. 3). In this case, it seems likely that the nonlinear rheology of dense suspensions is coupled to the glassy dynamics. This notion is supported by work on the yielding of colloidal glasses and thinning of dense colloidal fluids [29, 111]. In order to investigate this further, we now make a simple calculation of hydrodynamic relaxation times in a colloid, so that we may compare these to the relaxation times associated with the glassy dynamics.

5.3.1 Hydrodynamic relaxation times

To calculate a hydrodynamic relaxation time, we begin by assuming that it is dominated by pairs of particles, 'bound' by hydrodynamic forces, which tend to prevent relative motion of two near neighbours. We calculate a diffusion coefficient for motion along the line of centres, from which we obtain the lifetime of the hydrodynamic 'bond'. This pair approximation is motivated by the fact that there are few contacts which are sufficiently close to result in long relaxation times, and so there are fewer situations in which three particles are in very close proximity. Thus we expect that relaxations are dominated by that of particle pairs. Besides this expectation, the cooperative caging of particles is exactly the phenomenon described by MCT: here, we are attempting to illustrate the fact that hydrodynamics alone (*ie*, without the cooperative slowing down due to the cage) is not responsible for large relaxation times.

Relaxation of hydrodynamic pairs

In a system of particles interacting hydrodynamically the velocity $\mathbf{u}_i$ of particle i may be written as [2]

$$\mathbf{u}_i = \sum_j \underline{\underline{\omega}}_{ij} \cdot \mathbf{F}_j. \tag{5.2}$$

$\underline{\underline{\omega}}_{ij}$ is a mobility tensor, giving the velocity of particle i due to a force $\mathbf{F}_j$ acting upon particle j. This means that if particle 1 experiences a force, say through collisions with solvent molecules, particles $2, 3, 4 \ldots$ (as well as particle 1) will attain a velocity, as they 'feel' the movement of particle 1 through hydrodynamics. We may superpose velocities in this way, provided that the linear Stokes' equations are a good description of the fluid mechanics, a situation which typically holds in the low Reynolds numbers flows relevant to colloidal suspensions [2].

In a colloidal suspension, particles are constantly subjected a barrage of collisions from the solvent molecules. This results in diffusion, with the diffusivity D determined by the mobility and the thermal energy kT. In a dilute system the mean square displacement obeys

$$\langle \mathbf{r}(t)\mathbf{r}(t) \rangle = 2D\underline{\underline{I}}t \tag{5.3}$$

with the diffusion coefficient D given by $D = kT\omega$, with $\omega = \frac{1}{6\pi\eta a}$ the mobility of an isolated sphere. In the presence of a second sphere, the diffusivity of sphere 1 is modified

by hydrodynamic interactions with sphere 2. We can split the motion into that of the centre of mass position ($\mathbf{r}_{cm}$) and that of the relative motion ($\mathbf{r} \equiv \mathbf{r}_2 - \mathbf{r}_1$). The latter obeys $\langle(\mathbf{r}(t) - \mathbf{r}_o)(\mathbf{r}(t) - \mathbf{r}_o)\rangle = 2\underline{\underline{\mathbf{D}}}t$, where $\underline{\underline{\mathbf{D}}} = 2kT(\underline{\underline{\omega}}_{11} - \underline{\underline{\omega}}_{12})$ and $\mathbf{r}(t=0) \equiv \mathbf{r}_o$ [2].

We wish to calculate the typical time for two particles, initially at some small separation r_o, to escape from one another: *ie*, we wish to know the lifetime of a hydrodynamic 'bond'. In a dilute system, the typical relaxation timescale is the time taken for a particle to diffuse over a distance equal to its own radius. In analogy, here we take the relaxation time of a hydrodynamic bond to be the typical time for the relative separation to increase by a particle radius. To calculate this quantity, we utilise the diffusion coefficient for motion along the line of centres, given by $D_{||} \equiv \mathbf{r_o} \cdot \underline{\underline{\mathbf{D}}} \cdot \mathbf{r}_o$. In terms of this quantity, the mean square separation is given by $\langle(\delta r)^2\rangle = 2D_{||}t$, with $\delta r = (\mathbf{r}(t) - \mathbf{r}_o) \cdot \mathbf{r}_o$.

The hydrodynamic mobilities of two interacting spheres have been studied by Batchelor. For spheres of common radius a, they may be written [112]

$$\underline{\underline{\omega}}_{ij} = \frac{1}{6\pi\eta a}\left[A_{ij}(r)\frac{\mathbf{rr}}{r^2} + B_{ij}(r)\left(\underline{\underline{\delta}} - \frac{\mathbf{rr}}{r^2}\right)\right] \qquad (5.4)$$

where the A_{ij}, B_{ij} characterise the mobilities of the spheres along and perpendicular to the line of centres respectively. This form simply reflects that the response to any force perpendicular to $\mathbf{r}$ is equivalent (governed by B_{ij}), whilst forces parallel to $\mathbf{r}$ result in a different response. Symmetry dictates that $\underline{\underline{\omega}}_{ij}$ is symmetric in particle labels and that $\underline{\underline{\omega}}_{11} = \underline{\underline{\omega}}_{22}$.

Eq. 5.4 gives the diffusion coefficient at $t = 0$ (so that $\mathbf{r} = \mathbf{r}_o$) as

$$D(r) = \frac{2kT}{6\pi\eta a}(A_{11}(r) - A_{12}(r)). \qquad (5.5)$$

The separation dependent quantity $A_{11} - A_{12}$ is tabulated in Ref. [112]. In this work, we approximate $A_{11}(r) - A_{12}(r)$ by making a fit to the tabulated data. The expression

$$\begin{aligned} A_{11} - A_{12} \equiv f(x) \;=\; & 4(x-1)/(1 - (9/5)(2x-2)\log(2x-2) \\ & +0.0117203 + 2.88897(2x-2) \\ & +0.183829(2x-2)^2 - 0.00677877(2x-2)^3), \end{aligned} \qquad (5.6)$$

with $x \equiv r/2a$, fits the data well over the relevant range of separations, as shown in Fig. 5.3.

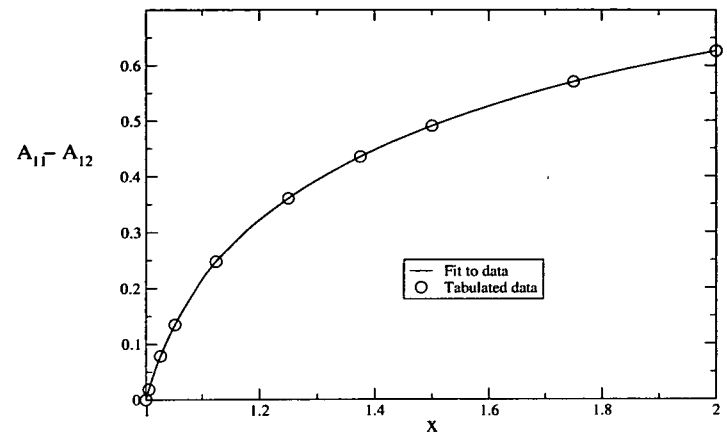

Figure 5.3: The difference between the hydrodynamic functions A_{11} and A_{12} as a function of the dimensionless separation $x = r/2a$. The points are the tabulated data from [112] and the line is a fit to this data. The leading two terms as $x \to 0$ in the expression for $A_{11} - A_{12}$ are known [113]: the fit was performed by adding higher order corrections to these leading terms.

From the diffusion coefficient for relative motion along the line of centres, we estimate the lifetime of a hydrodynamic bond between two particles at dimensionless separation x to be $\tau(x) \sim a^2/D(x)$ which gives

$$\tau(x) \sim \frac{6\pi\eta a^3}{2kTf(x)}. \tag{5.7}$$

This is only approximate: we have not accounted for the fact that, as the relative separation increases from the initial value, so does the mobility. Nor have we distinguished diffusion which reduces the separation from that which increases it. We shall not be concerned with these corrections, instead concentrating upon the order of magnitude, and the way in which the typical relaxation timescales change with volume fraction. In order to study this, we need the distribution of interparticle separations at a particular volume fraction – *ie*, the radial distribution function $g(r)$.

The distribution of relaxation times

The radial distribution function $g(r)$ (or, in terms of the dimensionless variable x, $\tilde{g}(x)$) provides us with the mean distribution of interparticle separations within a fluid. Here, we use

the Percus–Yevick radial distribution function (rdf) for hard spheres. An expression for this is given in [2].

We wish to calculate the distribution of relaxation times within a suspension at volume fraction ϕ. We cannot analytically invert our expression (Eq. 5.7) for $\tau(x)$ to give an analytic expression for the function $p(\tau)$ by relating $p(\tau)d\tau$ to $g(r)dr$. However, for a given value of the relaxation time (say τ_1), we can (via Eq. 5.7) calculate the corresponding interparticle separation, $x(\tau_1)$. The fraction of bonds surviving beyond time τ_1 is then just the probability that a particle chosen from random is within a dimensionless distance $x(\tau_1)$ of its nearest neighbour. If this distance lies outwith the nearest–neighbour shell in $\tilde{g}(x)$ then all bonds are unrelaxed at τ_1. For smaller values of $x(\tau)$, the fraction of unrelaxed bonds ($F_{bonds}(\tau_1)$) is given by an integral over the rdf which gives the fraction of particles within the nearest–neighbour shell which are also within a distance x from the origin. This gives

$$F_{bonds}(\tau_1) = \int_{\tau_1}^{\infty} p(\tau)\,\mathrm{d}\tau = \frac{\int_0^{x(\tau_1)} x^2\tilde{g}(x)\,\mathrm{d}x}{\int_0^{x^*} x^2\tilde{g}(x)\,\mathrm{d}x}, \tag{5.8}$$

where x^* corresponds to the limits of the nearest–neighbour shell – the position of the 1st minimum in $\tilde{g}(x)$. The normalisation integral in the denominator appears since $p(\tau)$ is normalised over all particles within the nearest neighbour shell, whilst $\tilde{g}(x)$ is normalised over all separations.

We show the results of this calculation in Fig 5.4. For volume fractions $\phi \lesssim 0.5$, the Percus–Yevick expression for the radial distribution function is a reasonable approximation to the hard–sphere rdf as found by computer simulation (see [72] for a comparison at $\phi = 0.49$). There is a quantitative error in the height of the main peak, but given the approximate nature of our calculation, this is of no concern. However, as one approaches random close packing, the Percus–Yevick rdf becomes unsatisfactory: the contact value of $g(r)$ ought to diverge upon reaching the close packed state, whilst the Percus–Yevick expression does not show a great change in the height of the first peak as random close packing is approached. Also, for large packing fractions ($\phi \approx 0.6$) the first minimum dips below zero! This prevents us from confidently predicting the distribution of hydrodynamic relaxation times for volume fractions approaching $\phi = 0.6$, as the rdf which we have used will predict too small an incidence of large relaxation times.

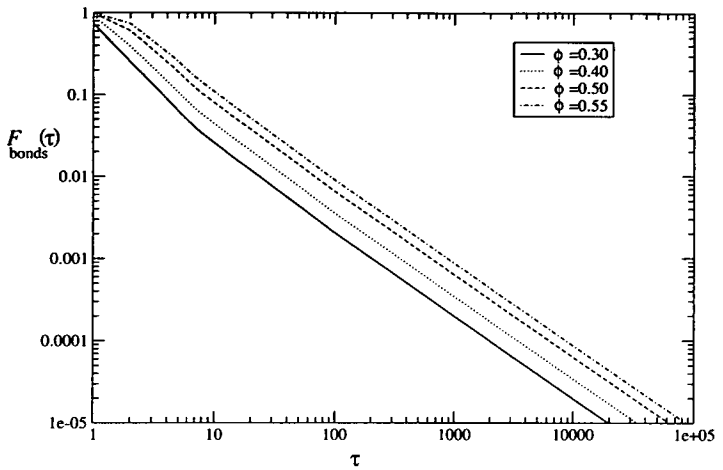

Figure 5.4: The fraction of hydrodynamic 'bonds' remaining at time τ in a hard–sphere colloid for a range of volume fractions. (Time is measured in units of the time τ_o for an isolated colloidal particle to diffuse a distance equal to its own radius.)

5.3.2 Is thickening due solely to hydrodynamics?

Raising the volume fraction of a colloid from $\phi = 0.3 \rightarrow \phi = 0.5$, one notices a strong slowdown in its dynamics, as well as a large increase in the viscosity [18]. At $\phi = 0.49$, typical relaxation times are about a factor of 50 greater than in a dilute system, and at higher volume fractions, the relaxation times become long compared with experimental timescales [76]. In contrast, typical hydrodynamic pair relaxation times show no sign of becoming macroscopically long: even for $\phi = 0.5$ the probability that a bond will last a time $50\tau_o$ is only about 1%. Also, predictions of the viscosity (see [13], and references therein) based upon a hydrodynamic slowdown shows a weaker increase in the viscosity than the experiments of [18] and predict that the viscosity does not diverge until random close packing, where interparticle gaps close to zero.

This backs up the notion that, in the vicinity of the glass transition, hydrodynamics do not play a significant part in creating the long relaxation times observed experimentally. The relaxation times are due instead to the cage effect, of which MCT seems to provide a reasonable description. Of course, at volume fractions approaching random close packing, the divergence of the

contact value of $g(r)$ implies that all particles have very close neighbours so that, in this limit, the time for two hydrodynamically 'bound' neighbours to escape one another can become arbitrarily large. At sufficiently high concentrations, had the glass transition not intervened, one would expect hydrodynamics alone to result in slow relaxations.

In shear thickening dense colloids, viscosities of the order 10^3 times the solvent viscosity can be observed, even at volume fractions well below random close packing [30]. If one presumes that the close link [18] between viscosity and relaxation times remains (at least approximately) valid in sheared systems, this implies a similar mark–up in the typical relaxation time. If this slowdown is due to hydrodynamics, rather than having anything to do with the nearby glass transition, Fig. 5.4 suggests that the particles must be pushed sufficiently close together that the hydrodynamic relaxation time increases by a factor $\sim$ 1000. In contrast, typical glassy relaxation times have a head–start, the viscosity (which we have argued is due to the glassiness and not to hydrodynamics) already being of the order 50 times that of the solvent [18].

A simple argument

So, can shearing produce a sufficiently strong increase in hydrodynamic relaxation times over those in the quiescent state to account for observations of shear thickening (Sec. 2.3.3)? A simple argument suggests that, at least in some cases, it can. Consider an amorphous hard sphere suspension of hard spheres, radius a, at a concentration ϕ. In a sense, we can attribute the relative viscosity $\eta_r(\phi)$ of this suspension to the osmotic pressure Π which (in a suitable experiment employing a semi–permeable mebrane) sets the volume fraction. In such a setup, the system resists osmotic compression since greater volume fractions increase the number of close contacts, lowering the entropy.

Theory ignoring the glass transition [107] predicts a form of the viscosity increase with concentration. (In this argument, we use this theory for the viscosity, rather than the calculation given above since, as we noted, the Percus–Yevick rdf fails at high concentrations.) The relative viscosity as a function of concentration $\eta_r(\phi)$ diverges as $\phi \to \phi_{RCP}$. Assuming this form we can calculate the osmotic pressure increase required to increase the relative viscosity of a suspension from an initial value η_r^i to a final value η_r^f. Firstly, we calculate the initial

and final volume fractions to be ϕ^i and ϕ^f, where these quantities are defined by $\eta_r(\phi^i) = \eta_r^i$ and $\eta_r(\phi^f) = \eta_r^f$. We then calculate the osmotic pressure difference between ϕ^f and ϕ^i as $\Delta\Pi = \Pi(\phi^f) - \Pi(\phi^i)$, thus giving the osmotic pressure increase required to raise the relative viscosity (according to hydrodynamics) from η^i to η^f.

We now argue that, if the main effect of shearing upon the microscopic structure of the colloid is to form close contacts (resulting in longer hydrodynamic relaxation times and a correspondingly greater viscosity), then this is a similar effect to increasing the osmotic pressure. In this case we expect that the shear stress required to increase the relative viscosity of a colloid by shear thickening is of the same order as the increase in osmotic pressure required to cause the same degree of 'thickening'. Thus, to increase the relative viscosity from η_r^i to η_r^f by shearing, requires the application of an additional shear stress $\Delta\sigma \sim \Delta\Pi$.

Using this argument, we now estimate the stresses required to cause varying degrees of shear thickening. We take the osmotic pressure of a (dense) colloidal suspension of particles, radius a, at volume fraction ϕ to be

$$\Pi \approx \frac{3\phi kT}{4\pi a^3}\frac{1.85}{0.64-\phi}. \tag{5.9}$$

This expression captures the correct form of the divergence [2]. Note that Eq. 5.9 suggests a size dependence of the shear stress required to produce a given increase in relative viscosity. Thus, in the above argument, it also alters the stress required to increase the relative viscosity from η_r^i tp η_r^f. (This is interesting given that experiments [30] find that the shear rate ($\dot{\gamma}_c$) required for discontinuous thickening varies with particle radius, possibly consistent with $\dot{\gamma}_c \sim 1/a^3$.)

We begin by considering the stress needed to cause shear thickening from a relative viscosity $\eta_r \sim 50 \rightarrow \eta_r \sim 500$. From hydrodynamic predictions [13] for the viscosity $\eta_r(\phi)$, $\phi^i \approx 0.54$ and $\phi^f \approx 0.6$. From Eq. 5.9, for $690nm$ diameter particles, this gives the additional stress required to cause this degree of thickening as $\Delta\sigma \sim 0.5Pa$ (at room temperature). Let us compare this to the stresses which arise in a corresponding experimental system: in [33], a suspension of $690nm$ diameter particles at a volume fraction $\phi \approx 0.56$ continuously shear thickens from a relative viscosity $\eta_r \approx 27$ to $\eta_r \approx 530$ upon increasing the stress from (approximately) $10 \rightarrow 700Pa$. Obviously the stress required is significantly greater than that

suggested by our argument. For smaller particles, our argument would predict that greater stresses were required. However, this dependence is not crucial in our comparison: for our argument to predict stresses as large as those found experimentally, the particle radius would need to be an order of magnitude smaller.

In the same experiments, more concentrated samples thickened discontinuously: for $\phi = 0.61$, a much smaller increase in the stress (from $\sigma \approx 5$ to $\sigma \approx 50$) increases the relative viscosity from $\eta_r \approx 173$ to $\eta_r \approx 2670$. Our argument predicts that such an increase in η_r requires an increase in stress of $\Delta\sigma \approx 1.5Pa$. Again, this is much smaller than the stress found experimentally.

This suggests that the stresses required to cause sufficiently close contacts for hydrodynamic shear thickening (up to $\eta_r \sim 1000$) are not prohibitively large. However, let us consider Bertrand's experiments: in this case, the viscosity, due to an applied stress, diverges. Ignoring the glass transition, in order to cause such a divergence of the viscosity by osmotically compressing one must create a random close packed state. This carries a large entropy penalty: in the (idealised) random close packed state, particles can no longer move relative to one another, resulting in the loss of degrees of freedom. Classically, each of these degrees of freedom can access an infinity of microstates, and so their loss formally results in a divergent entropy loss. This leads to a divergence of the osmotic pressure at ϕ_{RCP}.

If our argument above holds, this suggests that shearing a system into a state in which each particle contacts its neighbours also requires a divergent stress, suggesting that this is not the origin of experimental jamming. In contrast, let us regard these jammed states as stress induced glasses. Following a similar line of reasoning to the above argument, in order to produce a divergent viscosity, we need only a stress of the order $\Pi(\phi_g)$. This is certainly *not* divergent, arguably making this a more plausible scenario.

Summary

So, it seems that not all shear thickening phenomena are primarily governed by hydrodynamic interactions. Without taking the cage effect into account, one cannot fully capture the rheology of colloids at concentrations above their glass transition: neither can one understand the

experimentally observed jamming. It seems that the cage effect, and the slow dynamics which it entails, plays a rôle in shear thickening behaviour in dense systems. This points towards the need for an improved understanding of the rheology of concentrated colloids: ideally, one would devise a theory which captured the many–body cage effect, its effect upon flow (and vice–versa), *as well* as the hydrodynamic interactions between colloidal particles. (The relative influence of these distinct features might well shift with concentration.) This is obviously a challenging task (elucidating the effect of hydrodynamic interactions on the glass transition is quiescent colloids is hard enough [114]). The influence of hydrodynamic interactions upon the non–Newtonian rheology of colloids has been, and continues to be, studied extensively [115]. In contrast, the influence of the cage effect upon the non–Newtonian rheology seems less well understood. However, recent work [29, 82, 111] which has its basis in MCT, appears promising: in the following chapter, we proceed along this line of research.

Chapter 6

Modelling a Stress–Induced Glass

As mentioned in the previous chapter, we would like to better understand the rôle of the cage effect in governing the rheology of dense suspensions. In particular, we wish to investigate whether we might regard jammed suspensions as a stress induced glass. With this aim, we now describe a model of jamming in suspensions, based upon a schematic version of the MCT discussed earlier. We begin by disussing the effect that one expects stressing a dense suspension to have upon the glass transition.

6.1 The effect of stress and flow upon the glass transition

As discussed in Ch. 4, the coupling constants of the MCT are dependent upon the static structure of the system via $S(q)$. (Recall that this is the key way in which variables such as interparticle potential, temperature and density enter the theory.) Therefore, alterations to the structure alter the material's susceptibility to arrest. Intuition suggests that flow–induced structural alterations will tend to **promote**, rather than inhibit, dynamical arrest: since the equilibrium static structure of a quiescent (hard sphere) fluid is the most efficiently packed fluidlike structure at that density, a perturbed structure will have a greater number of close contacts, hindering particle diffusion and promoting arrest. The most obvious way to alter structure is to apply stress to the material. Stressing a solid distorts the microstructure, resulting in a free energy penalty which is manifested as elasticity. After the transient flow has ceased, both stress and

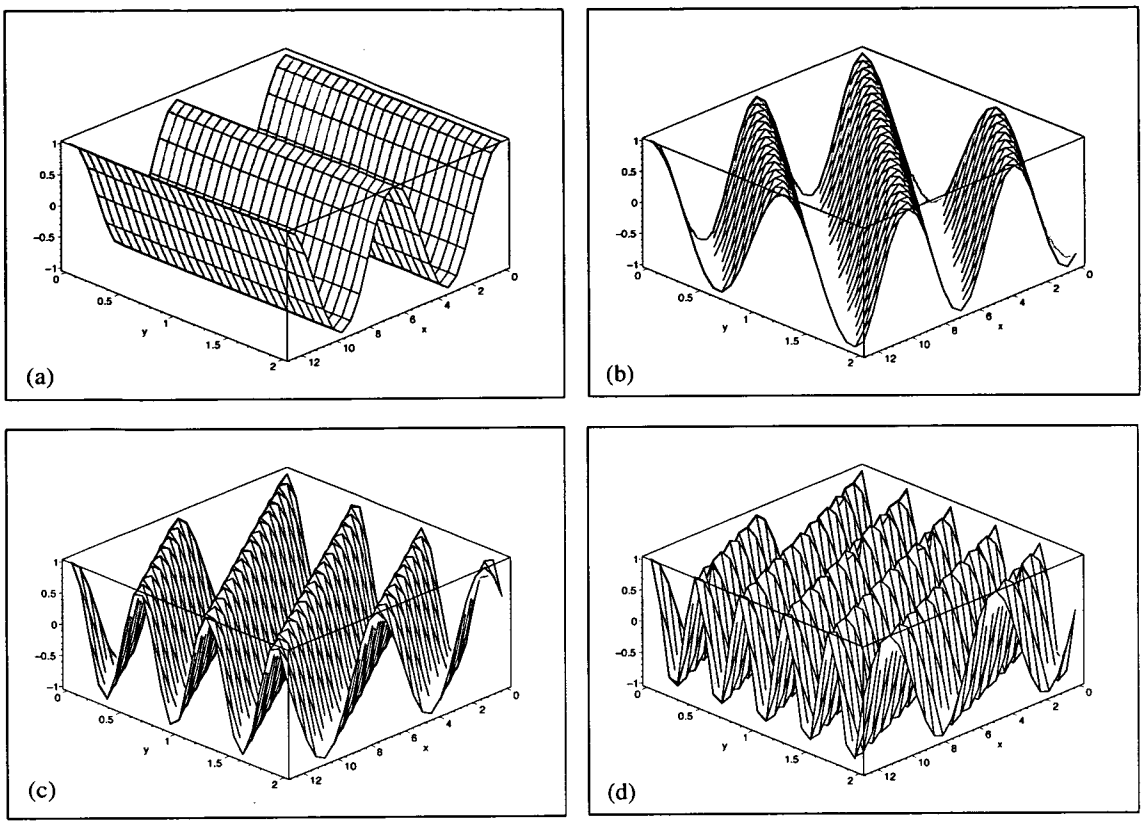

Figure 6.1: An illustration of the way in which advection by shear flow reduces the distance over which particle diffusion is necessary to relax a fluctuation with wavevector component in the flow direction. We show the evolution of a sinusoidal fluctuation in the x–direction (without Brownian motion) as it is advected by a flow $\mathbf{v} = \dot{\gamma} y \hat{\mathbf{x}}$. (a) is at zero–strain, (b) corresponds to a strain $\gamma = 5$, (c) to $\gamma = 10$ and (d) to $\gamma = 15$. Note how the distance between adjacent peaks (and troughs) is reduced by the shear flow.

the distorted structure remain. Thus one expects that stressing a material can 'shift' its glass transition.

Stressing a colloidal fluid can also alter the microstructure, but in this case, it is accompanied by steady–state flow. This has its own impact upon the tendency to arrest, distinct from the effect of a distorted structure. The flow shortens the lifetime of those fluctuations with wavevector components in the flow direction because diffusion over small distances, aided by advection with the flow, can relax a long–ranged fluctuation. This is illustrated in Fig. 6.1. Fluctuations orthogonal to the flow are not directly affected, but any coupling between fluctuations at differing wavevectors can ensure the premature relaxation of these fluctuations also [29, 82]. Since the onset of glassy behaviour is associated with the failure of fluctuations to relax, flow

prevents structural arrest.

Given the above arguments, we anticipate stress and flow having essentially opposite effects. One will tend to cause a slowdown of the dynamics, resulting in a more viscous material, whilst the other will tend to speed up relaxations and result in a less viscous response. However, the flow response to stress depends upon the viscosity, and so a material's state under a given imposed stress ought to be determined in a self–consistent fashion.

A microscopic approach?

Having identified the likely effects of shearing upon the colloidal glass transition, one would ideally like to formulate a first–principles theory which naturally captures both of these effects. A theory, based upon MCT, which captures the fluidisation under shear has already been devised [82, 29]. Expectation values of relevant quantities are obtained by calculation of overlap integrals with density fluctuations which, as in MCT, are treated as 'slow' variables. From first principles, this theory leads to predictions of the shear melting of colloidal glasses. It is found that, for nonzero shear rates, all fluctuations are ergodic.

In order to formulate a tractable theory, the authors were forced to make several approximations. One of these was to assume that the system remains near equilibrium, in the sense that internal forces in the material are taken to be described by the quiescent static structure factor. Whilst this approximation may suffice for the description of fluidisation under shear, it must preclude the theory from capturing dynamical arrest due to shear–induced changes to the structure. The difficulty of calculating such changes is a major obstacle to improving upon this situation. However, it is not the only one: as we have seen, in MCT, one approximates the nonlinear coupling between density fluctuations by projecting onto density pairs. In a simplified version of MCT, this is equivalent to writing the Hamiltonian of the system as an integral over a bilinear product of densities [116] with the direct correlation function acting as an effective potential. Since jamming may be associated with extended clusters, one might expect that an improvement to this harmonic approximation will be necessary – in other words $S(q)$ may not be a suffficiently good description of the structure to capture thickening and jamming.

So, it appears that the formulation of a microscopic theory which captures both of these effects

is a particularly challenging task. It seems likely that one would have to improve upon the quiescent MCT *as well* as adapt it to deal with sheared suspensions. In the work presented here, we take a simpler approach, utilising a schematic MCT model, altered to introduce competition between the effects described above. We shall also take a scalar approach: the only stress in the model shall be regarded as the shear stress, and the only deformation shall be the shear rate. Scalarising is a fairly common simplification to make in theories of nonlinear rheology [9] although, obviously, this is not wholly satisfactory.

6.2 The formulation of a schematic model

We shall now formulate a model based upon the schematic F2 model described in Ch. 4. Recall that the equation of motion for a density correlator within an schematic model for a colloidal suspension is

$$\phi(t) + \tau_o\dot{\phi}(t) + \int_0^t m(t-t')\dot{\phi}(t')\,dt' = 0, \tag{6.1}$$

with $m(t) = v_2\phi^2(t)$ for an F2 model. The wavevector dependent parent of this equation holds rigorously for a quiescent colloidal suspension. However, its derivation fails outwith thermodynamic equilibrium, where the fluctuation–dissipation theorem (FDT) no longer holds. (This is most easily seen in an alternative approach [117] to the projection operator formalism described in Appendix A. In this formalism, one derives separate equations for the correlation and the response: in the special case of equilibrium, the fluctuation–dissipation theorem allows one to collapse these equations onto the MCT described in Ch. 4). However, in the first–principles theory of rheology mentioned above, the authors obtain an equation which is remarkably similar to that of the quiescent MCT, with the caveat that the origin of time in their equations refers to the start–up of the flow. They also found that a schematic version of their model, in which the MCT vertices were altered to mimic their variation due to flow in the microscopic model, provided qualitatively similar results to the more sophisticated approach [82].

This suggests that the character of the MCT survives generalisation to sheared systems, whilst the memory function becomes altered by shear. With this in mind, we assume that we may describe sheared systems using a schematic model, whilst modifying the coupling 'constant'

in order to describe the effect of shearing upon the system's memory. The form of this dependence is motivated by simulation of sheared suspensions, experimental observations and intuition. However, the exact mathematical form is, unavoidably, somewhat arbitary. To guard against this affecting the results unduly, variations to the choices described below were also investigated. In the following, we will describe the model on which most time was spent, whilst highlighting those places in which alternative options were also considered. The results of those alternatives will be discussed in Ch. 8.

The effect of shear stress

The first alteration which we make to the static F2 model is to allow the coupling to increase with shear stress. The most obvious way to do this is to assume a regular expansion of the coupling about the unstressed state, *ie*,

$$v_2 \to v_o + a\sigma + b\sigma^2 + c\sigma^3 + \ldots \tag{6.2}$$

One can then neglect the odd powers of σ on the grounds of symmetry – the material should not respond differently to being sheared in opposite directions.

However, this approach is limited. It is best suited to cases in which one is interested in the region around $\sigma = 0$, as in order to make progress, one neglects higher order terms. But we have no reason to believe that this is the region of interest: if one is concerned with a region of stress away from $\sigma = 0$, a different approach may be needed. Therefore, in the following we consider a second case, in which we model the effect of stress by $v_2 \to v_o + \alpha\sigma$ (where σ should be regarded as an absolute magnitude so that symmetry is not violated). Whilst this prescription suggests a nonanalyticity at $\sigma = 0$, we do not consider it as a linearisation around the unstressed state. Rather, it is a way in which we can account for a sub–quadratic (specifically linear) rise in the coupling at values of stress away from zero (which is certainly not forbidden by symmetry). One can consider this approach as a linearisation of the coupling around some nonzero stress, in which case v_o need not exactly coincide with the coupling at zero–shear. Thus, this approach is somewhat complementary to that of expanding around the unstressed state: in the latter, whose results we shall show in Ch. 8, one expects to capture the

correct behaviour for $\sigma \to 0$, whilst the former is less restrictive for larger stresses (and will turn out to result in richer phenomenology).

The effect of shear flow

The second modification that we make is to recognise the fluidising effect of flow. The effect of this upon the memory function in an MCT–like theory has been calculated by Fuchs and Cates [82]. Wavevectors q are advected by the flow to higher values $q(t) = \sqrt{q^2 + 2k_x k_y + k_x^2 \dot{\gamma}^2 t^2}$ (for a flow in the x–direction with gradient in the y–direction: *cf* Fig. 6.1). Such advected wavevectors appear within the vertex in their theory, 'killing off' the coupling at late times (through the vertex) and thus restoring ergodicity for any flow rate.

In the models presented here, we allow for a vertex which vanishes at large accumulated strains. In the primary model which we discuss, we choose an exponential decay $m(t) \sim \mathrm{e}^{-\dot{\gamma}t}$ (more precisely, we should consider the absolute magnitude of the shear rate). Similarly to the situation regarding the stress, we are primarily interested in $\dot{\gamma}t \gtrsim 1$, and so the apparent nonanalytic dependence at small strains is again immaterial. However, in order to ensure that this choice does not unduly influence the results, in Ch. 8 we consider a second model for which $m(t) \sim \frac{1}{1+\dot{\gamma}^2 t^2}$.

The memory function under shear

Depending upon the precise mathematical form chosen, various memory functions are possible. The main body of our work has focused on the memory function defined by the primary choices described above, giving

$$m(t) = (v_o + \alpha\sigma)\mathrm{e}^{-\dot{\gamma}t}\phi^2(t). \tag{6.3}$$

As mentioned, we will return to variations of this form, and make a comparison of the results.

The viscosity

In the proposed memory function (and generalisations thereof), the effect of shear appears in two quite separate ways, via the applied stress σ and the resulting shear rate $\dot{\gamma}$. These two

quantities are, of course, not independent, but are related through the viscosity $\eta \equiv \sigma/\dot{\gamma}$, which may vary. In order to complete the definition of our scalar model, we need a prescription for the viscosity, so that upon specifying an applied stress, all other quantities are fixed. In linear response theory, the shear viscosity is expressed as the time integral of a stress correlator [72]. In our schematic model, we have only one correlator, and choose

$$\eta = \int_0^\infty \phi(t)\, dt = \tau, \tag{6.4}$$

where we have chosen units such that stresses are dimensionless. Thus, the viscosity equates to a characteristic relaxation time τ.

Whilst we are not studying just the linear regime in this work, this prescription is, we believe, a suitable choice. In MCT, the shear viscosity diverges as the relaxation time of correlators as one approaches the glass transition (and this correspondence in not lost under shear [29, 82]): this is captured by Eq. 6.4. Writing η as (say) the integral of ϕ^2, would also capture this, but leads to very similar results. With this prescription, dynamical arrest implies a divergent viscosity and hence zero shear rate. This is consistent with the idea, discussed above, that shear flow prevents arrest.

Our model is now fully defined: we have

$$\phi(t) + \tau_o \dot{\phi}(t) + \int_0^t m(t-t')\dot{\phi}(t')\, dt' = 0, \tag{6.5}$$

$$m(t) = (v_o + \alpha\sigma)\mathrm{e}^{-\dot{\gamma}t}\phi^2(t), \tag{6.6}$$

$$\eta = \int_0^\infty \phi(t)\, dt. \tag{6.7}$$

Having devised the model, we now proceed to study it in some depth. We do so by a combination of analytic and numerical work.

6.3 Solution of the model

The conventional F2 model may be studied analytically by asymptotic expansions around the glass transition. Close to the transition, these techniques yield the characteristic signatures of the MCT glass transition (see Ch. 4). Here, we adapt these techniques to deal with the additional complexity present in our model over the F2 model.

The F2 model has also been studied numerically, using a standard algorithm [118]. To adapt this technique to the present situation, one needs to adapt a code which solves the standard F2 model in a simple way – this is outlined later. Firstly though, we describe our analytic study of the model.

6.3.1 Analytic solution

Many of the following methods are adapted from standard techniques used in solution of the MCT equations of motion (See, *eg* [95]). We begin by defining a Laplace transform:

$$f(z) \equiv \mathcal{L}[f(t)](z) \equiv i \int_0^\infty f(t) \mathrm{e}^{izt}\, dt; \;\; Im(z) > 0. \tag{6.8}$$

Then, Laplace transforming Eq. 6.1, we obtain

$$\phi(z) = \frac{-1}{z - \frac{1}{i\tau_o + m(z)}}. \tag{6.9}$$

Close to a glass transition, the condition $|\tau_o| \ll |m(z)|$ will hold for low frequencies – in other words, close to the glass transition the dominant source of low–frequency friction arises from the cage effect, which the mode–coupling approximation to the memory function describes. Since we are interested in low-frequency dynamics, we make the approximation of ignoring the regular part of the memory function. For clarity in what follows, we shall label the position in parameter space by the vector $\mathbf{v} \equiv (v_o, \alpha, \sigma)$ – these labels shall appear as subscripts. Ignoring the regular part of the memory, we have

$$\frac{z\phi_{\mathbf{v}}(z)}{1 + z\phi_{\mathbf{v}}(z)} = z m_{\mathbf{v}}(z). \tag{6.10}$$

A familiar result

We split the correlator into the sum of its late–time limit and a (time–dependent) remainder: we write $\phi_{\mathbf{v}}(t) = f_{\mathbf{v}} + g_{\mathbf{v}}(t)$. Now let us assume that, for suitable values of the relevant parameters, our model admits nonergodic solutions. In a nonergodic state the relaxation time τ is divergent and so $\dot{\gamma} = 0$ for any finite stress. Therefore, upon taking the zero-frequency limit of Eq. 6.10, we obtain the result

$$\frac{f_{\mathbf{v}}}{1 - f_{\mathbf{v}}} = V f_{\mathbf{v}}^2, \tag{6.11}$$

where $V = v_o + \alpha\sigma$. Here, we have used the fact that, since $g_{\mathbf{v}}(t)$ tends to zero at late times, terms $\sim g_{\mathbf{v}}(t)$ give rise to singularities weaker than $\sim 1/z$ as $z \to 0$.

This result fixes the nonergodicity parameter of a glassy state with coupling V: it has nonzero solutions for $f_{\mathbf{v}}$ provided $V \geq 4$, indicating that glassy solutions become possible beyond this value of the coupling. However, this need not imply that our model undergoes a glass transition at $V = 4$, since we have calculated this by assuming *a priori* that we are in a glassy state, and thus $\dot{\gamma} \equiv 0$. By doing so, our model reduces exactly to the F2 model, and so this result, which holds for the F2 model, is inevitable. It has been shown that the nonergodicity parameter is the largest of the solutions to Eq. 6.11 [95]. (The smaller solution would require that the nonergodicity parameter becomes smaller upon increasing coupling, which seems unlikely.)

MCT glass transitions lead to a characteristic behaviour of the nonergodicity parameters: they jump discontinuously from zero on the liquid side of the transition, to a finite value as the transition is breached. Further increasing the coupling, there is a nonanalytic (square root) variation from the value at the transition. Eq. 6.11 tells us that such behaviour will be present in the current model if and only if the transitions occur at the F2 value of $V = 4$. We shall return to this point at a later stage. (Of course, it still remains for us to investigate where in parameter space these transitions occur, if indeed they exist at all.)

A Low–frequency expansion

We now consider the behaviour of correlation functions close to transition points (assuming that the latter exist). We write $\phi_{\mathbf{v}}(t) = f_{\mathbf{v}_c} + g_{\mathbf{v}}(t)$, where $f_{\mathbf{v}_c}$ is the long time limit of the

correlator at a point $\mathbf{v}_c$ on the locus of transition points to nonergodic states. Since we study correlators close to the transition points $|\mathbf{v} - \mathbf{v}_c|$ is a small quantity.

To guide our treatment of Eq. 6.10, we consider what we know of conventional MCT behaviour (which, from the previous section, tells us the behaviour of the correlator at transition points in the current model). A glassy correlator decays onto a plateau on the β–relaxation time, where it then remains for all time. In the current model, transitions will be at $V \geq 4$, and we might expect the inequality to hold, due to the fluidising term in the memory. Thus, on timescales for which $\dot{\gamma}t \ll 1$, the correlators $\phi_{\mathbf{v}}(t)$ and $\phi_{\mathbf{v}_c}(t)$ will be very similar. By considering $|\mathbf{v} - \mathbf{v}_c|$ arbitrarily small, we can ensure that they do not become strongly separated until $\phi_{\mathbf{v}_c}(t)$ has essentially reached its long time limit. Thus, there will be a regime of time for which $g_{\mathbf{v}}(t)$ is a small quantity.

In Laplace–space, the separation of the correlator into a constant plus a remainder reads $z\phi_{\mathbf{v}}(z) = -f_{\mathbf{v}_c} + zg_{\mathbf{v}}(z)$. In line with standard MCT techniques [95], we now treat $g_{\mathbf{v}}(z)$ perturbatively in the Laplace transformed equation of motion, Eq. 6.10. Expanding the LHS in powers of $g_{\mathbf{v}}(z)$, we find

$$\begin{aligned}\frac{z\phi_{\mathbf{v}}(z)}{1+z\phi_{\mathbf{v}}(z)} &= \left(\frac{-f_{\mathbf{v}_c}}{1-f_{\mathbf{v}_c}} + \frac{zg_{\mathbf{v}}(z)}{1-f_{\mathbf{v}_c}}\right)\left(1 - \frac{zg_{\mathbf{v}}(z)}{1-f_{\mathbf{v}_c}} + \frac{z^2g_{\mathbf{v}}^2(z)}{(1-f_{\mathbf{v}_c})^2} + \mathcal{O}(z^3g_{\mathbf{v}}^3(z))\right) \\ &= \frac{-f_{\mathbf{v}_c}}{1-f_{\mathbf{v}_c}} + \frac{zg_{\mathbf{v}}(z)}{(1-f_{\mathbf{v}_c})^2} - \frac{z^2g_{\mathbf{v}}^2(z)}{(1-f_{\mathbf{v}_c})^3} + \mathcal{O}(z^3g_{\mathbf{v}}^3(z)). \qquad (6.12)\end{aligned}$$

We now wish to approximate the RHS in the same regime of frequency. Considering the memory function in the time domain, we expect that $\dot{\gamma}t$ (as well as $g_{\mathbf{v}}(t)$) can be treated perturbatively, since it is the shear–induced memory loss which prompts the growth of $g_{\mathbf{v}}(t)$. We also treat the separation from the transition as small: we write

$$V = V_c + \epsilon, \qquad (6.13)$$

where V_c is the value of V at the transition point $\mathbf{v}_c$. We find the (time–domain) memory function to be

$$m(t) = (V_c + \epsilon)\left(f_{\mathbf{v}_c}^2 + 2f_{\mathbf{v}_c}g_{\mathbf{v}}(t) + g_{\mathbf{v}}^2(t)\right)\left(1 - \dot{\gamma}t + \mathcal{O}(\dot{\gamma}^2t^2)\right). \qquad (6.14)$$

In the time regime of interest, terms $\mathcal{O}(g(t)\dot{\gamma}t)$ and $\mathcal{O}\left(g^2(t)\right)$ are negligible with respect to terms $\mathcal{O}\left(g(t)\right)$. Additionally, terms $\mathcal{O}\left(\epsilon g(t)\right)$ and $\mathcal{O}\left(\epsilon\dot{\gamma}t\right)$ may be neglected with respect to

terms $\mathcal{O}(\epsilon)$. The RHS of Eq. 6.10 then becomes

$$zm(z) \approx -Vf_{\mathbf{v}_c}^2 + 2f_{\mathbf{v}_c}V_c z g_{\mathbf{v}}(z) - V_c f_{\mathbf{v}_c}^2 z\dot{\gamma}\mathcal{L}[t](z). \tag{6.15}$$

Using Eq. 6.11 (evaluated at the transition), we find that Eq. 6.10 becomes, asymptotically close to the transition,

$$zg_{\mathbf{v}_c}(z)\left(\frac{1}{(1-f_{\mathbf{v}_c})^2} - 2f_{\mathbf{v}_c}V_c\right) + zV_c f_{\mathbf{v}_c}^2\dot{\gamma}\mathcal{L}[t](z) + f_{\mathbf{v}_c}^2\epsilon = 0. \tag{6.16}$$

Performing the back Laplace transform, we find the correlator in the time domain to be

$$\phi(t) \approx f_{\mathbf{v}_c}\left(1 + \frac{\epsilon f_{\mathbf{v}_c}}{\frac{1}{(1-f_{\mathbf{v}_c})^2} - 2f_{\mathbf{v}_c}V_c}\right)\left(1 - \frac{V_c f_{\mathbf{v}_c}\dot{\gamma}t}{\frac{1}{(1-f_{\mathbf{v}_c})^2} - 2f_{\mathbf{v}_c}V_c + \epsilon f_{\mathbf{v}_c}}\right), \tag{6.17}$$

or, expressed more succinctly,

$$\phi(t) = f\,(1 - t/\tilde{\tau}) \tag{6.18}$$

with f and $\tilde{\tau}$ defined appropriately. This expression is consistent with an exponential decay from the plateau at late times: we shall show in Ch. 7 that an exponential decay from the plateau does indeed agree with the numerical results which we have obtained.

Transition points

We now investigate the possibility of 'jamming transitions', distinct from the conventional F2 transition at $V = 4$, within our model. We begin by evaluating Eq. 6.9 at $z = 0$ to deduce

$$\tau = \tau_o - im(0). \tag{6.19}$$

We have just shown that, close to the transition, the correlator is consistent with an exponential at late times. Motivated by numerical results, we assume that this is the correct late–time form of the correlation functions. As we approach a jamming transition, the relaxation time of this exponential diverges (since the shear rate vanishes at the transition point), whilst the β-relaxation timescale remains finite[1]. Therefore, at the transition, the contribution from the

[1] At an MCT transition, both the α and β relaxation timescales diverge. However, in general the transitions described here do not occur at these points, and so the β relaxation time remains finite

exponential completely dominates over the short time (non-exponential) contribution. Accordingly, Eq. 6.19 becomes

$$\tau = \tau_o + V\int_0^\infty \exp(-\dot{\gamma}t)\phi^2(t)\,dt \tag{6.20}$$

$$\approx V\int_0^\infty \exp(-\dot{\gamma}t) f^2 \exp(-2t/\tilde{\tau})\,dt, \tag{6.21}$$

where we have approximated the correlator by $\phi(t) = f\exp(-t/\tilde{\tau})$ over the whole temporal range, and dropped the (non–divergent) contribution from the regular part of the memory function. By definition, $\tau = \int_0^\infty \phi(t)\,\mathrm{d}t$, and so we require $\int_0^\infty f\exp(-t/\tilde{\tau}) = \tau$, giving $\tilde{\tau} = \tau/f$.

We now write this as an iteration: the nth approximation to the relaxation time is calculated using the $(n-1)th$ value to determine the shear rate. Thus

$$\tau^{(1)} \approx f^2 \int_0^\infty V\mathrm{e}^{-\sigma t/\tau^{(0)}}\mathrm{e}^{-2ft/\tau^{(1)}}\mathrm{d}t, \tag{6.22}$$

which we can solve to give the ratio of $\tau^{(1)}$ to $\tau^{(0)}$:

$$\frac{\tau^{(1)}}{\tau^{(0)}} = \frac{f}{\sigma}\left(Vf - 2\right). \tag{6.23}$$

The key point to note is that the ratio is independent of $\tau^{(0)}$: thus, no matter how large the initial guess, the iteration leads to a larger value if the RHS is greater than unity. This suggests that, where this is the case, the relaxation time is divergent. Thus, setting the RHS=1 in Eq. 6.23, we conclude that the transitions to glassy states occur at stresses σ_c which obey

$$f_c\left[(v_o + \alpha\sigma_c)f_c - 2\right] - \sigma_c = 0, \tag{6.24}$$

where f_c is given by the largest solution of $\frac{f_c}{1-f_c} = (v_o + \alpha\sigma_c)f_c^2$ (from Eq. 6.11).

These transition points do not coincide with the F2 transition and have a different character to MCT transitions in general. These differences shall be investigated later. From a rheological point of view, we have found values of the stress for which the shear rate first becomes zero – *ie*, jamming transitions. The location of these transitions according to Eq. 6.24 will later be checked against a numerical solution for the full flow curves.

Behaviour at large stresses

As well as finding the transition points, one would like to build up a picture of the flow behaviour. Let us begin by investigating the large-stress behaviour of the system. We begin by postulating a situation in which the relaxation time diverges in the limit of large stress: in this case, Eq. 6.23 tells us that

$$\lim_{\sigma\to\infty} \frac{\tau^{(1)}}{\tau^{(0)}} \geq 1 \tag{6.25}$$

which, implies that

$$\lim_{\sigma\to\infty} \alpha f^2 \geq 1. \tag{6.26}$$

This can only be satisfied if $\alpha \geq 1$, since in a glass the nonergodicity parameter f approaches unity in the limit of large stress (see Eqs. 6.11 and 6.13). Therefore, nonergodic solutions may only be admitted in the limit of large stress if $\alpha \geq 1$.

Therefore, we can be sure that, for $\alpha < 1$, the shear rate can be made arbitrarily large by ramping up the stress, since the relaxation time does not grow unbounded. In this case, we can calculate the relaxation time in the large stress limit from Eq. 6.20. Only the region $t \sim 1/\dot{\gamma}$ contributes significantly to the integral, and for large shear rates this region becomes arbitrarily small. Thus, we may expand the correlator in powers of t [119], giving

$$\int_0^\infty \mathrm{e}^{-\dot{\gamma}t}\phi^2(t)\mathrm{d}t \approx \int_0^\infty \mathrm{e}^{-\dot{\gamma}t}\left(\phi^2(0) + \mathcal{O}(t^2)\right)\mathrm{d}t, \tag{6.27}$$

where we have used the initial condition that $\dot{\phi}(0) = 0$. We use the second boundary condition ($\phi(0) = 1$) to give

$$\tau \approx \tau_o + V\int_0^\infty \mathrm{e}^{-\sigma t/\tau}\mathrm{d}t \tag{6.28}$$

which is solved in the limit of large stress by

$$\tau = \frac{\tau_o}{1-\alpha}. \tag{6.29}$$

These results suggest that at $\alpha = 1$ the large–stress relaxation time diverges. Let us now consider the situation for which both the shear rate and the relaxation time grow unbounded for large stresses: this occurs if τ grows sublinearly with σ at large stresses. In this case we have that $\alpha \geq 1$ *and* $\tau = \frac{\tau_o}{1-\alpha}$, implying that $\alpha = 1$, else the relaxation time becomes negative.

This analysis shows that $\alpha = 1$ is a 'watershed' between ergodic and nonergodic solutions in the limit of large stress. For $\alpha < 1$, solutions are ergodic with the viscosity approaching a constant value; for $\alpha = 1$ there is the rather unusual situation that both the viscosity and the shear rate grow unbounded with applied stress; and for $\alpha > 1$, we have that, at sufficiently large stresses, the system is a solid and there is no (steady state) flow.

Small coupling behaviour

For completeness, we outline a way to find asymptotes at small values of the stress, provided that v_o is also small (although this condition will not be met for a system representing a dense supension).

To zeroth order in the coupling V, Eq. 6.1 becomes the simple differential equation

$$\phi(t) + \tau_o \frac{\mathrm{d}\phi}{\mathrm{d}t} = 0$$

with solution $\phi(t) = \exp(-t/\tau_o)$. For small values of the coupling, one expects that the correlator remains exponential to a good approximation, but with an altered relaxation time. Therefore, let us construct a zeroth–order memory function by taking ϕ to be an exponential with some (as yet undetermined) relaxation time. (Fixing the relaxation time as τ_o, one simply recovers the known zeroth–order correlator.) The largest timescale in the system is τ, and so $\dot{\gamma}t \lesssim \dot{\gamma}\tau \equiv \sigma$ which we may choose arbitrarily small. Therefore, we may approximate the fluidising exponential term by unity.

These approximations result in a memory function $m^{(0)}(t) = V\exp(-2t/\tau)$. We then wish to solve the equation

$$\phi^{(1)}(t) + \tau_o \dot{\phi}^{(1)}(t) + \int_0^t m^{(0)}(t-t')\dot{\phi}^{(1)}(t')\,dt' = 0 \tag{6.30}$$

for $\phi^{(1)}(t)$. Taking a Laplace transform and simplifying, we obtain

$$\phi^{(1)}(z) = \frac{z\tau + 2\tau i\tau_o + Vi}{2/\tau_o - iz - z^2\tau - 2iz\tau/\tau_o - iVz}. \tag{6.31}$$

Factorising the denominator and expanding in partial fractions allows us to perform the inverse transform, which gives the solution in the time domain as a sum of two exponentials. This

reminds us that (save for the trivial case $V = 0$) our initial guess as to the form of the correlator was incorrect, since this is not self–consistent. However, the two correlators should agree in the limit of small coupling: this is ensured by demanding that they have the same relaxation time, *ie*, $\tau^{(1)} \equiv \int_0^\infty \phi^{(1)}(t)\,\mathrm{d}t = \tau$. Doing so gives the relaxation time of the system in the limit of small coupling as

$$\tau = \frac{2\tau_o}{2 - V}. \tag{6.32}$$

6.3.2 Numerical solution

MCT models may be solved numerically using an established algorithm [118]. The difficulty in finding solutions to these models obviously results from the convolution integral. This algorithm simplifies the integral term in the following way. Eq. 4.15 is written (ignoring inertia, dropping **q**–subscripts, and absorbing Ω^2 into the memory function)

$$\phi(t) = M(t) - \frac{d}{dt}\int_0^t M(t - t')\phi(t')\,dt'. \tag{6.33}$$

In this form, the correlation function at time t may calculated from those at earlier times. The integral I in this equation is re–written in terms of a constant term and two integrals:

$$I = \phi(t/2)M(t/2) + \int_0^{t/2} \dot{M}(t - t')\phi(t')\,dt' + \int_0^{t/2} \dot{\phi}(t - t')M(t')\,dt'. \tag{6.34}$$

The important point is that the integrands are the product of a term which varies quickly only for early times (*eg*, $\dot{\phi}(t')$) and one which varies quickly only for late times (*eg* $M(t - t')$). When these integrals are discretised, this allows the slowly varying term to be treated as constant over a small interval, simplifying the integrals. The neglected term is cubic in the timestep. By evaluating the integral in this manner, the temporal evolution of the correlator may be calculated. For full details, see the original reference [118].

In order to adapt this algorithm to deal with our model, we employ the following procedure:

1. Input the parameters (α, v_o and σ) which one wishes to study.

2. Make a guess at the relaxation time of the correlation function for these parameters.

3. Calculate the shear rate using this relaxation time and the chosen value of the stress. This defines a time dependent F2 vertex.

4. Solve the time–dependent F2 model as outlined above to yield a correlation function.

5. Re–calculate the relaxation time by integrating the correlator.

6. Repeat from step 3 onwards using the new value of the relaxation time until it converges upon a self–consistent solution.

The code used was adapted from a FORTRAN F2 solver by Matthias Fuchs. It has been checked that it reproduces the expected F2 results for $\sigma = 0$. The code was used to generate values of the relaxation time τ, as well as plots of the correlation function $\phi(t)$ for a given parameter set.

For some parameters close to a nonergodicity transition, the code becomes slow to converge. In these cases, the initial guessing of the relaxation time becomes important, in that for a 'bad' initial guess, long runs are required for the code to converge upon the self–consistent solution. A work–around to this problem is for users to manually iterate their guesses at the relaxation time: one guesses an initial value then, according to whether this value increases or decreases upon computational iteration, one makes another estimate, attempting to obtain bounds upon the correct value. Once the correct value is known roughly, the code may be left to obtain it to the desired accuracy, but in some cases it proved simpler and quicker to continue 'by hand' in the manner described above until a satisfactory bound upon the value was obtained. The stability of results obtained in this manner was then checked by entering the upper and lower bounds as initial guesses, and checking that in each case the code returned a value within the expected range. This crude but effective method could no doubt be improved upon with a more sophisticated code.

In the following chapter, the results obtained numerically are presented and compared with the analytical results derived in the previous section.

Chapter 7

Results of the Jamming Model

In this chapter we present results obtained from the model described in Ch. 6. We begin by showing the flow curves obtained for a range of parameters. We then concentrate upon the jamming transitions showing, via 'phase diagrams', that parameter space splits into regions of ergodicity/nonergodicity. We also show results for the correlation functions of the model close to these transitions.

7.1 Model flow curves

The steady state rheological behaviour of our model is completely characterised by the flow curves, since we have reduced the stress and deformation tensors to two scalars. Upon varying the parameters, our model leads to a wide variety of flow curves. We might expect that the most interesting behaviour will be found close to the glass transition, as in that region there is the possibility for interplay between the long relaxation times and the effect of shearing. Recalling the 'meaning' of the parameters v_o and α, we therefore expect that the most interesting behaviour will be found for $v_o \approx 4$. For hard sphere colloids, discontinuous thickening tends to occur for concentrations $\phi \gtrsim 0.5$, for which the zero shear viscosity is around 50 times that at zero–concentration [79]. Thus, we shall begin by studying values of v_o for which the zero–shear viscosity (relaxation time) $\tau \gtrsim 50$: here, and in the rest of this chapter, we use units such that $\tau_o = 1$. As the parameter α does not have such an obvious experimental analogue, it

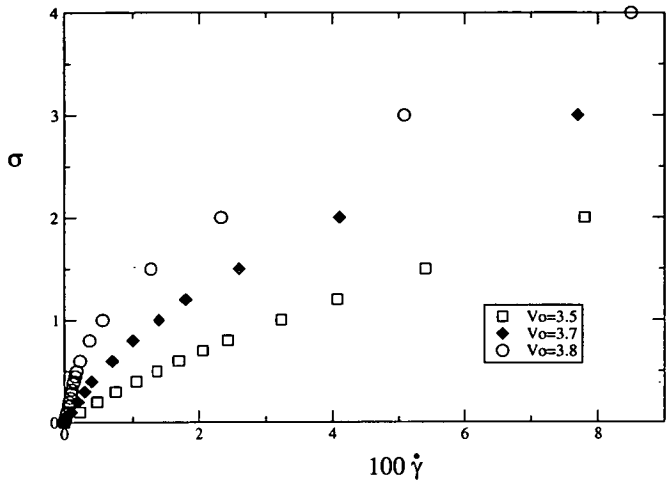

Figure 7.1: Model flowcurves for $\alpha = 0.95$. For this range of v_o, shear thinning is clearly present and, for $v_o = 3.8$, thickening is just about discernable at low stresses. At larger values of the stress, small variations in the viscosity are present (*eg*, for $v_o = 3.5$ the viscosity increases from $\tau = 18.9$ at $\sigma = 20$ to $\tau = 19.0$ at $\sigma = 30$). However, these variations are sufficiently small that they are not obvious on the flow curves.

is not so obvious what values to start with. However, from the previous chapter, we expect that values of order unity can lead to stress–induced nonergodicity, so we concentrate upon values in this range.

By taking the viscosity as equal to a relaxation time, we have made the stress dimensionless: therefore, stresses σ in the model should be compared to experimental stresses $\sigma_{exp} \sim \sigma G$ where G is the characteristic modulus of the material of interest (Ch. 1). In the model, we expect the stress to result in interesting behaviour when it is sufficiently large that $v_o + \alpha\sigma \sim 4$.

7.1.1 Variation of v_o

We begin by choosing a value $\alpha = 0.95$ and varying the value of v_o within the range $3.5 \leq v_o \leq 3.8$. (For $v_o = 3.5$, the viscosity at zero shear is $\tau = 45.6$, and so this corresponds to hard sphere concentrations in the vicinity of the equilibrium phase transition.) The flow curves for some parameters in this range are shown in Fig. 7.1. The most obvious feature is that, in

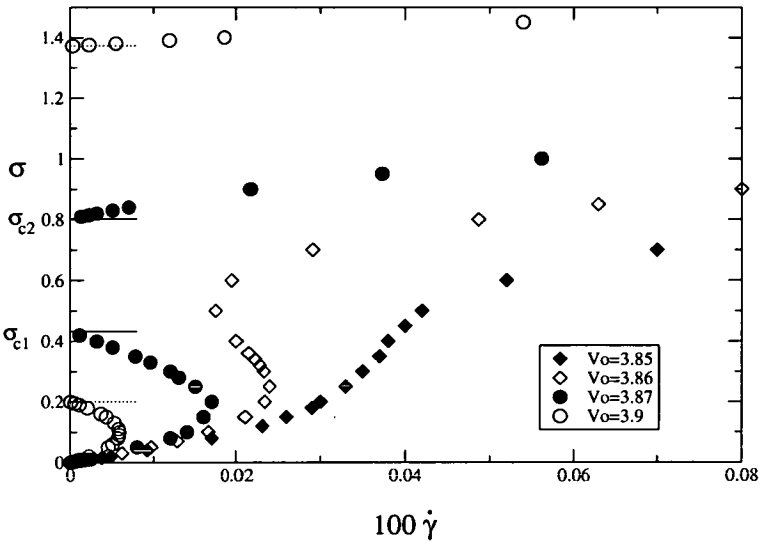

Figure 7.2: Flow curves, for $\alpha = 0.95$, for larger values of v_o. Shear thickening is apparent to such a degree that the curves become 'S-shaped' and, for the two largest values of v_o, there is a window of stress for which the viscosity (relaxation time) diverges. The limits of this window (denoted σ_{c1} and σ_{c2}, as shown here for one of the parameter sets), are 'jamming' transitions. The values of the stress at which these occur, according to Eq. 6.24, are shown as horizontal lines near the stress axis.

all cases, there is a regime of shear thinning. For the largest value of v_o, the shear thinning is proceeded by thickening at small applied stresses.

To investigate whether this trend to shear thickening develops, let us now move closer to the glass transition, and study the range $3.9 \leq v_o \leq 4$. In contrast to the rather gentle curves of Fig. 7.1, this leads to some rather more dramatic behaviour – see Fig. 7.2. As v_o is increased from 3.8, the predominately shear thinning behaviour shown in Fig. 7.1 is interrupted by strong shear thickening. For $v_o = 3.85$, the thickening is rather modest, whilst for the larger values of v_o shown, the thickening becomes so strong that regions of negative slope appear. In these regions, increasing the stress *lowers* the shear rate, which is exactly the opposite effect to that which it has in 'normal' circumstances. Recall that, as discussed in Ch. 2, regions of negative slope should be unstable to inhomogeneities – we shall discuss possible experimental signatures of an 'underlying' flow curve such as those in Fig. 7.2 in Ch. 9. Regardless of questions about stability, S–shaped flow curves such as there describe a situation in which too large a stress actually inhibits the flow of the material, reminiscent of many jamming situations.

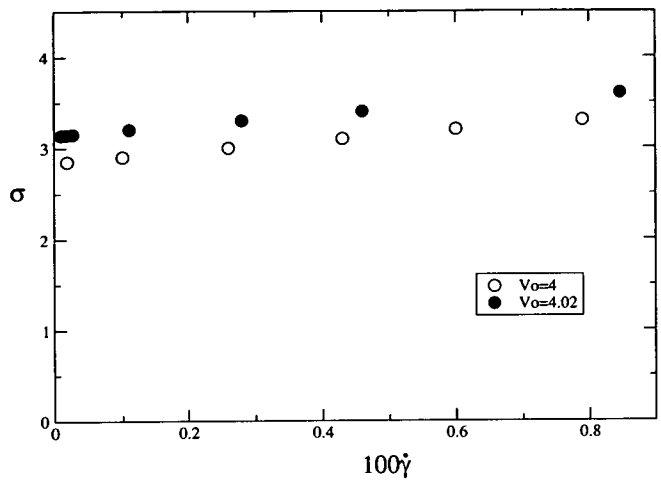

Figure 7.3: Flow curves for $\alpha = 0.95$, with v_o above the quiescent glass transition. Note the existence of a yield stress in each case – stresses below some threshold appear to result in divergent relaxation times, and so there is no steady–state flow. At stresses beyond the yield stress, the glass melts, and steady–state flow is possible.

For the two largest values of v_o shown, there is a window of stress for which the relaxation time has diverged – the system has became nonergodic due to the applied stress. We call the boundaries of the nonergodic state 'jamming transitions'. Their positions in parameter space, as calculated analytically in the previous chapter (Eq. 6.24), are seen to agree well with the numerical results. That such 'full jamming' occurs at all is not obvious from the definition of our model – particularly at late times, the vertex can decrease with increasing stress. We shall examine in detail the nature of these transitions at a later stage: for now, we continue surveying the behaviour for different values of the parameters.

By studying $v_o \geq 4$, we can examine the behaviour of systems which are nonergodic in the absence of shear. In this case, as shown in Fig. 7.3, there is no steady–state flow unless the stress is increased beyond a yield stress which increases with v_o. Given the behaviour at lower values of v_o for $\alpha = 0.95$, the presence of a yield stress is not surprising: Fig 7.2 shows that, at small stresses, there is a tendency to thicken. Therefore, it is not surprising that, for $v_o \geq 4$, small stresses cannot fluidise the system. The application of stresses beyond the yield stress lead to 'shear melting' of the glass, followed by a thinning viscosity, similar to the behaviour

at stresses above σ_{c2} in Fig. 7.2.

For smaller values of v_o than those discussed here, the rheology is much closer to Newtonian. For $v_o = 3$, for example, the viscosity changes only by $\sim 15\%$ upon increasing the stress between zero and $\sigma = 5$. Also, increasing v_o further introduces no new qualitative features: the yield stress increases monotonically with v_o, as one would expect. The results for $\alpha = 0.95$ can then be summarised as follows: far from the quiescent glass transition ($v_o \lesssim 3$), the rheology is quasi–Newtonian; for $3 \lesssim v_o \lesssim 3.8$, shear thinning is the main feature in the rheology. In the range $3.8 \lesssim v_o < 4$, shear thickening becomes more pronounced: upon increasing v_o the flow curve first becomes nonmonotonic, and then (for $v_o \gtrsim 3.866$) the curve reaches all the way back to the stress axis, indicating a jamming transition to a nonergodic state. Finally, for $v_o > 4$, a yield stress appears, below which there is no (steady–state) flow. Above this yield stress, behaviour is similar to that above σ_{c2} in the 'full–jamming' flow curves.

7.1.2 Variation of α

Having played around with the proximity to the quiescent glass transition, we now fix the value of v_o and investigate the effect of varying α. As we have mentioned earlier, the experimental meaning of α is not so obvious: it controls the extent to which the mode coupling vertex increases due to applied stress, and so seems related to the susceptibility of the static structure to external forcing.

If α is chosen sufficiently small (for a given value of v_o) then there is only shear thinning. This becomes of interest if the quiescent state is glassy, as this state can be fluidised by shearing. The nature of this fluidisation is not trivial, and so we shall return to this point later in this chapter. For now, we choose to vary α around 1, as this is large enough to provide competition between the thinning and thickening terms in the memory function. We initially choose $v_o = 3.9$ (for which the zero–shear viscosity is $\tau = 813.73$), which is sufficiently close to the quiescent glass transition to uncover some interesting behaviour.

Flow curves for a range of α less than unity are shown in Fig. 7.4. The variation in the curves with increasing α is qualitatively similar to that in Fig. 7.2, with the shear thickening becoming increasingly strong as α is increased. In contrast, for $\alpha \geq 1$, we expect to find a change in the

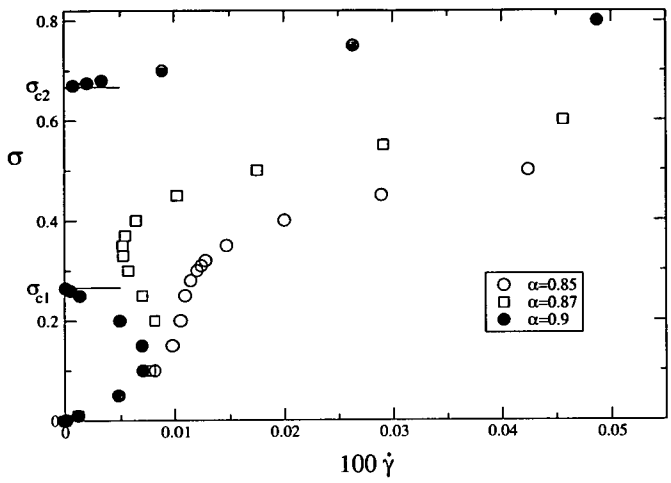

Figure 7.4: Flow curves at $v_o = 3.9$, which is close to the quiescent glass transition, for a range of values of α. For the largest value of α, there are jamming transitions at σ_{c1}, σ_{c2}. The analytical calculation of the transition points are shown as horizontal lines close to the stress axis.

behaviour, since in this case (Ch. 6), the large stress limit of the viscosity diverges. We present the flow curves arising in this region of parameter space in Fig. 7.5. In this case, the the system becomes nonergodic at some value of the stress but, in contrast to the previous case, does not 'unjam' upon increasing the stress. This is consistent with the result that, for $\alpha > 1$, $\lim_{\sigma\to\infty} \tau = \infty$. However, it is not the only possibility: there is a very small (for $v_o = 3.9$) range $1 < \alpha \lesssim 1.0032$ for which the system refluidises upon increasing the stress (as in, *eg*, Fig. 7.2), followed by a *second* region of jamming. Upon increasing the stress further, the system remains in this second nonergodic region. This behaviour is illustrated for $\alpha = 1.002$ in Fig. 7.6. As α is increased towards $\alpha^* \approx 1.0032$, both σ_{c2} and σ_{c3} tend to σ_{c1}, and thus the high–stress fluid region vanishes leading to the scenario of Fig. 7.5.

A final flow scenario is found at $\alpha = 1$. However, in this case it is difficult to resolve some important details of the flowcurve numerically: there is nontrivial structure to the flowcurve in regions where σ, $\dot\gamma$ and τ are all large. There is a 'low–stress' window of nonergodicity for $0.165 \lesssim \sigma \lesssim 5.935$. Upon increasing the stress further, the jammed state yields, followed by a second regime of thickening, in which the flow curve again has a region of negative slope, and τ

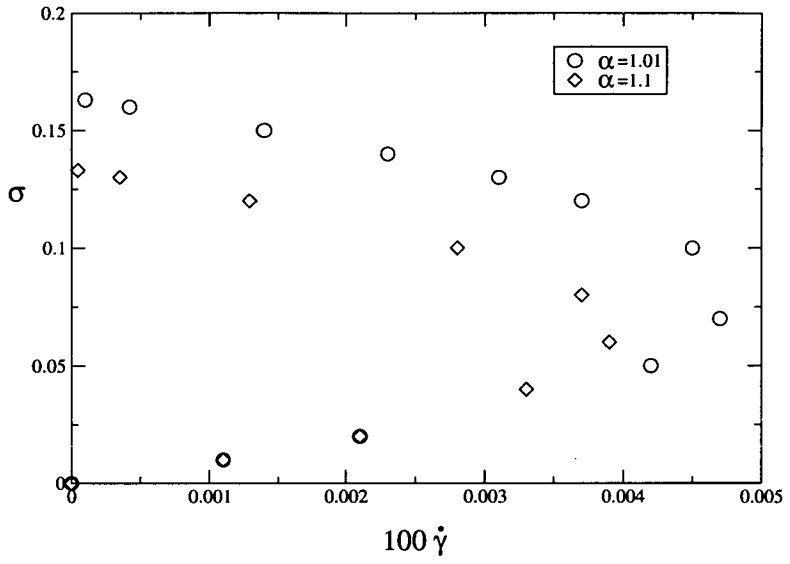

Figure 7.5: For these parameters, there is no refluidisation from the jammed state to a high stress fluid – one cannot break the jam by 'brute force'. As might be expected, larger values of α result in the jam occuring at lower values of the stress. At low stresses, the two curves are very similar.

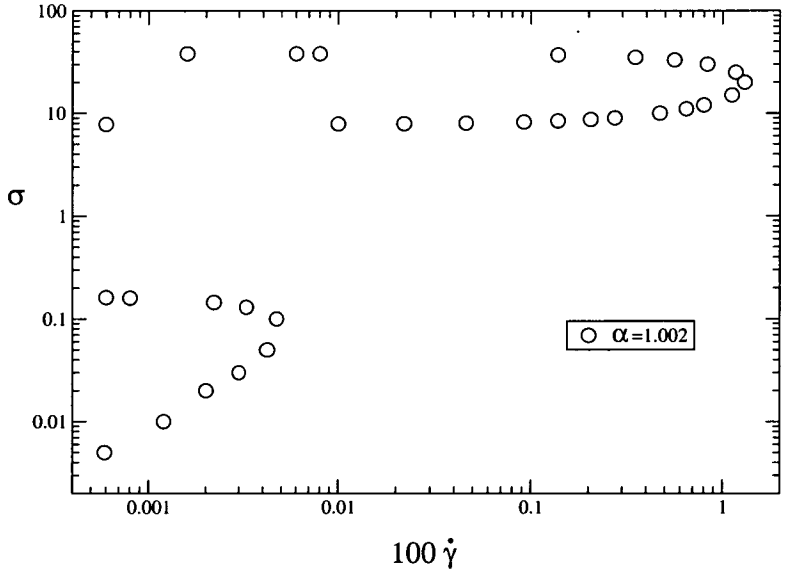

Figure 7.6: The flowcurve for $\alpha = 1.002$ (in a log–log plot). In this case, there are *two* windows of nonergodicity. Fluidisation from the second window by increasing the stress is not possible.

becomes too large to track. Numerically, this gives the impression that a second nonergodicity transition occurs: however, we shall see shortly (by examining Eq. 6.24) that this is not the case.

This concludes our initial survey of the model's rheology. The flow curves presented above cover the main scenarios that were found, and so we will not bore the reader by trotting out the curves for further parameter sets. In order to get an overview of the behaviour over a wide range of parameters, we now concentrate upon the jamming transitions, using Eq. 6.24 to elucidate their positions in parameter space, and then studying the nature of the transitions.

7.2 'Phase behaviour'

Using the analytical work of the previous chapter, we can calculate a 'phase diagram' for our model. To do so, we choose a value of v_o, then solve Eq. 6.24 (using the symbolic maths software Maple) to find the transition points for a range of values of α. This yields a line of transitions in parameter space, splitting it into ergodic and nonergodic regions. The phase diagrams provide us with an overview of the behaviour for a range of parameters without numerically calculating the flow curves for each case. The phase diagrams of the model for a range of v_o are shown in Fig. 7.7 and Fig. 7.8.

The phase diagrams show that, at a given value of v_o, there will be transitions to a nonergodic state provided α is sufficiently large. As v_o is decreased, the minimum value of α necessary for nonergodicity increases: for $v_o \lesssim 3.83$, there is no transition unless $\alpha > 1$, in which case a transition is guaranteed regardless of v_o. For $v_o \gtrsim 3.80$, there is a window in α for which the nonergodic region is finite in σ (see Fig. 7.8). If this window includes $\alpha > 1$, there is a second (infinite) range of stress in which the system is nonergodic (we saw this for the case $v_o = 3.9$ in the previous section).

Is there a yield stress?

As we approach the quiescent glass transition ($v_o = 4$), the minimum stress required to jam the system approaches zero (at fixed $\alpha > 0$). For $v_o \geq 4$, the system is glassy without shearing. In

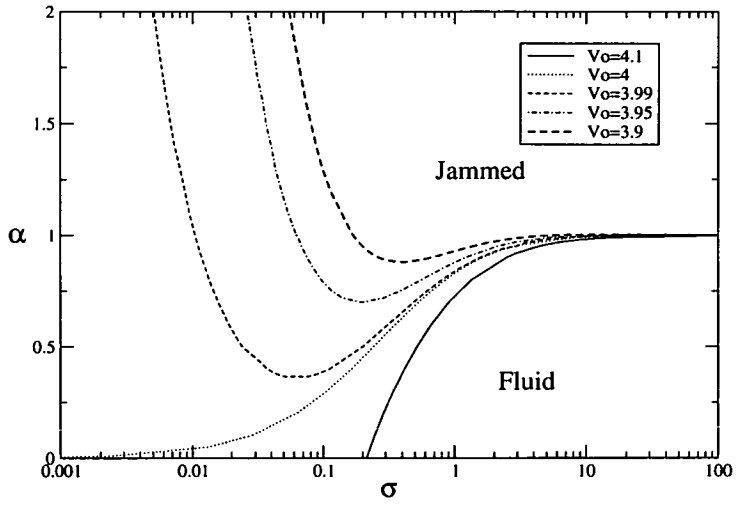

Figure 7.7: 'Phase diagrams' for the model at various v_o. The lines denote transitions in the (α, σ)–plane. All states below the curve for a given value of v_o are fluid states, whilst those above (and on) the line are nonergodic, jammed states.

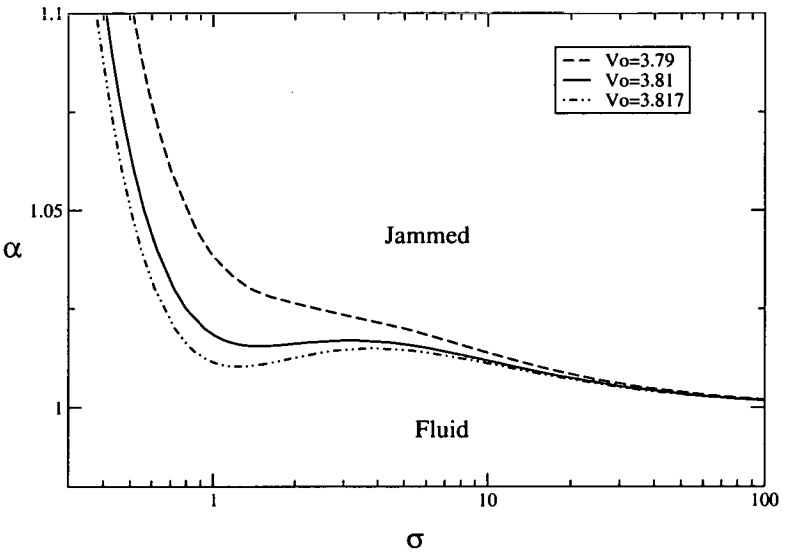

Figure 7.8: Phase diagrams for smaller values of v_o. Note that the diagram is on a different scale to Fig. 7.7 so that the features appear more clearly. As before, jammed states lie on or above the line for a given value of v_o. For this range of v_o, jammed states only appear for $\alpha > 1$.

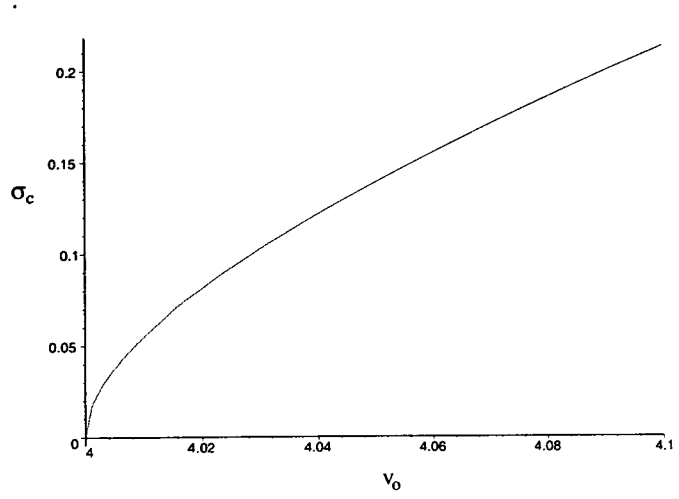

Figure 7.9: The yield stress of the 'shear thinning only' case $\alpha = 0$. The yield stress increases smoothly from zero at $v_o = 4$.

this case, provided α is not too large, we can cause fluidisation by shearing. This may be seen for the cases $v_o = 4$ and $v_o = 4.1$ in Fig. 7.7. It is interesting to ask whether or not a glass has a yield stress – *ie*, will any nonzero stress melt the glass, resulting in steady–state flow? For $v_o = 4.1$ it is rather obvious that a yield stress does indeed exist, but for $v_o = 4$ the situation as $\alpha \to 0$ is not clear from the diagram. To answer this question, we examine Eq. 6.24 with $\alpha = 0$. This gives an expression for the stress σ_c at the transition, in terms of v_o:

$$\sigma_c = v_o/2 - 2 + (v_o/2 - 1)\sqrt{1 - 4/v_o}. \tag{7.1}$$

We show, in Fig. 7.9, the $\alpha = 0$ yield stress as a function of v_o. The yield stress vanishes at $v_o = 4$. Thus, *at* the glass transition, an arbitrarily small stress is predicted to melt the glass. This is at odds with related work [82], in which a nonzero yield stress appears at the glass transition. We return to this point in Ch. 9.

Large stress behaviour

We note that the large stress behaviour is governed by α, in agreement with the approximate analysis of Sec. 6.3.1. By $\sigma \sim 100$, the phase shows only a weak dependence upon v_o:

the system is in a nonergodic (ergodic) state for $\alpha \gtrsim 1$ ($\alpha \lesssim 1$). The line $\alpha = 1$ is of particular interest, as we were unable to elucidate the behaviour in this case using numerics. As mentioned above, if v_o is sufficiently small there are no transitions at finite σ unless $\alpha > 1$. For $\alpha = 1$, the system remains ergodic at all finite stresses if v_o is less than a threshold value $v_o \approx 3.83$. For larger values of v_o (such as the case $v_o = 3.9$ which we studied numerically) there is a finite window in stress for which the solutions are nonergodic (unless $v_o \geq 4$ in which case the system is jammed for any finite stress): beyond this window the system remains ergodic for all finite stress. This is in contrast to the impression given by a numerically determined flow curve: since the relaxation time becomes very large, the flowcurve suggests the presence of transitions beyond the initial window of nonergodicity.

The nature of the jamming transitions

Having considered the position of the transitions in parameter space, let us note that they are rather different in character to the conventional MCT glass transitions. The jamming transitions are not associated with the first appearance of nonergodic solutions (which occurs at $v_o + \alpha\sigma = 4$), but rather with the *disappearance* of the ergodic, flowing solutions. At the jamming transitions, $v_o + \alpha\sigma > 4$: this implies that, for the jamming transitions to have any significance, flowing solutions (where they exist) must be stable with respect to glassy ones (or else the jamming transitions would be hidden by the usual nonergodicity transition at $v_o + \alpha\sigma = 4$). This is correct under numerical iteration (hence the resulting flow curves), but physical stability does not obviously follow. However, in the preceeding analysis, we have assumed this to be the case: we shall return to this point in Ch. 9, where we shall also discuss the differences between the jamming transitions and the usual MCT glass transitions in some more depth.

7.3 Correlation functions

All of the results presented so far have only contained information regarding the relaxation time (viscosity) for a given set of parameters. But MCT makes important predictions regarding the form of the correlation functions, rather than just their late time limit, and the same goes for the

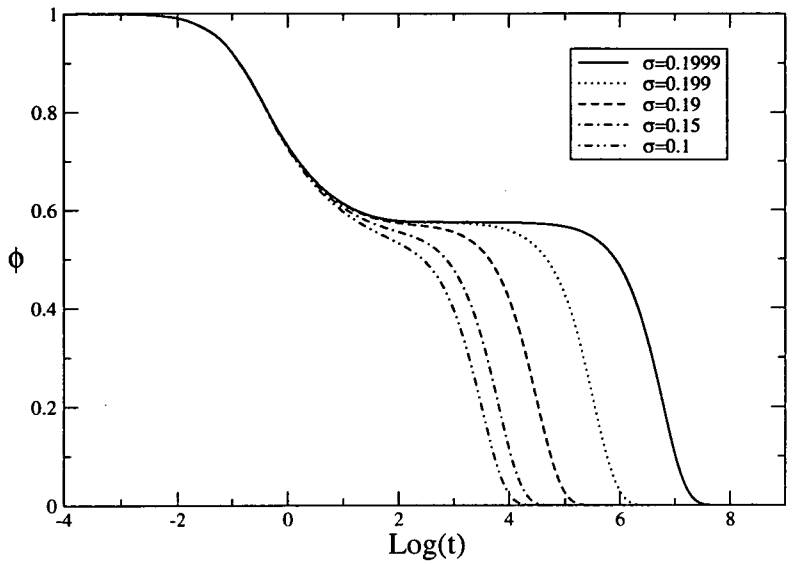

Figure 7.10: Correlation functions for a range of stresses approaching the first jamming transition (at $\sigma_{c1} = 0.2$) for $v_o = 3.9$, $\alpha = 0.95$. Note that, sufficiently close to the transition, there is a clear separation between the β–decay and the flow–induced final decay, resulting in a very well–defined plateau.

current model. In this section we show model correlators for a range of parameters, comparing them to correlators obtained from the conventional F2 model. We begin by presenting the correlators approaching a jamming transition. Fig. 7.10 shows the correlation functions for $v_o = 3.9$, $\alpha = 0.95$ for a series of values of σ approaching the jamming transition at $\sigma_{c1} = 0.2$. We see that, at early times the different correlators are very similar. They differ significantly only at late times, when the flow 'kills off' the memory, resulting in decay from the plateau region. As the transition is approached, the timescale on which this occurs (essentially τ) grows strongly. As one nears an MCT glass transition, both the β relaxation timescale (on which the plateau is approached) and the α–relaxation time (on which the correlator decays below the plateau) diverge. At a jamming transition, there is only a single divergent timescale. The β–relaxation occurs on a finite timescale, resulting in the very well–defined plateau which we see in Fig. 7.10. This is again due to the fact that the jamming transitions do not occur at MCT critical points: on timescales $t \ll 1/\dot{\gamma}$, the dynamics are essentially those of the F2 model at the appropriate coupling. At the jamming transition, this coupling is $v_2 > 4$, for which the β–relaxation occurs in a finite time, and so it is no surprise that we have but a single divergent timescale.

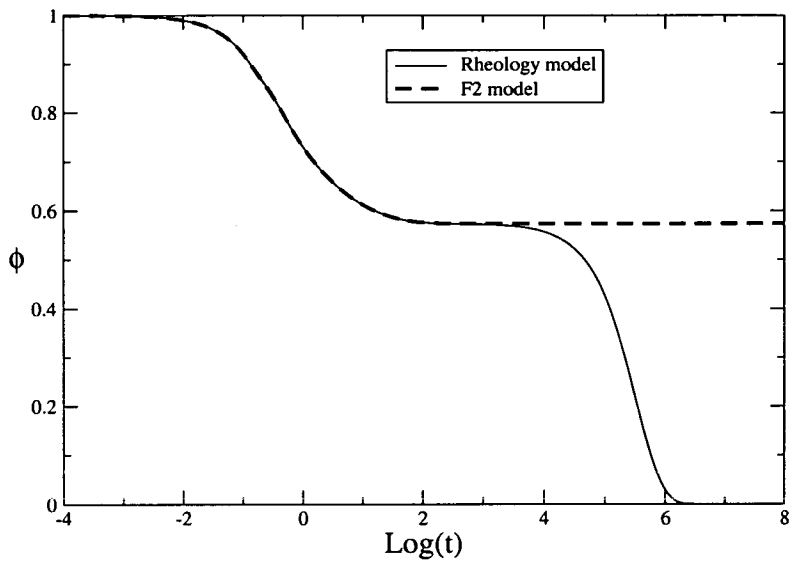

Figure 7.11: The correlation functions for our model with $v_o = 3.9$, $\alpha = 0.95$ and $\sigma = 0.199$, compared with the correlation function for the F2 model with $v_2 = 3.9 + (0.95 \times 0.199) = 4.08905$. At $\sigma = 0.199$, the shear rate is $\dot{\gamma} = 1.04 \times 10^{-4}$ (the jamming transition for these parameters is at $\sigma = 0.2$). As we would expect, the dynamics in the two cases are similar until $\dot{\gamma}t \sim 1$.

We show, in Fig. 7.11, that the early–time dynamics are identical to an F2 model with appropriate coupling. For times $t \lesssim 1/\dot{\gamma}$, the decay of the correlation functions are indistinguishable to the eye. This shows that, close to the jamming transitions, the late–time dynamics are governed by the shear–induced fluidisation. In the absence of this fluidisation in the memory function, there would be no α–relaxation, since we would be within the glass. This raises questions regarding the late–time dynamics in the vicinity of jamming transitions in this scenario: is the characteristic stretching of the final decay (Ch. 3), found in the vicinity of the glass transition, also present close to jamming transitions? Given the brief argument above, one might expect that it is not: we shall return to this point in Ch. 8.

Functional form of the late–time decay

In our calculation of the transition points we assumed that, in the vicinity of a transition, the late–time decay of the correlation functions were of exponential form. In Figs. 7.12 and 7.13, we demonstrate (for one particular parameter set) that an exponential does indeed fit the numerics very closely, both for $\sigma \approx \sigma_{c1}$ and $\sigma \approx \sigma_{c2}$. The same conclusion was reached for

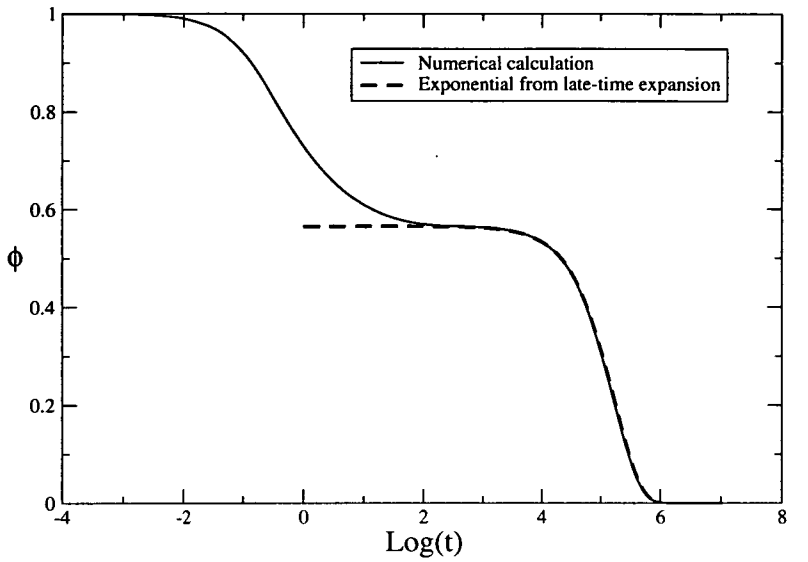

Figure 7.12: The correlation function close to a jamming transition for $v_o = 3.9$, $\alpha = 0.99$ and $\sigma = 0.172$ (the transition occurs at $\sigma_{c1} = 0.174$), along with the exponential decay consistent with Eq. 6.17, using the numerically determined shear rate at those parameters.

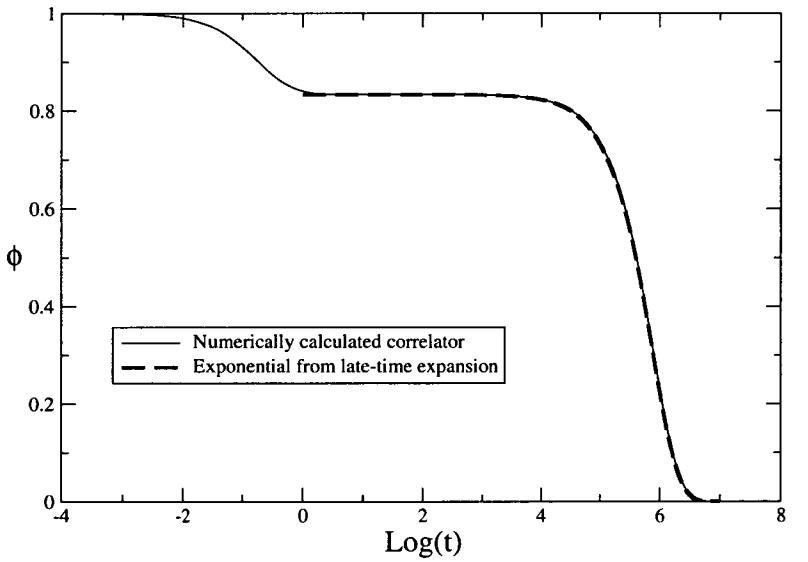

Figure 7.13: The correlation function at a stress ($\sigma = 3.334$) just above the window of nonergodicity ($\sigma_{c2} = 3.333$), for the same parameters as Fig. 7.12. At early times ($\dot{\gamma}t \ll 1$) the coupling is greater than that at the initial jamming transition, and so the plateau is much higher. Again, the exponential is that consistent with the late–time expansion of the correlation function, with the shear rate calculated from the numerical calculation of τ at this stress.

all other parameter sets that were examined, vindicating our calculation of the transition points.

7.4 Summary of results for the rheology model

We now summarise the key results obtained in studying our MCT based rheology model. We have shown that, similiarly to MCT models, the parameter space (defined by the values of v_o, α and σ) splits into two regions. In the first region, the correlation functions decay to zero on a timescale τ. These solutions correspond to an ergodic fluid. In the second region, the correlations do not decay to zero: rather, there is a nonzero long–time limit $f_{\mathbf{v}}$. These solutions correspond to nonergodic solids. Dependent upon the parameters, upon increasing the stress, we have found the following scenarios:

1. there are no jamming transitions;
2. there is a window of stress for which the solutions are nonergodic;
3. there is a single transition into a jammed state;
4. increasing stress leads to nonergodicity, followed by melting into a fluid, which then re–jams upon further increasing the stress;
5. the quiescent system is glassy, and is fluidised (or not, for $\alpha > 1$) upon increasing the stress.

The nonergodic solutions map directly onto the F2 model, since in this case the shear rate, which distinguishes the current model from F2, is identically zero. However, the manner in which these states are approached differs substantially from that of the F2 model. The transitions are shifted from the MCT transition points: therefore, there is but a single divergent timescale upon approaching the transition; and the variation in the nonergodicity parameter upon entering the glass state is analytic, except for the discontinuity at the transition. The transitions do not occur at the lowest coupling for which nonergodic solutions are available. Rather, they are associated with the disappearance of ergodic solutions. In Ch. 9, we shall discuss these results within the context of experimental results on jamming in suspensions. Firstly though, in the following chapter we consider the effect of alterations to the model.

Chapter 8

Variations of the Model

As promised in Ch. 6, we now turn to consider some variations of the model. These are

- Building on an F12 model, rather than upon an F2 model.
- Allowing a quadratic stress dependence of the vertex.
- Choosing an algebraic form $m(t) \sim \frac{1}{1+\dot{\gamma}^2 t^2}$, rather than an exponential form, for fluidisation under flow.

In this chapter, we present the results of these alterations, and discuss the stability of the model's predictions in light of these results.

8.1 An F12 model

8.1.1 Motivation

In the model defined by Eqs. 6.5 and 6.6, we found that, close to jamming transitions, the final decay of correlators was exponential. Close to an MCT glass transition, this final decay is not of exponential form, but rather has the form of a stretched exponential – see Ch. 4. However, the F2 model is anomalous, in that it does not show this stretching. Thus, one cannot attribute

the exponential decay found in our jamming F2 model to the difference between our jamming transitions and a standard F2 glass transition.

In contrast, the static F12 model does display the stretched exponential decay which fits both experiments and MCT predictions. Thus, in order to to investigate whether the exponential decay is meaningful, we studied a jamming F12 model. This is defined by the usual equation of motion for the correlation functions (Eq. 6.1), and the memory function

$$m(t) = \left((v_1 + \alpha_1\sigma)\phi(t) + (v_2 + \alpha_2\sigma)\phi^2(t)\right) \mathrm{e}^{-\dot{\gamma}t}. \tag{8.1}$$

The static F12 model has a locus of transitions in the $\{v_1, v_2\}$ plane [95]: for $v_2 < 1$, upon increasing v_1, one passes through what is known as a 'type A' transition. As one does this, the nonergodicity parameter increases smoothly from zero. These transitions are not thoughht to be connected with the experimental glass transition. For $v_2 > 1$, upon increasing v_1 beyond a critical value $v_{1c}(v_2)$, the system encounters a 'type B' transition, which corresponds more closely to the experimental glass transition: there is the usual discontinuity in the nonergodicity parameter and, in the vicinity of the transition, the stretching of the dynamics discussed above occurs. As v_2 approaches 4, the critical value of v_1 tends to zero, consistent with our knowledge of the F2 transition.

8.1.2 Results

Results were obtained for the jamming F12 model by simply adapting the code used to solve the F2 rheology model. No analytic solutions were attempted.

Rheology

Numerically, one obtains flow curves which are qualitatively similar to those of the F2 rheology model. For sufficiently large parameters (v_1, v_2, α_1 and α_2), the shear rate appears to vanish at certain values of the stress, suggesting jamming transitions to a nonergodic state, as found in the original model. Similiarly to the F2 rheology model, there are parameters for which we found (i) no transitions; (ii) a transition to a jammed state with no re–fluidisation; (iii)

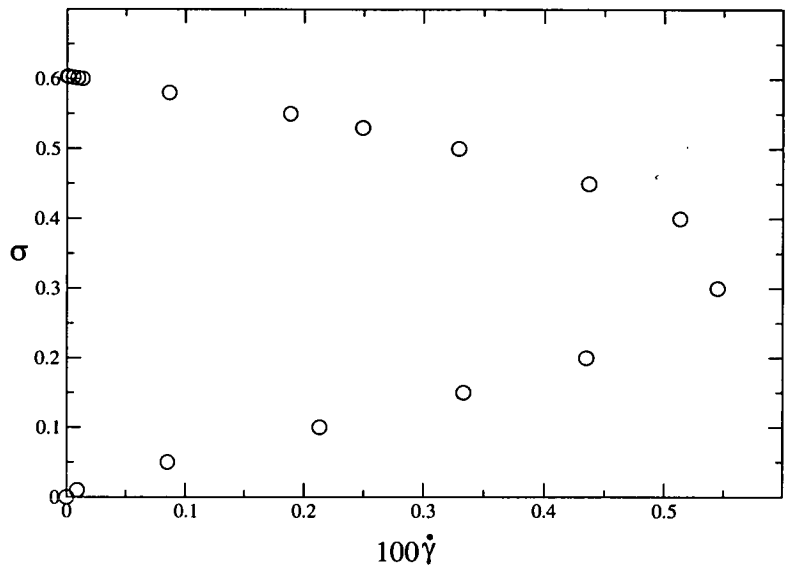

Figure 8.1: The steady–state rheology of the F12 model with parameters $v_1 = v_2 = 0.95$, $\alpha_1 = \alpha_2 = 0.9$. There appears to be a transition to a nonergodic state, but for these parameters there is no high stress fluid state.

jamming, followed by re–fluidisation; and (iv) a quiescent glass state which is melted upon shearing. Other scenarios may of course be present, but we have not found them. Fig. 8.1 shows an example of the flow curves which may be obtained in the F12 based model.

In the model studied in Ch. 7, we noted that the behaviour at $\alpha = 0$, for which the yield stress vanished continuously at the quiescent glass transition, differed from the results of related work [82]. In the case of our F12 based model, it is more difficult to elucidate this point, since we do not have an analytic expression for the transition points: therefore, we must turn to numerics. However, we can ease progress by modifying the numerical code: for $\alpha_1 = \alpha_2 = 0$, the memory function does not explicitly depend upon σ. In order to specify the memory function, one just needs to choose a value of $\dot{\gamma}$ (as well as v_1 and v_2). Having done so, we calculate the correlation function from the memory function in the usual way, and integrate to obtain the viscosity (and thus the stress). In this case, as in the unsheared F2/F12 models, there is no need for an iteration of τ.

Fig. 8.2 shows the rheology of the F12 based model, in the shear thinning only case ($\alpha_1 = \alpha_2 = 0$), in the vicinity of its quiescent glass transition (we have chosen $v_2 = 2$, for which

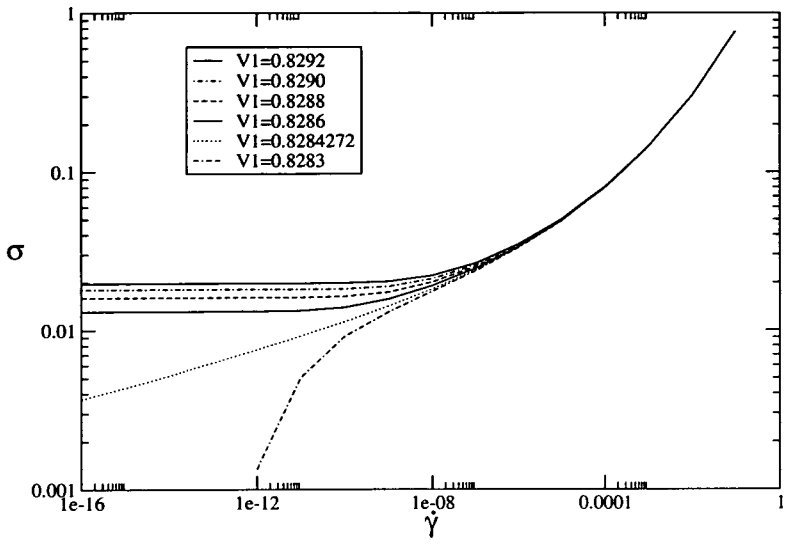

Figure 8.2: The low shear rate rheology of the F12 model with $v_2 = 2$, $\alpha_1 = \alpha_2 = 0$, for values of v_1 which straddle the quiescent glass transition (which, for $v_2 = 2$, occurs at $v_1^{crit} = 2\sqrt{2} - 2 \approx 0.82842712$). The data for larger v_1 lie above that for smaller values. For the four largest values of v_1 shown, the presence of a yield stress is suggested by the fact that the flow curve begins to level off around $\dot{\gamma} \sim 10^{-10}$. In this range of shear rate, there is no apparent levelling off for $v_1 = 0.8284272$.

the transition occurs at $v_1 = v_1^{crit} = 2\sqrt{2} - 2 \approx 0.82842712$). For the four largest values of v_1 shown (all of which are within the glass) the stress clearly approaches a constant value (the *yield stress*) within the range of shear rate shown. For $v_1 = 0.8284272$, the flow curve also approaches a constant value, but does not do so until $\dot{\gamma} \approx 10^{-22}$. Since v_1^{crit} is irrational, we cannot study the rheology exactly at the transition: therefore, in Fig. 8.3, we plot the yield stress (σ_y) *vs.* the distance to the transition ($\epsilon \equiv v_1 - v_1^{crit}$) in the hope that a pattern will emerge. However, this is not conclusive: a simple power law cannot describe the data convincingly over the range of ϵ studied. Neither does the yield stress obviously approach a constant value as $\epsilon \to 0$. Therefore, we are unable to conclusively state that the yield stress does, or does not, vanish smoothly as the transition point is approached.

Late time dynamics

Our main motivation for extending the study to an F12 model is to investigate whether or not the late time exponential relaxation found in the original model survives. In order to do so, the final relaxation of correlation functions, close to jamming transitions, were fit with

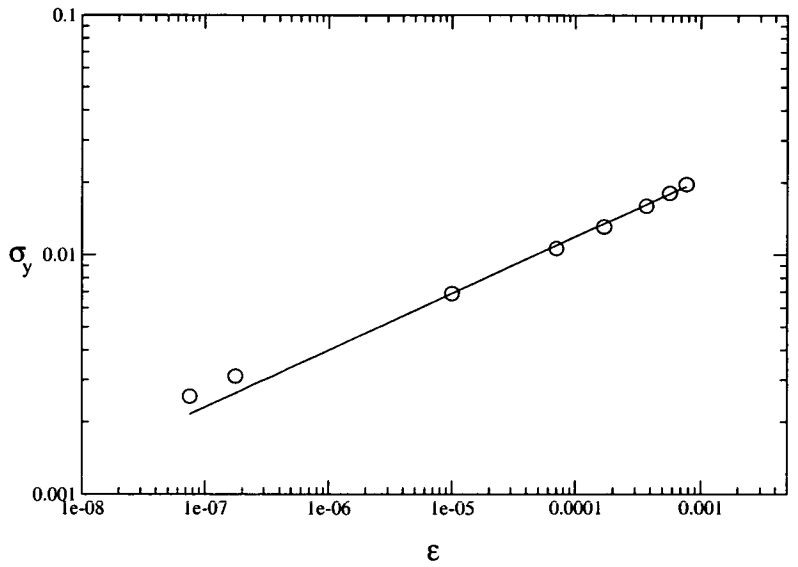

Figure 8.3: The points show yield stresses of the F12 based model for $v_2 = 2$ and $v_1 = v_1^{crit} + \epsilon$, plotted against ϵ. The continuous line is a power law fit to the data: $\sigma_y = 0.10575\,\epsilon^{0.237289}$.

exponentials. Fig. 8.4 shows an exponential fit to the correlation function for the parameters $v_1 = v_2 = 0.95$, $\alpha_1 = \alpha_2 = 0.9$ (the same as those used in Fig. 8.1) at $\sigma = 0.6032$. The exponential provides a good description of the final decay in this case.

However, unlike in the case of the F2 rheology model, for other parameters the final decay was ill–fitted by an exponential. For the parameters $\alpha_1 = 0.4$, $\alpha_2 = 0.55$, $v_1 = 0.75$ and $v_2 = 2.2$, one finds a jamming transition followed by re–fluidisation. Close to the latter, an exponential fits the final decay well, but close to the former, it does not, as shown in Fig. 8.5.

This is not the only parameter set for which the exponential fit is less than satisfactory – other examples have been found. This is in marked contrast to the case in the F2 model in which, for *all* cases tested, the tail of the relaxation was well fitted by an exponential, suggesting that this form of the decay is an artefact of the original model.

8.2 Quadratic stress dependence of vertex

The next alteration that we allow for is a quadratic, rather than linear, dependence of the vertex upon stress in an F2 based model. *ie*, we use a memory function $m(t) = (v_o + \alpha\sigma^2)\mathrm{e}^{-\dot{\gamma}t}\phi^2(t)$.

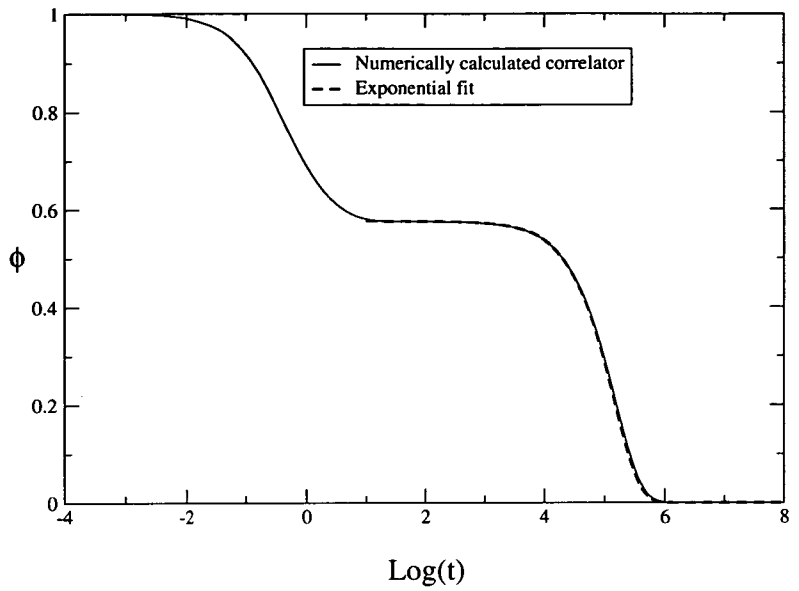

Figure 8.4: The correlator close to the jamming transition ($\sigma = 0.6032$) for the same parameters as Fig. 8.1. The final decay of the correlation function is well described by an exponential fit.

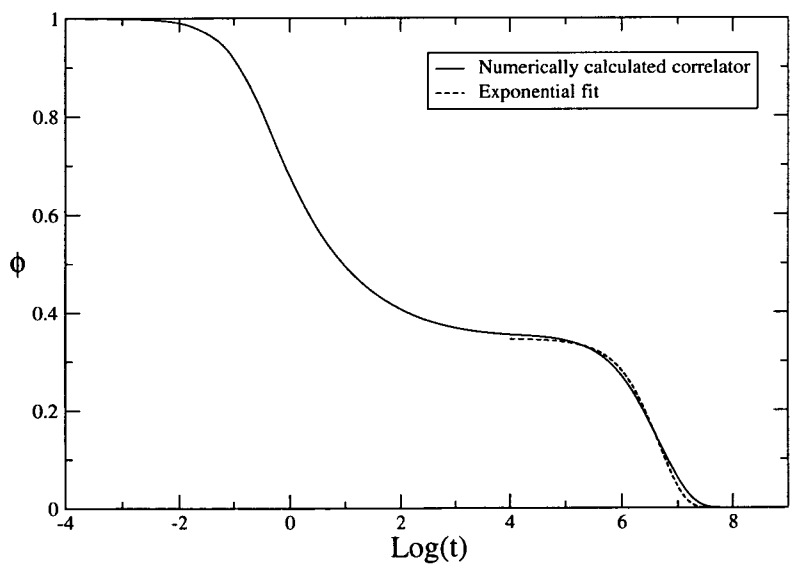

Figure 8.5: The correlator for the parameters $\alpha_1 = 0.4$, $\alpha_2 = 0.55$, $v_1 = 0.75$ and $v_2 = 2.2$, and $\sigma = 0.0322$ which is close to the initial jamming transition. The fit is an exponential fit to the correlator for times $t > 10^4$.

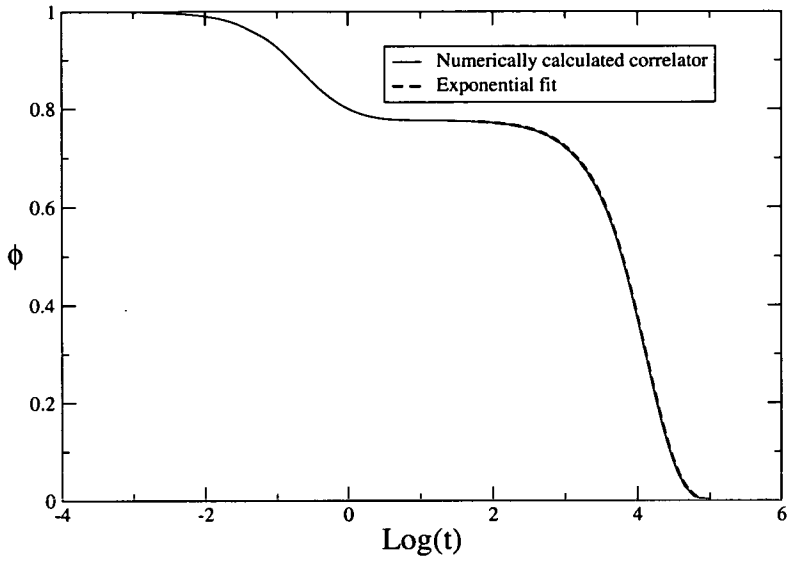

Figure 8.6: The correlator for the parameters $v_o = 3.9$, $\alpha = 0.5$ and $\sigma = 1.938$ with a quadratic stress dependence of the correlator. The transition occurs at $\sigma = 1.939$. Note that the tail is well fitted by an exponential.

In this case, the analysis leading to Eq. 6.18 remains essentially unchanged. Thus we might expect that the exponential decay at late times survives the current alteration. This has been checked numerically for several parameter sets: the exponential fits are every bit as convincing as those in the original model. An example is given in Fig. 8.6.

8.2.1 Phase diagrams

Since the tail retains the exponential character, the locus of transitions in parameter space is found by trivially altering the analysis leading to Eq. 6.24. This allows us to obtain phase diagrams, as shown in Fig. 8.7, for the new model. In this case, the model shows a qualitative difference to the original version. For all values of $\alpha > 0$ and $v_o \leq 4$, there is a transition to a glassy state at sufficiently high stress, but there is no re–entrant fluid for any values of α. For $v_o \geq 4$, one finds glassy states at zero applied stress (as expected): these may or may not be melted by shearing, dependent upon the value of α and v_o. If they are melted, they re–jam, so that they are nonergodic in the large stress limit. This leads to flow curves for which, upon increasing the stress, one melts a glass before causing thickening and jamming. An example of

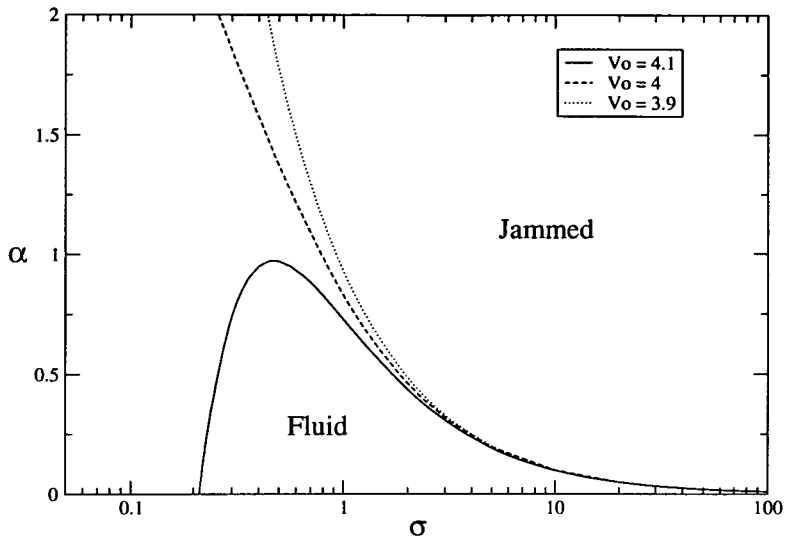

Figure 8.7: Phase diagrams for the model with a quadratic stress dependence of the vertex. The 'phase–behaviour' is somewhat different to that found in Ch. 7, with all states being jammed at sufficiently high stress.

such a curve is shown in Fig. 8.8.

8.2.2 Flow curves

The transitions aside, the rheology of this model is interesting. One can find shear thinning at low applied stresses, before the onset of shear thickening – such behaviour did not appear in the model studied in Ch. 7. Fig. 8.9 shows the flow curves for $v_o = 3.9$, $\alpha = 0.2$, for which full jamming is present: compare this to the flow curves for $v_o = 3.9$ in the initial model (Fig. 7.4) – in that case a value of $\alpha \gg 0.2$ is required to jam the system.

8.2.3 A final possibility

We have argued in Ch. 6 that a quadratic stress dependence is the correct form at low stresses, but that we have no reason to require such a form away from $\sigma = 0$. Thus, it is interesting to consider the results which arise from a vertex which has a quadratic dependence at small stresses, but which goes over to a linear form at larger values. With such a vertex, there is a tendency to shear thin at both low and high stresses, whilst jamming is possible for intermediate

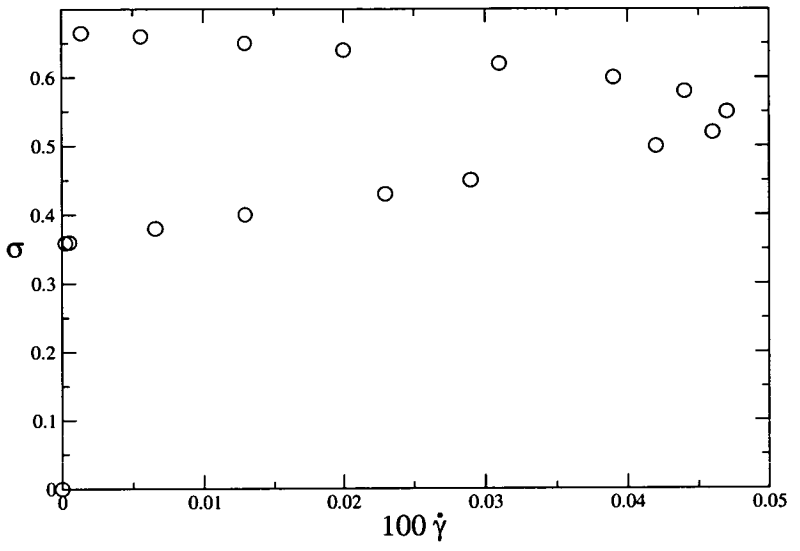

Figure 8.8: The flowcurve which results from a vertex which is quadratic in the stress, for the parameters $v_o = 4.1$, $\alpha = 0.9$. In the absence of stress, the system is a glass, which is melted upon imposition of a sufficiently large stress. However, upon increasing the stress further, there is strong thickening and jamming.

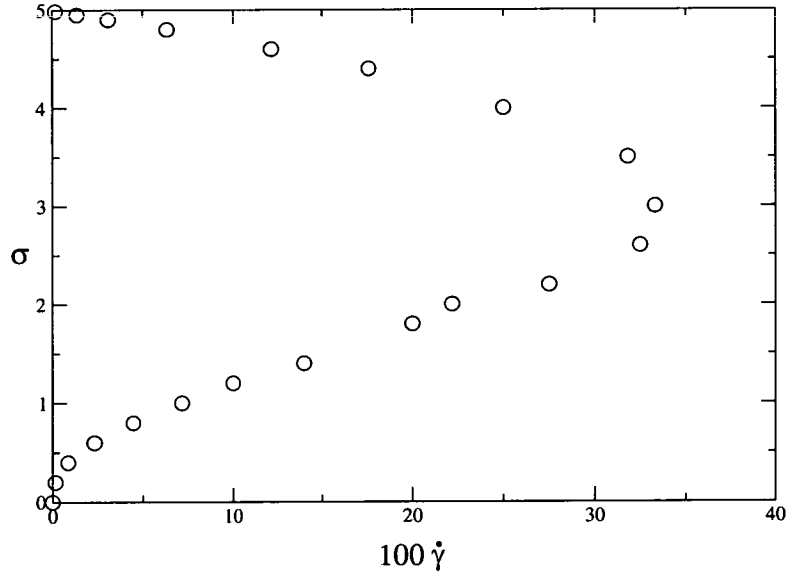

Figure 8.9: The steady–state rheology for $v_o = 3.9$, $\alpha = 0.2$ with a vertex which is quadratic in the applied stress. Note the presence of thinning at low stresses, followed by thickening and jamming. No fluidisation after a stress induced jamming is found for these (or any) parameters with this model.

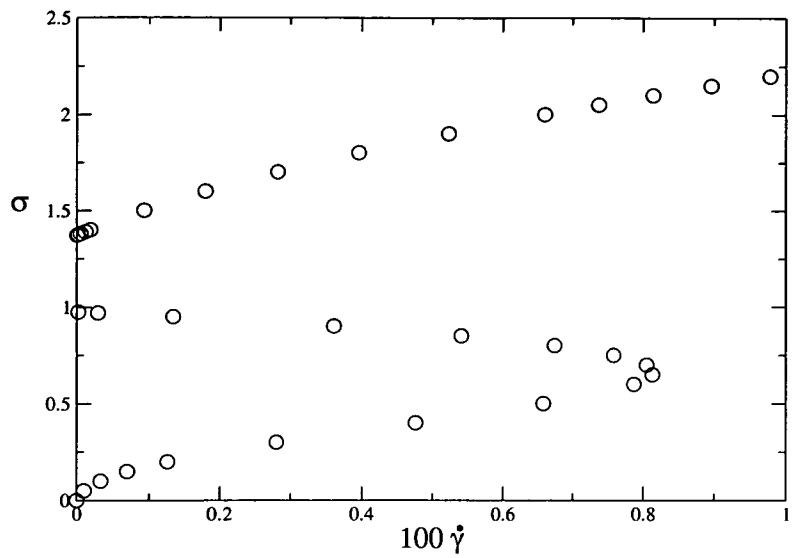

Figure 8.10: The flow curve which arises for $v_o = 3.9$, $\alpha = 0.95$ if one allows for variation of the coupling with stress which is quadratic at low stresses ($\sigma < 1$), and linear for large stresses ($\sigma > 1$). In this case thinning proceeds the jamming.

values. The simplest manner to allow a linear vertex at large stresses whilst retaining the quadratic form around $\sigma = 0$ is to choose a vertex for which $m(t) = (v_o + \alpha\sigma^a)\mathrm{e}^{-\dot{\gamma}t}\phi^2(t)$, with $a = 2$ for $\sigma < 1$ and $a = 1$ for $\sigma > 1$. Results from this choice are shown in Fig. 8.10.

If the unsheared state is a glass, this scenario allows for it to melt upon shearing, followed by thickening and jamming of the resulting fluid as the stress is further increased. In this case, we obtain behaviour such as that shown in Fig. 8.11.

8.3 Algebraic fluidisation

Finally, we investigate the effect of the manner in which flow enters the memory function by replacing the exponential of our original model with the algebraic form $m(t) \sim 1/(1 + \dot{\gamma}^2 t^2)$.

As in the case of the F12 based model, this change makes analytic progress difficult – the results presented here were obtained numerically. The rheology of this model is qualitatively similar to the original model, with jamming and re–fluidising scenarios easily found. We do not show any jamming flow curves, as they add nothing new.

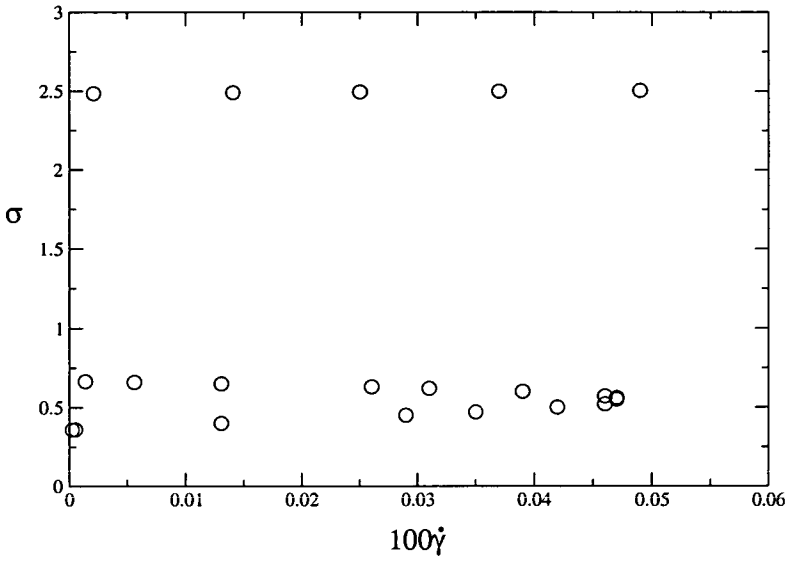

Figure 8.11: The steady rheology arising from a vertex which is quadratic in stress for $\sigma < 1$ and linear for $\sigma > 1$, for $v_o = 4.1$ and $\alpha = 0.9$. In the absence of applied stress the system is a glass: this is shear melted upon the application of a sufficiently large stress. Upon further increasing the stress, there is thickening and full jamming. At the highest stresses ergodicity is restored.

However, the yielding behaviour of this model is of interest. We have already investigated whether or not the schematic model upon which we base our work affects the behaviour in the case $\alpha = 0$, in particular, whether or not a yield stress appears discontinuously at the quiescent glass transition. We now ask the same question regarding the form of the fluidisation factor in the memory function.

The flow curves for this model with $\alpha = 0$, and values of v_o straddling the glass transition (at $v_o = 4$) are shown in Fig. 8.12. Sufficiently deep within the glass, the stress approaches a constant value as $\dot{\gamma} \to 0$, suggesting the presence of a yield stress. At the transition point, no such plateau is evident in Fig. 8.12: rather, over several orders of magnitude, the rheology appears consistent with a power law fluid. However, in Fig. 8.13, we show the $v_o = 4$ flow curve at smaller shear rates: doing so, we see that the stress does saturate, but not until $\dot{\gamma} \sim 10^{-28}$. Thus, it appears that choosing algebraic (rather than exponential) fluidisation leads to a discontinuously appearing yield stress.

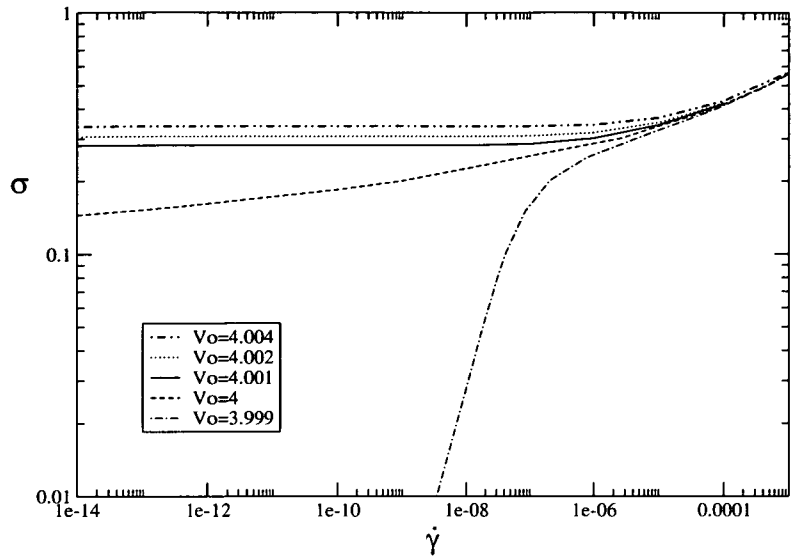

Figure 8.12: $\alpha = 0$ flow curves of the model with algebraic fluidisation. Sufficiently deep into the glass, a yield stress is apparent. The situation is not so clear as the transition is approached from above.

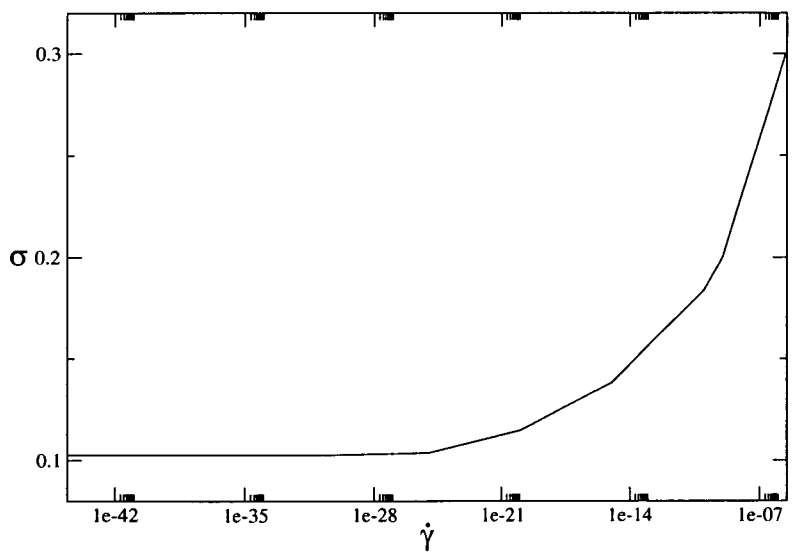

Figure 8.13: The $\alpha = 0$ flow curve of the model with algebraic fluidisation, at the transition point $v_o = 4$. At sufficiently small shear rates, the flow curve *does* level off, showing that in this case the yield stress does appear discontinuously at the glass transition.

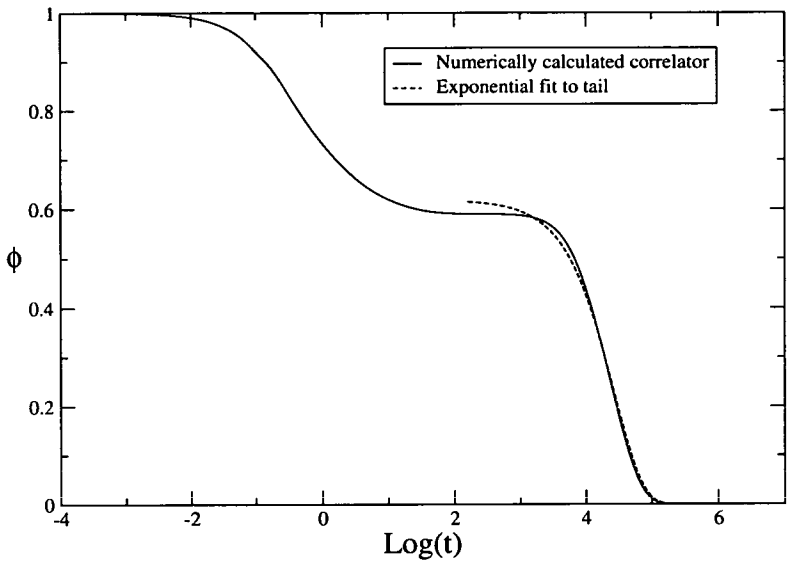

Figure 8.14: The correlation function of the model with an algebraic dependence upon shear rate, for the parameters $v_o = 3.9$, $\alpha = 0.3$ and $\sigma = 0.78$: this stress is just above the second critical stress $\sigma_{c2} \lesssim 0.775$, and so the material is in the high stress fluid state.

8.3.1 Late time dynamics

Also of interest is the late–time relaxation of correlators in systems close to jamming. Similiarly to the results of the jamming F12 model, the quality of exponential fits to the late–time dynamics is variable. Some correlators (of systems close to a transition) are manifestly non-exponential – an example is given in Fig. 8.14 which shows a correlator for $\sigma \approx \sigma_{c2}$. Other examples (including cases in the vicinity of the initial transition) were also found.

8.4 Structural stability of the model

In the preceeding part of this chapter, and in Ch. 7, we have described the results of making different choices in the formulation of a simple model of jamming. If the results of the model were particularly sensitive to these choices then it would be difficult to have any confidence in its predictions. With this in mind, we now discuss the stability of the model to these changes.

8.4.1 Flow scenarios

We have seen that the basic rheological scenarios resulting from the model are not altered by either using an F12 model or by varying the form of fluidisation to the algebraic form studied in the previous section. In contrast, choosing the vertex to vary quadratically with stress, regardless of its value, alters the flow behaviour somewhat: provided $\alpha \neq 0$, in the limit of large stress the system jams regardless of other parameters. This behaviour is unphysical (since dilute colloids do not shear thicken), and results from the form of the vertex at large stress: the more general flow behaviour is recovered if we allow a vertex which become linear at large stress.

Thus, the flow scenarios which we have found require only that the vertex does not increase too quickly at large stress. We have not attempted to obtain a precise criterion for this condition.

8.4.2 Late–time dynamics

As shown in this chapter, the main effect of altering the fluidising form of the model, or of building upon an F12 model, was to alter the late–time decay of correlations in the vicinity of the jamming transitions. Unlike the basic rheological scenarios, the exponential decay found in Ch. 7 is not robust with respect to arbitary choices which were made, and so cannot be regarded as significant.

As an aside, this raises the interesting question of whether or not, in the vicinity of a jamming transition, one expects to find the dynamical stretching which appears in unsheared supercooled liquids. In the proximity of a conventional glass transition, the late–time relaxations occur via a cooperative, many body relaxation. In the scenario discussed in Ch. 6, this relaxation is assisted by the shear advection of fluctuations. At high accumulated strain (since the zero of time), diffusion over small lengthscales can relax the fluctuations, thus a cooperative movement of many particles might be avoided. Since this result from the model appears to be sensitive to details however, it cannot shed any light upon the validity of this speculation.

8.4.3 Yielding behaviour

In [82], Fuchs and Cates investigate schematic models of shear thinning, including one which is a combination of two of the variants studied here (at $\alpha = 0$). The memory function is

$$m(t) = \frac{1}{1 + (\dot{\gamma}t)^2} \left(v_1 \phi(t) + v_2 \phi^2(t) \right) . \tag{8.2}$$

In this case a yield stress appears discontinuously at the quiescent glass transition. In their work, this model appears as a simplified version of a seperate model which has a microscopic basis: this microscopic model also predicts a discontinuously appearing yield stress.

This is in contrast to the model studied in Ch. 7 (with $\alpha = 0$), in which we saw that the yield stress goes to zero smoothly as $v_o \to 4^+$. We have seen that replacing the exponential fluidisation with the same algebraic term as used in [82] recovers the discontinuity in σ_y, whilst the effect of building upon an F12 model, whilst retaining the exponential fluidisation, is unclear. Thus, as with the functional form of the correlation functions, this aspect of the results *is* rather sensitive to the mathematical details of the model and so we must be cautious in interpreting these results. One would tend to lean towards the predictions of the microscopic model.

Chapter 9

Discussion

In this chapter we shall interpret the results of our models in the context of experimental observations. We will also return to the arguments made in Ch. 5 regarding the relevance of glassiness to nonlinear rheology. Firstly though, we discuss the nature of the jamming transitions in relation to conventional MCT glass transitions, and return to the question of physical stability, raised in Ch. 7.

9.1 The jamming transitions

Recall from Ch. 6 that, for sufficiently large v_o, α and σ, glassy solutions to our models are always available. However, even where they exist, they are not the only possible solutions – as we have seen, ergodic, flowing solutions are also possible for some parameters. As mentioned in Ch. 7, our analysis assumes that, where they exist, the flowing solutions (to which our iteration converges) are physically stable with respect to the nonflowing glassy solutions. We discuss this assumption below, but firstly, presuming that it holds, we compare the jamming transitions to those of conventional, static MCT.

9.1.1 Comparison of jamming transitions with MCT glass transitions

In the F2 (and other MCT models) the glass transition occurs at points in parameter space where nonergodic solutions become available. At these *critical points* [1] there is a bifurcation in the long–time limit (f) of the correlation function: at these points it jumps from its value in the fluid ($f = 0$) to a nonzero value f_c, followed by a nonanalytic variation as the coupling is further increased ($f - f_c \sim \sqrt{\epsilon}$, where ϵ is the separation from the transition in the space of coupling constants). At lower values of the coupling, no such nonergodic solution is possible.

In the case of our jamming transitions, this is not the case: rather (at fixed v_o and α) the system jams at values of the stress for which the ergodic, flowing solutions vanish. These points are not critical points: they do not correspond to a bifurcation in f. Therefore, the initial jump in f at jamming transitions is followed by an analytic variation with coupling (*ie*, with the stress if other parameters are fixed). This point is illustrated by the variation of the nonergodicity parameter f with σ, as shown in Fig. 9.1. In the figure, there is a range of stress for which a glassy solution has become available (indicated by the existence of nonzero f in the upper part of the diagram) but is not chosen – rather, the system remains flowing (as indicated in the lower part by a nonzero shear rate). Only when the viscosity of the flowing solution diverges (at σ_{c1}), signalling that flowing solutions are no longer possible, does the system become nonergodic. At σ_{c2}, a flowing solution again becomes available.

This key difference – that jamming transitions do not occur at critical points – has other implications. The β relaxation timescale τ_β (as well as the longer structural relaxation timescale τ) diverges at an MCT transition – *ie*, at a critical point. In our model, transitions do not occur at these points. Therefore, the β relaxation of the underlying F2 model (that with $v_2 = v_o + \alpha\sigma$) occurs on a finite timescale. By moving arbitrarily close to a jamming transition, we can make the shear rate sufficiently small that $\dot{\gamma}\tau_\beta \ll 1$, therefore ensuring that the β relaxation of the unsheared system is unchanged by the flow. Thus, in the neighbourhood of jamming, we have a pre–plateau relaxation which occurs on a finite timescale, followed at arbitrarily late times by a flow induced final relaxation. This leads to a (very) well–defined plateau region if one looks sufficiently close to a jamming transition – see *eg*, Fig. 7.10.

[1] This is the standard terminology, although these points have nothing whatsoever to do with the usual critical points of equilibrium statistical mechanics.

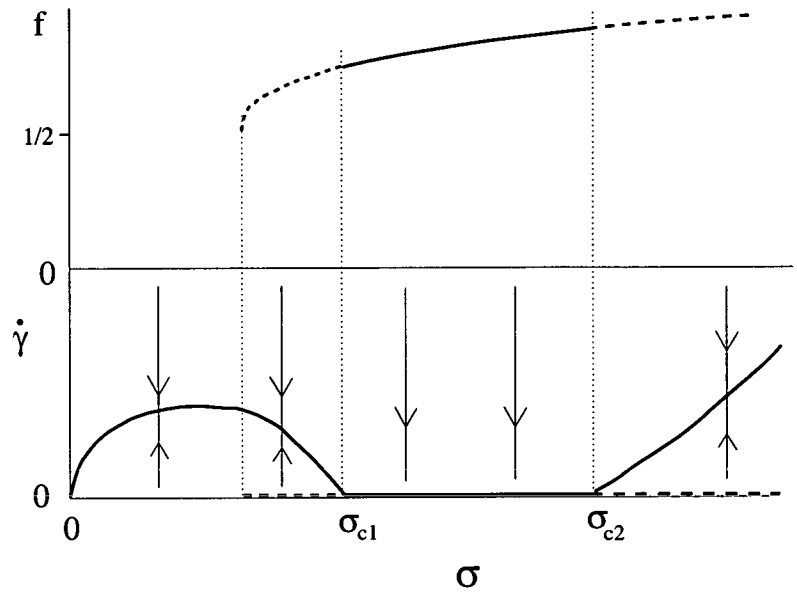

Figure 9.1: Schematic variation of $\dot{\gamma}$ and f upon varying σ. Solid (dashed) lines denote stable (unstable) solutions under the iteration described in Ch. 6. Arrows indicate flow of $\dot{\gamma}$ under the iteration. Note that the ergodic solution remains stable beyond the critical point where a nonergodic solution first becomes valid, *ie*, $v_o + \alpha\sigma > 4$. Therefore, around the jamming transitions, there are no nonanalyticities after the discontinuity in f.

9.1.2 Stability of ergodic *vs.* nonergodic solutions

Under numerical iteration, ergodic solutions to our models are stable: where ergodic solutions exist, any finite initial guess of the relaxation time τ leads to convergence upon that solution (Fig. 9.1). However, as written, the iteration does not directly map onto temporal evolution, and so stability under iteration does not imply physical stability. This said, the nature of the iteration suggests that transient violations of Eq. 6.4, resulting in an infinitesimal shear rate in the nonergodic state, lead the system towards the flowing state. Can one make a correspondence between flow of the solutions under iteration (as illustrated in Fig. 9.1) and temporal evolution? To do so would require a physical model for the temporal evolution of the viscosity as it is perturbed from a steady state value (consistent with our solutions). We have not been able to formulate such a model, and so cannot argue rigorously that the solutions which are stable under iteration are also physical stable. However, we have tacitly assumed this to be the case.

If our assumption is correct, then we have a model which shows an interesting range of non-

linear rheology, including nonergodicity transitions which differ from those of MCT. What if it is not? In this case, our models would shown none of the novel phenomenology which we have described. There would be but a single nonergodicity transition at $v_o + \alpha\sigma = 4$ with much of the phenomenology of the usual F2 model. Rheologically, this would imply that (at fixed v_o and α), upon increasing the stress beyond $\sigma^* = (4 - v_o)/\alpha$, the material (which for smaller values of the stress is flowing) chooses to abruptly arrest, even although a flowing solution remains a valid possibility. This scenario is in marked contrast to both the usual MCT transition, and to the jamming transitions described above, in which the relaxation timescale diverges smoothly. In this case, the relaxation time would jump from a finite value to a divergent one. Rheologically, this would result in a discontinuity in the flow curve, with the shear rate jumping from a finite value to zero at σ^*.

To us, this seems somewhat unlikely, particularly since the shear rate at σ^* need not be small, or even decreasing. If the shear rate were to jump to zero, it would seem to suggest that the material *prefers* to be in a nonergodic state, which goes against the usual notion that it becomes trapped there, unable to explore phase space. Finally, such a situation would seems to be in contrast to the many reports of flow at high stresses in discontinuously thickening colloids (*eg*, [30, 33]).

If our intuition is correct, then where flowing solutions exist, the nonergodic state is metastable. This opens up the possibility of hysteresis: if one can take the system into a jammed state, then it might be possible to lower (raise) the stress below (above) σ_{c1} (σ_{c2}), whilst remaining in the nonergodic state. The model predicts no limit to this at large stresses, but this situation could not persist below σ^*, since below this point there are no nonergodic solutions. We discuss the possibility of hysteresis further in the following section.

9.2 Comparison of model rheology with experiment

Quantitative comparison of our models with a specific experimental system is difficult, since restricting attention to schematic models results in loss of quantitative predictive power. (In an F2 model, one could take the interpretation of v_2 as the height of the first peak in $S(q)$

literally, but such a minimilistic approach seems unlikely to tally with reality on a quantitative level. Indeed, as stated in Ch. 3, the predictions of the F2 model do significantly differ from experimental results.) However, we *can* compare the basic scenarios which we have found with experiments.

9.2.1 Does 'full jamming' in our models correspond to experimental stress induced solidity?

As mentioned in Ch. 2, Bertrand and co–workers have performed experiments in which an initially fluid suspension was transformed into a persisting solid by shearing [42]. Similar phenomena have been observed in industrial situations [91]. In Bertrand's experiments, this phenomenon occurred only for a particular range of concentrations: at lower volume fractions, shear thickening was observed, whilst at higher concentrations, the sample was solid in its quiescent state.

In our model, for suitable values of α, upon increasing v_o we find a similar sequence of behaviour, provided we make the obvious link between v_o and concentration (although the most suitable variation of α with concentration is not clear). It is tempting to identify the jamming transitions of our model with the stress induced solid found experimentally.

However, such an identification is not trivial: the particles used in the experiments are perhaps too large for the notion of glassiness to be relevant. They are slightly outwith the range of sizes usually regarded as colloidal, having radii $a \sim 3\mu m$, suggesting that Brownian forces are small compared with forces such as gravity. Also, in such a system it is certainly not clear that stress transmission is due to thermodynamic forces rather than direct contacts. It would be of great interest to ascertain whether suspensions of smaller particles, in which Brownian motion is more important, can also be jammed into a solid. The industrial experiments mentioned above show that (in some cases at least) they can. For obvious reasons these experiments, similarly to those of Ref. [42], do not utilise the simple model systems favoured by physicists. Thus, further experiments investigating jamming, particularly on model systems [89] would be welcome.

Secondly, our model ignores the question of how the stressed material mantains its solidity

after the external forcing is removed. If, as in the experiments, the solid state persists after removal of the external driving, our model suggests it remains stressed. This was discussed in Ch. 5: we believe that capillary forces at the surface of the sample can sustain the stress which is imparted by the rheometer plates. We have not attempted to capture this aspect of the physics in the model.

These points make it difficult to unambiguously identify the jammed states found experimentally with that of our model. However, the similarities between the two scenarios are encouraging. In both cases, there is a parameter which one can increase to produce shear thickening, cause jamming, and then create a glassy state in the absence of applied stress.

Another aspect of our work cannot be easily compared to Ref. [42]. In the theory, jammed states may be refluidised, depending upon parameters and the precise mathematical form, whilst in these experiments reproducible rheological measurements could not be made in cases for which jamming occurred, and so it is not clear whether or not refluidisation is possible upon steadily increasing the stress. However, this aspect of our work seems relevant to other rheological experiments, in that the basic shape of a material's constitutive flow curve is crucial to its macroscopic rheology.

9.2.2 Shear thickening scenarios

As we discussed in Ch. 2 experimental observations of shear thickening (*eg*, Fig. 2.5) often show an essentially vertical section of the flow curve (in its usual representation): beyond a certain point, increasing the stress has little or no impact upon the shear rate. The shear rate may even appear to decrease with shear stress (even although, classically, this is disallowed). If the shear rate is controlled, thickening appears even more catastrophic: the rheometer increases the stress in an attempt to attain the shear rate which has been programmed, sometimes leading to stresses so large that the rheometer is damaged.

If one assumes the usual instability of regions of the flow curve with negative slope, this behaviour may be inferred from the 'S–shaped' flow curves which appear in our model. (The situation is rather similar to the shear thinning of wormlike micelles – see Ch. 2.) One expects that, upon increasing the shear rate, the stress must jump from the lower to the upper branch,

leading to the observed behaviour. If the experiment is stress controlled, one expects that for a window of stress, the shear rate remains approximately constant, as the material forms a high viscosity band whose extent grows with the applied stress until it fills the cell, at which point the material is wholly on the high viscosity branch.

Of course, dependent upon the situation, there may or may not be a high viscosity branch available to the system: in some cases the model shows no fluidisation upon increasing the stress from the nonergodic state, essentially setting a maximum rate at which the material can flow, regardless of the applied stress [30, 33]. In this case, our model suggests that increasing the stress will result in a jammed state. But, if regions of the flow curve with negative slope are unstable, how might one cause jamming in a material whose constitutive flow curve has the form shown in Fig. 9.1, where a high viscosity flowing branch is allowed? One cannot simply raise the stress beyond σ_{c1}, as doing so will result in banding. The answer might be to access the second branch, above σ_{c2}, before gradually decreasing the stress below this value. Doing so, the shear rate might remain on the high viscosity branch until σ_{c2}, at which point full jamming would occur. Once in the jammed state, it might be possible to (carefully) lower the stress below σ_{c1} without leaving the jammed state: as mentioned previously, this is limited by σ^*, below which nonergodic solutions do not exist. This scenario is illustrated in Fig. 9.2. Hysteresis can be observed upon increasing and then decreasing the applied stress (Fig. 2.5), but jamming has not been observed in this manner.

9.2.3 Glassy or hydrodynamic thickening?

So, whilst the model cannot be easily mapped onto specific experimental systems, it offers a natural explanation, via the S–shaped constitutive flow curves, for the discontinuous thickening observed in dense colloids. (Note that a similar approach to ours, based also upon glassiness, via the SGR model, results in qualitatively similar flow curves to those of the current model [63].) It is arguable that hydrodynamic explanations do not provide such a natural explanation for *discontinuous* thickening. They do not seem to offer the possibility of the nonmonotonic constitutive flow curves which arise in the current approach. Neither do they seem to offer an explanation of stress induced solidity – as we argued in Ch. 5, creating an arbitrarily large

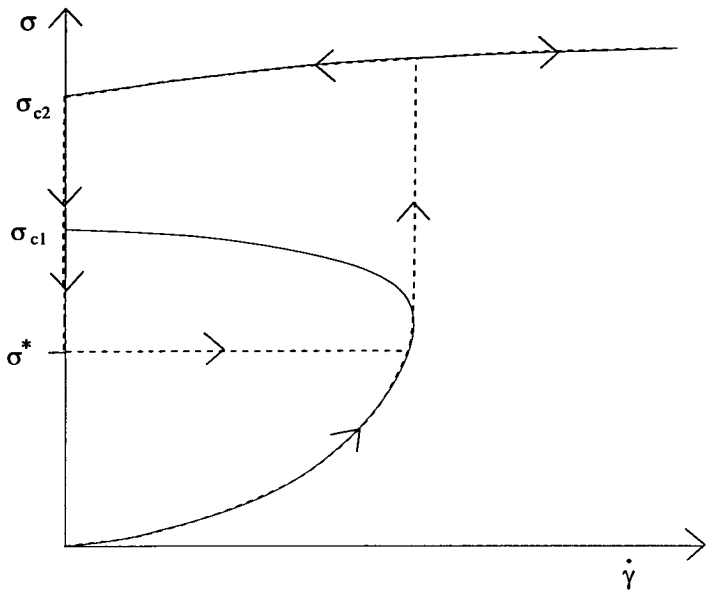

Figure 9.2: An illustration of the hysteresis which might be expected, given the classical instability of regions of the flow curve with negative slope. Upon increasing the stress above σ_{c2}, the system reaches the high viscosity branch. Upon consequently decreasing the stress, it remains on the high viscosity branch, resulting in full jamming at σ_{c2}. As the stress is decreased, the system might remain jammed until σ^*: at lower stresses, nonergodic solutions do not exist and thus jamming is forbidden.

viscosity via hydrodynamics requires an arbitrarily large stress.

Finally, we note that the hydrodynamic picture [120] predicts that thickening occurs at large Peclet numbers. This is in contrast with our work in which, depending upon the parameters, thickening may occur at much lower Peclet numbers – see Fig. 7.2, in which thickening begins at Pe$\sim 10^{-4}$. Whilst experiments do typically show thickening at Peclet numbers of order ten or so, this is not always the case: even keeping the concentration approximately constant, a range of experimental systems show quite a range in the Peclet number at the onset of thickening [43]. Also, increasing volume fraction typically decreases the Peclet number required to cause thickening: in [33], discontinuous thickening is observed at Pe≈ 5 for $\phi = 0.59$ (within the glass), whilst at lower volume fractions a larger value is required, even for continuous thickening, (*eg*, Pe~ 100 for $\phi = 0.56$). This suggests that mechanisms other than hydrodynamics are at work in shear thickening colloids.

To summarise, hydrodynamics arguments (as outlined in Ch. 2) alone do not appear to be capable of describing all aspects of shear thickening phenomena, although such arguments

undoubtedly have some bearing on the non–Newtonian rheology of dense suspensions. In particular, the authors of Ref. [120] claim that their theory provides an understanding, in terms of hydrodynamics, of continuous thickening. This may be so, but in more concentrated systems, one must account for the cooperative nature of particle relaxations. We suggests that it is this *cage effect*, rather than hydrodynamics, which plays the leading rôle in controlling the flow of dense suspensions.

Chapter 10

Conclusions

In this thesis, we set out to investigate the role played by the cage effect in determining the nonlinear rheology of dense suspensions, in particular their propensity to *shear thicken* and *jam*. This was motivated, at least in part, by the experiments of Bertrand *et al* [42] and by similar observations in industrial systems [91]. These observations seem somewhat at odds with purely hydrodynamic explanations of shear thickening. With this in mind, we have investigated a simple model in which the glassy dynamics of a dense suspension are intertwined with its rheology.

The experiments mentioned above also motivate questions regarding the stability of jammed suspensions once external driving is removed: why does the stress induced solid not return to its original state when the external stress is removed? What are the microscopic differences between the jammed solid and the more stable fluid? These questions, as well as the physics of shear thickening and jamming, are relevant to the industrial process of high shear granulation, whereby materials (*eg*, washing powder) may be prepared in a granular form. We have suggested answers to these questions.

In this chapter, we draw conclusions from the work which has been presented. In addition, we highlight open questions regarding jamming in particulate systems, and its relation to the glass transition, suggesting areas where future work would be of benefit.

The cage effect and shear thickening

Hydrodynamic interactions alone cannot explain all shear thickening phenomena, particularly those in very dense suspensions. It is natural to suppose that the cage effect has a bearing upon shear thickening: however, a first–principles theory (originating from MCT or some other microscopic theory of the glass transition) capable of capturing thickening appears some way off. In this case, *ad hoc* models such as that presented here have a rôle to play.

We have shown that, allowing for a vertex which can increase with stress, whilst being eroded by flow, a simple MCT–like model can reproduce much of the phenomenology found in shear thickening dense colloids. The S–shaped flow curves which arise from the model, when coupled with classic flow instabilities, rather naturally lead to scenarios consistent with experiment: discontinuous shear thickening is inferred from the constitutive behaviour.

In addition, the model predicts 'full–jamming' scenarios: that is, S–shaped flow curves can extend back to the σ–axis, indicative of stressed, nonflowing states. In the context of the model, this is a stress induced glass, which has the properties of the idealised glass state of MCT. However, the model predicts that jamming transitions are distinct from conventional MCT glass transitions: they are associated with the disappearance of ergodic solutions, rather than the appearance of nonergodic ones. This results in transitions which are not associated with a bifurcation of the nonergodicity parameter. Because of this difference, much of the phenomenology of these transitions is missing: there is but a single divergent timescale at a jamming transition; and, after the discontinuity at the transition, the nonergodicity parameter varies analytically with the vertex.

It is natural to associate the jammed state of the model with the stress induced solids found experimentally, although this identification is not trivial. However, the simple argument of Ch. 5 suggests that, to cause a divergence of the viscosity via hydrodynamic interactions between particles, one requires very large (formally divergent) stresses. In contrast, the same argument suggests that the stress required to cause a similar divergence due to particle caging is rather more modest.

In short then, an MCT–like model in which vertices may increase with applied stress, whilst being eroded due to flow advection, accounts for many features of the rheology of dense colloids,

including some aspects whose description in terms of hydrodynamics appears inadequate. This is not to say that hydrodynamic forces in shear thickened suspensions are irrelevant, but rather that this is not the only piece of physics relevant to the problem. The large degree of cooperativity required for large scale motion (*the cage effect*) is an important factor which must be accounted for.

Persisting jammed states

If our picture of stress induced arrest is correct, then the jammed samples found experimentally remain stressed, even after external forcing has ceased. We suggest that the stress is sustained by capillary forces at the sample boundary, caused by particles protruding from the interface due to dilatancy. If this is so, decreasing particle size or increasing sample size can preclude surface forces from sustaining the jammed solid, and so this suggestion may be tested rather simply. A rough scenario based upon this notion seems to account for the observed bistability of the samples. However, a detailed understanding of this scenario has yet to be developed.

Jamming: unanswered questions

Jamming occurs in a wide range of situations. Grain in a hopper, sheared dense suspensions, and motorway traffic can all jam up. However (even leaving aside traffic jams) it is not yet clear how different jamming situations are related. A question of interest is whether jammed states are related to glasses: an improved microscopic theory of colloid rheology, incorporating the cage effect, possibly via an MCT–like theory, might go some way towards answering this question in colloids. But linking the glass transition, in which thermodynamics are vital, to jammed granulars in which they are irrelevant, seems an even harder goal. Whilst our model suggests a relation between glassiness and jamming, and despite intriguing similarities between different systems (*eg* granulars and glasses), it remains to be seem to what extent the same physics really does underly the behaviour of these materials.

The question, raised earlier, regarding the nature of stress transmission in jammed materials is a pertinent one. What is the nature of stress transmission in systems which are both particulate and thermal in nature? *ie*, what is the nature of stress transmission in jammed colloids?

With this question in mind, further systematic experimental investigation of jamming in model suspensions (such as that of Ref. [89]), through a range of particle size, would be welcome indeed. Such an investigation might shed light on the question of whether, as we have assumed in much of this thesis, the notion of a stress induced glass is correct. If, in jammed colloids, stress transmission is of a similar nature to that in a glass, this would seem to be the case. An alternative possibility is that sufficient Brownian motion can prevent full jamming. In that case, a jammed state could not be supported by thermodynamic forces, suggesting a granular–like transmission of forces.

Experimental validation of our model would support the basic ideas which underly it – *ie*, that of jamming as stress induced glassiness. If our model is valid, one might be able to create a fully jammed state in discontinuously thickening suspensions by bringing the system into the strongly thickened state, and then carefully decreasing the stress. Also, measurements of the nonergodicity parameter f in jammed samples would be of interest: assuming a correspondance between the parameter v_o and the concentration, the coupling could, in principle, be varied. Such experiments would test our prediction that the nonergodicity parameter varies analytically after the initial jump at the transition.

We hope that the work presented in this thesis will motivate further work, both theoretical and experimental, aimed at increasing our understanding of jamming phenomena and their relationship to the glass transition.

Appendix A

The Zwanzig–Mori formalism

In this appendix, we use the projection operators defined in Ch 4 to derive formally exact equations of motion for dynamical variables and their correlations. This formalism is due to Zwanzig and Mori, and is covered in various standard texts [72, 94, 121].

Taking the time derivative of Eq. 4.5 gives the time derivative of the variables in the set $\{A_i\}$ as, in vector notation,

$$\dot{\mathbf{A}}(t) = \mathrm{e}^{i\mathcal{L}t} i\mathcal{L}\mathbf{A}, \tag{A.1}$$

into which we can insert the unit operator to give

$$\begin{aligned} \dot{\mathbf{A}}(t) &= \mathrm{e}^{i\mathcal{L}t}(\mathcal{P}+\mathcal{Q})i\mathcal{L}\mathbf{A} \\ &= \mathrm{e}^{i\mathcal{L}t} i\underline{\underline{\Omega}} \cdot \mathbf{A} + \mathrm{e}^{i\mathcal{L}t}\mathcal{Q}i\mathcal{L}\mathbf{A}, \end{aligned} \tag{A.2}$$

where we have defined a projection operator

$$\mathcal{P}B \equiv (B, \mathbf{A}^\dagger) \cdot \underline{\underline{\chi}}^{-1} \cdot \mathbf{A}, \tag{A.3}$$

and its complement $\mathcal{Q} \equiv 1 - \mathcal{P}$, using the scalar product defined in the main text. The dagger denotes a Hermitian conjugate in the space of $\mathbf{A}$ (rather than in the Hilbert space of dynamical variables). Thus $\mathbf{A}^\dagger$ is a row vector. The *frequency matrix* $\underline{\underline{\Omega}}$ is defined by $i\underline{\underline{\Omega}} \equiv (i\mathcal{L}\mathbf{A}, \mathbf{A}^\dagger) \cdot \underline{\underline{\chi}}^{-1}$.

A geometrical interpretation of the operators $\mathcal{P}$ and $\mathcal{Q}$ is provided in the main text. These operators, as well as $\mathcal{L}$, are Hermitian in the vector space of dynamical variables. (One can

easily show that $\mathcal{L}$ is Hermitian by writing the equilibrium average as a phase–space integral and integrating by parts. Using the definition of $\mathcal{P}$, one easily deduces that the projectors are Hermitian.)

The second term on the RHS of Eq. A.2 can be simplified using the identity

$$e^{i\mathcal{L}t} = e^{i\mathcal{Q}\mathcal{L}t} + \int_0^t dt' e^{i\mathcal{L}(t-t')} i\mathcal{P}\mathcal{L} e^{i\mathcal{Q}\mathcal{L}t'} \tag{A.4}$$

which is proven [94] by Laplace transforming. This gives

$$e^{i\mathcal{L}t}\mathcal{Q}i\mathcal{L}\mathbf{A} = \mathbf{F}(t) + \int_0^t dt' e^{i\mathcal{L}(t-t')}\mathcal{P}i\mathcal{L}\mathbf{F}(t'), \tag{A.5}$$

where $\mathbf{F}(t) \equiv e^{i\mathcal{Q}\mathcal{L}t}\mathcal{Q}i\mathcal{L}\mathbf{A}$. This quantity is known as the *random force* or the *fluctuating force*, for reasons made clear in the main text. This quantity (also known as the fluctuating force) is orthogonal to the subspace spanned by the $\{A_i\}$, and so $\mathbf{F}(t') = \mathcal{Q}\mathbf{F}(t')$. This gives

$$\begin{aligned} \mathcal{P}i\mathcal{L}\mathbf{F}(t') &= (i\mathcal{L}\mathcal{Q}\mathbf{F}(t'), \mathbf{A}^\dagger) \cdot \underline{\underline{\chi}}^{-1} \cdot \mathbf{A} \\ &= -(\mathbf{F}(t'), (\mathcal{Q}i\mathcal{L})^* \mathbf{A}^\dagger) \cdot \underline{\underline{\chi}}^{-1} \cdot \mathbf{A} \\ &= -(\mathbf{F}(t'), \mathbf{F}^\dagger) \cdot \underline{\underline{\chi}}^{-1} \cdot \mathbf{A} \\ &= -(\mathbf{F}, \mathbf{F}^\dagger(-t')) \cdot \underline{\underline{\chi}}^{-1} \cdot \mathbf{A}, \end{aligned} \tag{A.6}$$

where we have used the Hermiticity of $\mathcal{L}$ and $\mathcal{Q}$, as well as TTI. We now define the *matrix of memory functions* via correlations of the random force

$$\underline{\underline{\mathbf{M}}}(t) \equiv (\mathbf{F}, \mathbf{F}^\dagger(-t)) \cdot \underline{\underline{\chi}}^{-1}, \tag{A.7}$$

which, with Eqs. A.5 and A.2 yields

$$\dot{\mathbf{A}} = i\underline{\underline{\mathbf{\Omega}}} \cdot \mathbf{A}(t) + \mathbf{F}(t) - \int_0^t dt' \underline{\underline{\mathbf{M}}}(t') \cdot \mathbf{A}(t - t'). \tag{A.8}$$

This equation is known as a *generalised Langevin equation* for the set $\{A_i\}$. Again, reasons for the names should become clear in the main text, where we apply some physical insight to these formal manipulations.

Finally, we multiply this equation on the RHS by the row vector $\mathbf{A}^\dagger$ and take a thermal average (*ie,* we take a scalar product) to give an equation for the correlation matrix

$$\dot{\underline{\underline{\mathbf{\Phi}}}}(t) = i\underline{\underline{\mathbf{\Omega}}} \cdot \underline{\underline{\mathbf{\Phi}}} - \int_0^t dt' \underline{\underline{\mathbf{M}}}(t') \cdot \underline{\underline{\mathbf{\Phi}}}(t - t'). \tag{A.9}$$

Bibliography

[1] R G Larson. *The Structure and Rheology of Complex Fluids*. Oxford University Press, New York, 1999.

[2] W B Russel, D A Saville, and W R Schowalter. *Colloidal Dispersions*. Cambridge University Press, Cambridge, 1991.

[3] W C K Poon. A day in the life of a hard sphere suspension. In M E Cates and M R Evans, editors, *Soft and Fragile Matter*, pages 1–8. Institute of Physics Publishing, Bristol, 2000.

[4] U Gasser, E R Weeks, A B Schofield, P N Pusey, and D A Weitz. *Science*, 292:258, 2001.

[5] H M Laun. *J Non–Newt Fluid Mech*, 54:87, 1994.

[6] J-B Salmon, A Colin, and D Roux. *Phys Rev E*, 66:31505, 2002.

[7] H A Barnes, J F Hutton, and K Walters. *An Introduction to Rheology*. Elsevier, New York, 1989.

[8] T C B McLeish. Rheology of linear and branched polymers. In M E Cates and M R Evans, editors, *Soft and Fragile Matter*, pages 79–111. Institute of Physics Publishing, Bristol, 2000.

[9] M E Cates. Structural relaxation and rheology of soft condensed matter. In J-L Barrat, M Feigelman, J Kurchan, and J Dalibard, editors, *Slow Dynamics and Nonequilibrium Relaxations in Condensed Matter*, pages 74–130. EDP Sciences–Springer, 2003.

[10] C W Macosko. *Rheology: Principles, Measurements and Applications*. VCH Publishers, New York, 1st edition, 1994.

[11] S M Fielding, P Sollich, and M E Cates. *J Rheol*, 44:323, 2000.

[12] P D Olmsted. *Curr Opin Coll Int Sci*, 4:95, 1999.

[13] J F Brady. *Curr Opin Colloid Int Sci*, 1:472, 1996.

[14] A Einstein. *Ann Phys*, 19:289, 1906.

[15] A Einstein. *Ann Phys*, 34:591, 1911.

[16] G K Batchelor. *J Fluid Mech*, 83:97, 1977.

[17] P N Segré, S P Meeker, P N Pusey, and W C K Poon. *Phys Rev Lett*, 75:958, 1995.

[18] W C K Poon, S P Meeker, P N Pusey, and P N Segré. *J Non–Newt Fluid Mech*, 67:179, 1996.

[19] C G de Kruif, E M F van Iersel, A Vrij, and W B Russel. *J Chem Phys*, 83:4717, 1985.

[20] G N Choi and I M Krieger. *J Coll Interface Sci*, 113:101, 1986.

[21] J C van der Werf and C G de Kruif. *J Rheol*, 33:421, 1989.

[22] T Shikata and D S Pearson. *J Rheol*, 38:601, 1994.

[23] P Sollich, F Lequeux, P Hebraud, and M E Cates. *Phys Rev Lett*, 78:2020, 1997.

[24] T G Mason and D A Weitz. *Phys Rev Lett*, 75:2770, 1995.

[25] T G Mason and D A Weitz. *Phys Rev Lett*, 74:1250, 1995.

[26] T G Mason, J Bibette, and D A Weitz. *Phys Rev Lett*, 75:2051, 1995.

[27] P Panizza, D Roux, C-Y D Lu, and M E Cates. *Langmuir*, 12:248, 1996.

[28] P Sollich. *Phys Rev E*, 58:738, 1998.

[29] M Fuchs and M E Cates. *Phys Rev Lett*, 89:248304, 2002.

[30] W J Frith, P d'Haene, R Buscall, and J Mewis. *J Rheol*, 40:531, 1996.

[31] J Bender and N J Wagner. *J Rheol*, 40:899, 1996.

[32] V T O'Brien and M E Mackay. *Langmuir*, 16:7931, 2000.

[33] P d'Haene, J Mewis, and G G Fuller. *J Coll Int Sci*, 156:350, 1993.

[34] J F Brady. *Chem Eng Sci*, 56:2921, 2001, and references therein.

[35] T N Phung, J F Brady, and G Bossis. *J Fluid Mech*, 313:181, 1996.

[36] J R Melrose and R C Ball. *Europhys Lett*, 32:535, 1995.

[37] R C Ball and J R Melrose. *Adv Colloid Interface Sci*, 59:19, 1995.

[38] J R Melrose, J H van Vliet, and R C Ball. *Phys Rev Lett*, 77:4660, 1996.

[39] R L Hoffman. *Trans Soc Rheol*, 16:155, 1972.

[40] R L Hoffman. *J Coll Int Sci*, 46:491, 1974.

[41] H M Laun *et al.* *J Rheol*, 36:743, 1992.

[42] E Bertrand, J Bibette, and V Schmitt. *Phys Rev E*, 66:60401(R), 2002.

[43] R L Hoffman. *J Rheol*, 42:111, 1998.

[44] J R Melrose. *Faraday Discuss*, 123:355, 2002.

[45] R S Farr, J R Melrose, and R C Ball. *Phys Rev E*, 55:7203, 1997.

[46] M Doi and S F Edwards. *The Theory of Polymer Dynamics*. Clarendon Press, Oxford, 1986.

[47] N A Spenley, M E Cates, and T C B McLeish. *Phys Rev Lett*, 71:939, 1993.

[48] J K G Dhont. *Phys Rev E*, 60:4534, 1999.

[49] D Bonn, J Meunier, O Greffier, A Al-Kahwaji, and H Kellay. *Phys Rev E*, 58:2115, 1998.

[50] M M Britton and P T Callaghan. *J Rheol*, 41:1365, 1997.

[51] J L Goveas and P D Olmsted. *Eur Phys J*, 6:79, 2001.

[52] O Radulescu, P D Olmsted, and C-Y D Lu. *Rheol Acta*, 38:606, 1990.

[53] P Boltenhagen, Y Hu, E F Matthys, and D J Pine. *Europhys Lett*, 38:389, 1997.

[54] G Picard, A Ajdari, L Bocquet, and F Lequeux. *Phys Rev E*, 66:051501, 2002.

[55] A Ajdari. *Phys Rev E*, 58:6294, 1998.

[56] S M Fielding and P D Olmsted. *Phys Rev Lett*, 90:224501, 2003.

[57] R Bandyopadhyay, G Basappa, and A K Sood. *Phys Rev Lett*, 84:2022, 2000.

[58] R Bandyopadhyay and A K Sood. *Europhys Lett*, 56:447, 2001.

[59] J-B Salmon, A Colin, and D Roux. *Phys Rev E*, 66:031505, 2002.

[60] L Hilliou and D Vlassopoulos. *Ind Eng Chem Res*, 41:6246, 2002.

[61] M E Cates, D A Head, and A Ajdari. *Phys Rev E*, 66:025202(R), 2002.

[62] D A Head, A Ajdari, and M E Cates. *Europhys Lett*, 57:120, 2002.

[63] D A Head, A Ajdari, and M E Cates. *Phys Rev E*, 64:061509, 2001.

[64] C Derec, A Ajdari, and F Lequeux. *Eur Phys J E*, 4:355, 2001.

[65] A Aradian and M E Cates. cond–mat/0310660, 2003.

[66] S M Fielding and P D Olmsted. cond–mat/0310658, 2003.

[67] P G Debenedetti. *Metastable Liquids: Concepts and Principles*. Princeton University Press, Princeton, 1st edition, 1996.

[68] W Kob. Supercooled liquids and glasses. In M E Cates and M R Evans, editors, *Soft and Fragile Matter*, pages 259–284. Institute of Physics Publishing, Bristol, 2000.

[69] M D Ediger, C A Angell, and S R Nagel. *J Phys Chem*, 100:13200, 1996.

[70] D Tabor. *Gases, Liquids and Solids*. Cambridge University Press, Cambridge, 3rd edition, 1991.

[71] W van Megen and S M Underwood. *Phys Rev E*, 49:4206, 1994.

[72] J P Hansen and I R McDonald. *The Theory of Simple Liquids*. Academic Press, London, 1st edition, 1976.

[73] P N Pusey. Colloidal suspensions. In J P Hansen, D Levesque, and J Zinn-Justin, editors, *Liquids, Freezing and the Glass Transition*, pages 763–942. North-Holland, Amsterdam, 1989.

[74] S P Lee, W Tscharnuter, and B Chu. *J Poly Sci: Poly Phys Ed*, 10:2453, 1972.

[75] W Götze. *Z Phys*, 60:195, 1985.

[76] P N Pusey and W van Megen. *Phys Rev Lett*, 59:2083, 1987.

[77] W van Megen and P N Pusey. *Phys Rev A*, 43:5429, 1991.

[78] S-E Phan, W B Russel, Z Cheng, J Zhu, P M Chaikin, J H Dunsmuir, and R H Ottewill. *Phys Rev E*, 54:6633, 1996.

[79] S P Meeker, W C K Poon, and P N Pusey. *Phys Rev E*, 55:5718, 1997.

[80] V Viasnoff, S Jurine, and F Lequeux. *Faraday Disc*, 123:253, 2003.

[81] L Ramos and L Cipelleti. *Phys Rev Lett*, 87:245503, 2001.

[82] M Fuchs and M E Cates. *Faraday Disc*, 123:267, 2003.

[83] A Ajdari. Mechanical aging and nonlinear rheology. In J-L Barrat, M Feigelman, J Kurchan, and J Dalibard, editors, *Slow dynamics and nonequilibrium relaxations in condensed matter*, pages 43–73. EDP Sciences–Springer, 2003.

[84] L Berthier, J-L Barrat, and J Kurchan. *Phys Rev E*, 61:5464, 2000.

[85] M E Cates, J P Wittmer, J-P Bouchaud, and P Claudin. *Phys Rev Lett*, 81:1841, 1998.

[86] A J Liu and S R Nagel. *Nature*, 396:21, 1998.

[87] J Bergenholtz, W C K Poon, and M Fuchs. *Langmuir*, 19:4493, 2003.

[88] V Trappe, V Prasad, L Cipelletti, P N Ségre, and D A Weitz. *Nature*, 411:772, 2001.

[89] M D Haw. cond–mat/0308615, 2003.

[90] J R Rice. *J Geophys Res*, 80:1531, 1975.

[91] Patrick Warren. Private communication.

[92] B J Ennis, G Tardos, and R Pfeffer. *Powder Tech*, 65:257, 1991.

[93] H Goldstein, editor. *Classical Mechanics*. Addison–Wesley, Reading, MA, 1980.

[94] J-P Boon and S Yip. *Molecular Hydrodynamics*. McGraw–Hill, New York, 1980.

[95] W Götze. Aspects of structural glass transitions. In J P Hansen, D Levesque, and J Zinn-Justin, editors, *Liquids, Freezing and the Glass Transition*, pages 287–503. North-Holland, Amsterdam, 1989.

[96] J Bosse, W Götze, and M Lücke. *Phys Rev A*, 17:434, 1978.

[97] G Szamel and H Löwen. *Phys Rev A*, 44:8215, 1991.

[98] S J Pitts and H C Andersen. *J Chem Phys*, 113:3945, 2000.

[99] W Götze. *Condens Matter Phys*, 1:873, 1998.

[100] W Kob. Supercooled liquids. In J-L Barrat, M Feigelman, J Kurchan, and J Dalibard, editors, *Slow Relaxations and Nonequilibrium Dynamics in Condensed Matter*, pages 199–269. EDP Sciences–Springer, 2003.

[101] W Götze and L Sjögren. *Rep Prog Phys*, 55:241, 1992.

[102] U Bengtzelius, W Götze, and A Sjölander. *J Phys C*, 17:5915, 1984.

[103] W van Megen, S M Underwood, and P N Pusey. *Phys Rev Lett*, 67:1586, 1991.

[104] K N Pham *et al.* *Science*, 296:104, 2002.

[105] W Hartl. *Curr Opin Coll Int Sci*, 6:479, 2001.

[106] E Leutheusser. *Phys Rev A*, 29:2765, 1984.

[107] J F Brady. *J Chem Phys*, 99:567, 1993.

[108] O Reynolds. *Philosophical Magazine*, 20:469, 1885.

[109] G Y Onoda and E G Liniger. *Phys Rev Lett*, 64:2727, 1990.

[110] D M Wood. *Soil Behaviour and Critical State Soil Mechanics*. Cambridge University Press, Cambridge, 1990.

[111] K Miyazaki and D R Reichmann. *Phys Rev E*, 66:050501(R), 2002.

[112] G K Batchelor. *J Fluid Mech*, 74:1, 1976.

[113] M D A Cooley and M E O'Neil. *Mathematika*, 16:37, 1969.

[114] M Tokuyama and I Oppenheim. *Physica A*, 216:85, 1995.

[115] J Bergenholtz. *Curr Opin Coll Int Sci*, 6:484, 2001.

[116] M E Cates. cond–mat/0211066, 2002.

[117] J-P Bouchaud, L Cugliandolo, J Kurchan, and M Mezard. *Physica A*, 226:243, 1996.

[118] M Fuchs, W Götze, I Hofacker, and A Latz. *J Phys Condens Matter*, 3:5047, 1991.

[119] E J Hinch. *Perturbation Methods*. Cambridge University Press, Cambridge, 1991.

[120] J Bergenholtz, J F Brady, and M Vicic. *J Fluid Mech*, 456:239, 2002.

[121] D Forster. *Hydrodynamic Fluctuations, Broken Symmetry and Correlation Functions*. W A Benjamin, Reading, Mass., 1975.